2016

Assessing Seasonal Performance, Stiffness, and Support Conditions of Pavement Foundations

Yang Zhang
Iowa State University

Assessing seasonal performance, stiffness, and support conditions of pavement foundations

by

Yang Zhang

A dissertation submitted to the graduate faculty

in partial fulfillment of the requirements for the degree of

DOCTOR OF PHILOSOPHY

Major: Civil Engineering (Geotechnical Engineering)

Program of Study Committee:
David J. White, Major Professor
Pavana K.R. Vennapusa, Major Professor
Bora Cetin, Major Professor
Robert Horton
Peter C. Taylor
Charles T. Jahren

The student author and the program of study committee are solely responsible for the content of this dissertation. The Graduate College will ensure this dissertation is globally accessible and will not permit alterations after the degree is conferred.

Iowa State University

Ames, Iowa

2017

This work is dedicated to my parents, my parents in law, and my wife,

Xiaolin Zhang, Demei Liu, Dongfeng Chen, Yan Zhao, and Conglin Chen

TABLE OF CONTENTS

LIST OF TABLES

LIST OF FIGURES

ABSTRACT

Seasonal freeze-thaw cycles in cold regions are a key factor leading to pavement damage. The duration and penetration depth of freeze-thaw cycles in the foundation layers can significantly influence the pavement performance. Frost heaves and loss of support conditions are two direct results due to pavement freezing and thawing. Current research has brought great interests in this topic, which may benefit pavement design, construction, and maintenance.

Sufficient freezing depth, continuous water supply, and frost susceptible geomaterials are the three factors required resulting in pavement freeze-thaw related damage. When these factors are satisfied, stiffness and support conditions can be significantly affected due to the phase change of moisture within pavement structures. In various current pavement design guides, seasonal variation in foundation layers is taken into consideration by empirically adjusting the foundation layer moduli values. As various QC/QA testing methods is used in practice, different mechanistic properties can be derived. Even though only a few particular parameters are considered in current pavement design guides, empirical correlations were reported for transferring different properties. Values of these measurable properties change seasonally, which may differ from the values of design parameters after correlations. Therefore, it is necessary to evaluate if the seasonal mechanistic property values meet the design values and if the empirical correlations match to the in situ measurements.

This study focused on investigating the frost actions of pavement foundations that may affect pavement designs, such as frost penetration depths, number of freeze-thaw cycles, moisture conditions, and geomaterial frost susceptibility. QC/QA tests were conducted to assess the influences and performance on reconstructed and rehabilitated pavement

foundation stiffness and support conditions. Seasonal strength/stiffness results of pavement foundation layers were evaluated in comparison with design values in terms of empirical correlations.

Key words: seasonal; pavement foundation; stiffness; support condition; FWD; DCP; frost penetration; freeze-thaw cycle.

CHAPTER 1. INTRODUCTION

Seasonal freeze-thaw cycles in cold regions lead to various pavement damage. Focusing on this statement, this chapter describes the industry and technical problems with respect to the goals, objectives, and significance of this research. The final section of this chapter presents the organization of this dissertation.

1.1. Problem Statement

In climates like Iowa, pavement foundations are subject to freezing and thawing, which influence pavement systems associated with design, construction, and maintenance. This physical process is called the freeze-thaw cycle and results in all kinds of pavement problems, such as frost heave and thaw weakening in pavement foundation layers. In earthwork engineering, freeze-thaw cycles are a common situation that influences the road safety, serviceability (e.g., user comfort and confidence), durability, and maintenance costs of pavements for pavement designers, transportation agencies, contractors, road users, and taxpayers.

Frost-stiffening and thaw-weakening primarily result from ice forming and melting within geomaterials. The stiffness and strength of the roadbed material decrease as the phase of the moisture changes from solid to liquid and increase as the phase changes from liquid to solid (Janoo and Berg, 1996; Johnson, 2012; Zhang et al., 2016). Three elements, the freezing front, thawing front, and moisture contents of the pavement layers, primarily influence the mechanistic properties of pavement foundations (Konrad and Roy, 2000). The significant influence of cyclic freezing and thawing on pavement performance means that it is important to investigate freeze-thaw conditions and frost actions in pavements, such as frost penetration depths, numbers of freeze-thaw cycles, and the duration of freezing and thawing periods. To provide effective

pavement designs, changes in the in situ pavement foundation stiffness during and after freeze-thaw cycles and those pavement frost actions need to be better quantified.

Various thickness design procedures have been developed since the 1970s for concrete pavement design. PCA (1984) and AASHTO (1993) design procedures are currently the most popularly used methods by the highway agencies in the U.S., while there is increasing interest in implementing the newly developed mechanistic-empirical design guide by AASHTO (2008). While the AASHTO (2008) procedure is a significant advancement over the PCA (1984) and AASHTO (1993) procedures in terms of analyzing the pavement responses, the key design parameter used to characterize foundation layer support is still the modulus of subgrade reaction (k) value. Resilient modulus (M_r) value is one of design parameters in AASHTO (1993) and AASHTO (2008), but the M_r value is converted to a k value using empirical relationships in the design process. AASHTO (1993) provides suggested values for use in design as target M_r values for subgrade in frozen, thawed, and summer conditions. AASHTO (2008) deals with seasonal variations in a more sophisticated manner based on local climatic modeling data and laboratory test measurements to adjust modulus values for seasonal variations. However, limited research has been conducted to evaluate these adjustments and correlations used in these pavement design guides, and there is a need to appraise if seasonal variations in foundation layer mechanistic properties are properly addressed in pavement designs.

This study focuses on investigating the freeze-thaw performance of pavement foundations. The benefits to industry from this research are to improve the safety and durability of pavement systems, to reduce the costs of construction and maintenance, and to provide comfortable serviceability for road users. The results from this research provide guidance for improving pavement designs to address climatic induced pavement problems in seasonal frost areas.

1.2. Research Goal and Objectives

The principal goal of this research is to evaluate the freeze-thaw performance of pavement foundations. To address this goal, the detailed objectives of the study were:

- to investigate the frost penetrations in pavement foundations using different methods and evaluate the estimates comparing to the actual measurements;
- to assess the seasonal variations in pavement foundation mechanistic properties and compare these parameter values to the design values;
- to investigate the joint frost heave on deteriorated concrete pavements and determine the frost susceptibility of reconstructed foundation materials;
- to determine the stiffness and support conditions of reconstructed pavement foundation layers and evaluate the empirical correlations in pavement design guides; and
- to statistically compare the pavement slab stabilizations between using cementitious grout and high density polyurethane foam based on measuring foundation properties.

1.3. Organization of the Dissertation

This dissertation consists of seven chapters: a general introduction, four technical articles, one case study article, and general conclusions and recommendations for future research.

Following this chapter, Chapter 2 discusses the frost penetration estimations using modified Berggren equation and three other empirical models. Estimated results are compared with in situ measurements to evaluate the estimations and to analyze the impacts of key factors on the estimation accuracy. Chapter 3 discusses an in situ study on the pavement foundation mechanistic properties at different seasons. Results comparing to the design values and relationships between measurements and empirical correlations are presented. The relationships between the foundation layer properties and pavement performance are also discussed in the

article. Chapter 4 presents a case study investigating the frost heave deterioration at joint locations of concrete pavement. Vertical heaves measured at deteriorated joints and water conditions at layers are presented for assessing possible causes. The frost susceptibility of the reconstructed foundation materials is rated. Chapter 5 illustrates reconstructed pavement foundation layer stiffness and support conditions. Testing results from falling weight deflectometer (FWD), light weight deflectometer (LWD), and dynamic cone penetration (DCP) are compared between measurements, target design values, and empirical correlations. Chapter 6 compares pavement slab stabilizations between cementitious grout and high density polyurethane (HDP) foam based on statistical analysis accounting for foundation layer mechanistic properties. Chapter 7 summarizes the conclusions derived from this study and provides several suggestions and directions for future research.

CHAPTER 2. SEASONAL FROST PENETRATIONS IN PAVEMENTS WITH MULTIPLE LAYERS

A paper to be submitted to *ASCE Journal of Cold Regions Engineering*

Yang Zhang, Robert Horton, David J. White, and Pavana K.R. Vennapusa

2.1. Abstract

Seasonal freeze-thaw cycles and frost penetration depth in cold regions can be key contributors to pavement damage, and it is important as part of design practice to account for detrimental freeze-thaw conditions in the foundation layers. Empirical and numerical models have been developed to estimate frost penetration beneath pavement. In this study, the modified Berggren equation as well as three simple empirical models were used to estimate frost penetration at three test locations with different pavement structures. Each of the test locations had an array of buried temperature sensors. The simple empirical equations performed poorly, but the modified Berggren equation had more promising frost penetration depths. Modified Berggren equation calculations were performed with the computer program PCASE. The air and ground surface temperatures were monitored to verify influences of the n-factor transferring air to surface freezing index. Different geomaterial properties were used in calculations to explore ways to improve estimation accuracy. Results indicate that pavement type, foundation layer conditions, and local climate affect PCASE frost penetration estimates. Including site specific information improves the accuracy of frost penetration predictions.

2.2. Introduction

In seasonal frost areas, freeze-thaw and frost penetration depth have been reported as contributors to accelerated pavement problems (Cassagrande et al. 1931; Chamberlain 1986; DeGaetano and Wilks 2002). Estimating freezing depth has gained great importance for

pavement design and maintenance. Several researchers have investigated various empirical and numerical methods to predict frost penetration in pavement systems (Aldrich and Paynter 1953; DeGaetano et al. 2001; Jumikis 1955; McKeown et al. 1988).

Stefan (1890) presented an equation based on Fourier's law to calculate the rate of ice formation. There are critical assumptions and limitations associated with the Stefan equation. However, civil engineers used the equation for predicting frost penetration into bare ground, and later, they improved the Stefan equation (Aldrich and Paynter 1953; Andersland and Ladanyi 2004). Several simplified models have been developed, but model results indicate significant uncertainties (Baladi and Rajaei 2015; Yoder and Witczak 1975). The modified Berggren equation is widely used in civil engineering (Bianchini and Gonzalez 2012). For this model, a modified factor that was determined empirically was included in the Stefan equation to overcome the limitation of neglecting soil volumetric heat. (Aldrich and Paynter 1953; Freitag and McFadden 1997). Several computer programs and methodologies were developed for calculating heat transfer in multi-layer conditions, including pavements (Aitken and Berg 1968; Bianchini and Gonzalez 2012). However, limited research has been performed to evaluate the modified Berggren based methods by comparing the predicted results to actual in situ measurements.

In this study, pavement temperature sensors were installed at three locations in the State of Iowa. The principal objectives of this research are to determine the actual frost penetrations from in situ pavement temperature measurements, to estimate the frost penetrations with the traditional modified Berggren and other simplified empirical models, and to compare the predicted results to the actual measurements.

2.3. Background

2.3.1. Seasonal ground frost penetration

Climatic influences have been taken into consideration in recent pavement design guides (AASHTO 1993; AASHTO 2008). In seasonal frost areas, the design of mechanistic parameters of roadbeds (e.g., resilient modulus and modulus of subgrade reaction) was modified using values determined under different seasonal conditions (AASHTO 1993; AASHTO 2008). However, frost penetration depth is still a key factor and needs to be verified if pavements have the potential to undergo freezing and thawing. From historical weather station data, frost depth maps are available for the United States (DeGaetano et al. 2001). The frost depths were determined from one to two hundred year return periods for bare soil, bare soil with snow cover, and turf. The average maximum frost penetration depths in Iowa ranged from 100 to 120 cm using pavement temperature data. Andersland and Ladanyi (2004) reported the 0°C isotherm value as an approach for analyzing temperature variations in pavement structures for lengths of freezing and thawing periods in different layers. Frozen zones versus time can be estimated from the 0°C isothermal depth. Determination of the 0°C isotherm depth also represent the maximum frost penetration depth.

Hoover et al. (1962) investigated pavement freeze-thaw conditions over three winters (1957 through 1960) on US Highway 117 in Jasper County, Iowa using the modified Berggren equation. Seven thawing periods during the 1957–1958 winter and nine during the 1959–1960 winter were documented (Hoover et al. 1962). During the 1958–1959 winter, a large continuous frozen zone and several smaller, thawed zones were observed at shallow depths for short times within the frozen period. Hoover et al. (1962) also estimated that there were 11 freeze-thaw cycles based on air temperature data, but only one freeze-thaw cycle at the 0.4 m depth. The

maximum frost penetration reached around 1.05 m during the three winters. New empirical and numerical models were developed to estimate frost penetrations based on air temperature data (see Table 2.1). However, each model had particular limitations and assumptions, which led to variations in the estimated results. The simultaneous heat and water (SHAW) model is a one-dimensional model that is able to simulate heat and water movement in freezing and thawing soils (Flerchinger et al. 1998).

Table 2.1. Models for predicting frost penetrations using air temperature data.

Key Equation	Measurements	Initial Assumptions		Limitations	Reference
$X = \sqrt{\frac{48k(FI)}{L}}$	ɣ and ω – assumed or measured in lab; T – measured in field (air or surface); n – assumed based on literature values or measured in situ. (or measure soil thermal properties directly in situ)	Air T equals surface T; isothermal boundary T is 0°C; surface T is constant.	The soil is semi-infinite, uniform and isotropic; Surface temperature changes to below 0°C suddenly and keeps constant.	Overestimate X due to neglecting volumetric heat effect.	Stefan (1889) Freitag and McFadden (1997)
$X = \lambda\sqrt{\frac{48kn(FI)}{L}}$		Homogeneous soil; ground is bare soil with single layer (weighted soil properties if multi-layer).		Does not consider the movement of water in freezing soil; ground is one-dimensional.	Aldrich and Paynter (1953) Aitken and Berg (1968)
$FI = \frac{d_i L_i}{24n\lambda_i^2} \times R$		Surface temperature changes to below 0°C suddenly and keeps constant;			Bianchini and Gonzalez (2012)
$X = a(FI)^b$	T - measured in field (air or surface)	Bare single layer soil; temperature is the only significant influence on X.		Empirical correlations based on local data.	Rajaei and Baladi (2015)

Note: Equations are in US units. *X*: frost penetration depth; *k*: thermal conductivity; *FI*: Freezing Index; *n*: factor transfers air FI to surface FI; *L*: latent heat; *λ*: correction coefficient; *d*: layer depth; *R*: thermal resistance; ɣ: dry unit weight; ω: moisture content; T: temperature; a, b: constant; C: volumetric heat capacity; v_0: absolute value of the difference between the mean annual temperature below the ground surface and 32°F; v_s: absolute value of the difference between the mean annual ground surface temperature and 32°F.

2.3.2. Stefan equation and modified Berggren equation

The Stefan equation was originally created for calculating the growth rate of ice sheets (Bianchini and Gonzalez 2012; Freitag and McFadden 1997; Stefan 1889). Basically, it assumed

that the amount of heat flux flow through an existing ice sheet was equal to the amount of latent heat generated from the formation of new ice. The Stefan equation was then applied to model soil freezing. An equation was developed based on the Fourier's law, which could be used to calculate the thickness of an ice sheet or a frozen soil layer. The equation was a function of freezing index (FI), thermal conductivity (k), and latent heat (L) (Freitag and McFadden 1997). However, the three principal assumptions led to significant influences on the calculations: the air temperature was the same as the ground surface temperature; the temperature at the isothermal boundary was 0ºC; and the soil profile was homogeneous and isotropic (Jumikis 1955).

Weaknesses on applying the Stefan equation have been reported (Aldrich and Paynter, 1953; Bianchini and Gonzalez, 2012; Nixon and McRobert 1973). First, there is a possible misuse of the FI. In accordance with the process of deducing this equation, the FI was obtained by integrating the temperature difference between the frozen soil and the freezing temperature (0°C) (Bianchini and Gonzalez 2012). Even when the temperature is measured near the interface of the frozen soil and air, it still showed a significant difference between this temperature and the air temperature. This led to inclusion of an n-factor used to transfer the air FI to the ground surface FI (Hanson et al. 2010). Andersland and Ladanyi (2004) summarized the freezing and thawing n-factors of different types of ground (e.g., the freezing n is 0.25–0.95 for concrete pavement). Limited research has focused on determining this factor, although investigators have reported different assumed n values for different areas (Brown 1963). However, it can be inferred that local environmental conditions such as wind speed, radiation, and moisture content influence n-factor values (Andersland and Ladanyi 2004; Khoshkhoo et al. 2015).

Due to the original assumption, the sensible heat released from ice formation was not taken into consideration. As the ice mass increases, the volumetric heat of the frozen soil layer

increases. The sensible heat generated near the frozen surface increases as ice forms, while the equation only accounts for latent heat. This weakness leads to an overestimation of the frozen soil thickness (Aitken and Berg 1968; Freitag and McFadden 1997). For the purpose of reducing influences from these weaknesses, the modified Berggren equation was developed (Jumikis 1955; MIT 1957).

Aldrich and Paynter (1953) modified the Stefan equation to become the modified Berggren equation by introducing a correction coefficient, λ. This coefficient can be calculated through a semi-empirical correlation accounting for both the latent heat and the sensible heat (Braley and Connor 1989). Computer programs were developed to determine λ through transcendental equations, especially to iterate the λ values of multilayered ground and to estimate frost penetration depth (Bianchini and Gonzalez 2012; USDA and USDAF 1988). However, manual computation of λ is only accessible through an empirical correlation in terms of fusion parameter μ and thermal ratio α, where μ is the parameter accounting for sensible heat (Aldrich and Paynter 1953). Hoover et al. (1962) applied the modified Berggren equation to estimate historical frost penetration depths, and Orakoglu et al. (2016) used it to estimate maximum frost penetration depths. Averaged soil properties corresponding to assumed frost penetration depths were used to determine λ and soil thermal properties for the study reported by Orakoglu et al. (2016).

Following Braley and Connor (1989), Bianchini and Gonzalez (2012) reported an improved method for predicting multi-layered frost penetration using air FI values based on the modified Berggren equation. A computer program named “Pavement-Transportation Computer Assisted Structural Engineering” (PCASE) was developed based on this calculation process. The basic theory of this method is to calculate the portion of FI that is required to penetrate a specific thickness of ground layer. After the sum of the FI of each calculated layer becomes equal to the

surface FI, it indicates that the final depth in the lowest layer represents the calculated frost penetration depth (Bianchini and Gonzalez 2012). A minor weakness of this method and also the previous average method is that the dry unit weights and moisture contents of each layer need to be assumed if measurements are not available in order to determine the latent heat and thermal conductivity. These assumptions increase the uncertainty of the results (Orakoglu et al. 2016). The default values of moisture content and dry unit weight in PCASE for the US moist-cold zone are summarized in Table 2.2.

Table 2.2. Default moisture contents and dry unit weights for the moist-cold zone in PCASE.

	Moisture Content (%)	Dry Unit Weight (kg/m^3)
Asphalt Cement Concrete	0.5	2243
Portland Cement Concrete	0.5	2323
Base Coarse	5	2243
Subbase Coarse	8	2082
Subgrade (clay/silt)	16 – 21	1522 – 1682

2.4. In Situ Measurements

2.4.1. In situ pavement temperature monitoring

Thermocouples were installed at three locations in the state of Iowa, central Iowa Expo (Expo – 1) site 1, central Iowa Expo (Expo – 2) site 2, and the US Highway 30 (US 30) site during construction. The pavement structures differ at the three locations. At the Expo sites, thermocouples were installed in each pavement layer and solar powered data acquisition systems were set-up at the testing locations (Figure 2.1). Temperature data were monitored every minute, and the data were collected before winter freezing initiated until spring thaw occurred.

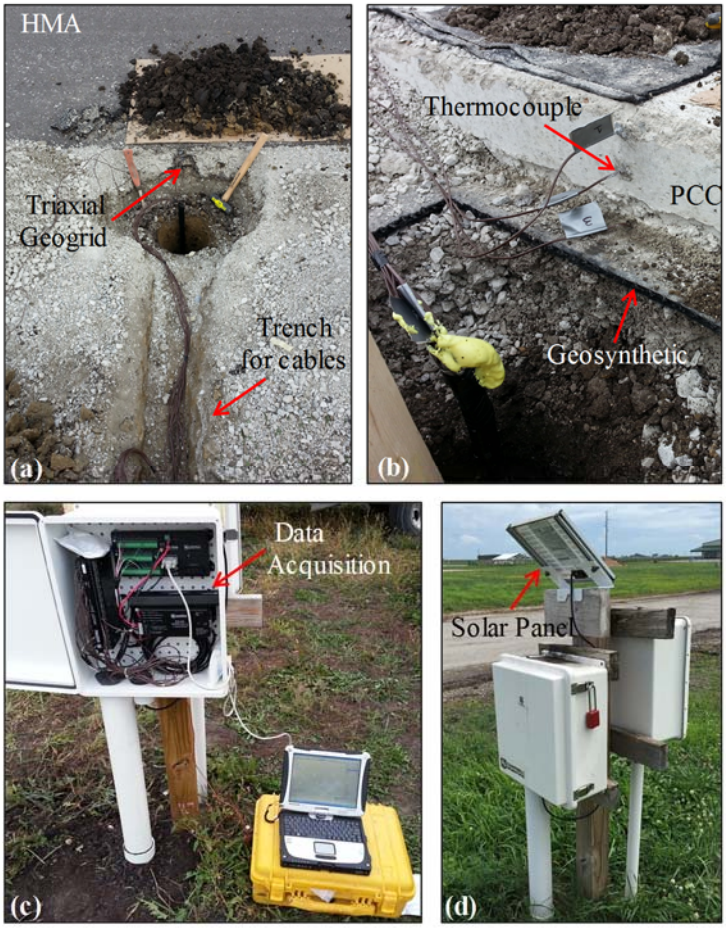

Figure 2.1. Installing thermocouples in pavements at the Expo site (a) Expo – 1 and (b) Expo – 2, (c) collecting data at site, and (d) data acquisition system.

At the expo sites, a total of 32 thermocouples were installed in October 2013 at Expo – 1 which had a HMA surface and at Expo – 2 which had a PCC surface (16 thermocouples each street), and two thermocouples were also placed near the ground surface to monitor the air temperature. Thermocouple 1 is placed 2.54 cm below the surface, and thermocouple 2 is 5.08 cm below the first thermocouple. Temperature data from thermocouple 1 were used to approximate boundary condition. Thermocouples 2 to 5 are 7.62 cm vertically apart from each other, and thermocouples below thermocouple 5 are spaced vertically by 10.16 cm. There is a modified subbase layer (MSB) under the 15 cm thick pavement layer at both streets, and a layer of geosynthetic was placed at Expo – 2 between the PCC and MSB layer. A layer of triaxial

geogrid was used at Expo – 1 at the bottom of MSB. Another 15 cm thick subbase layer was stabilized with portland cement and fibers at Expo – 2 above the natural subgrade. The detailed thermocouple layout and pavement profiles at the Expo site are shown in Figure 2.2.

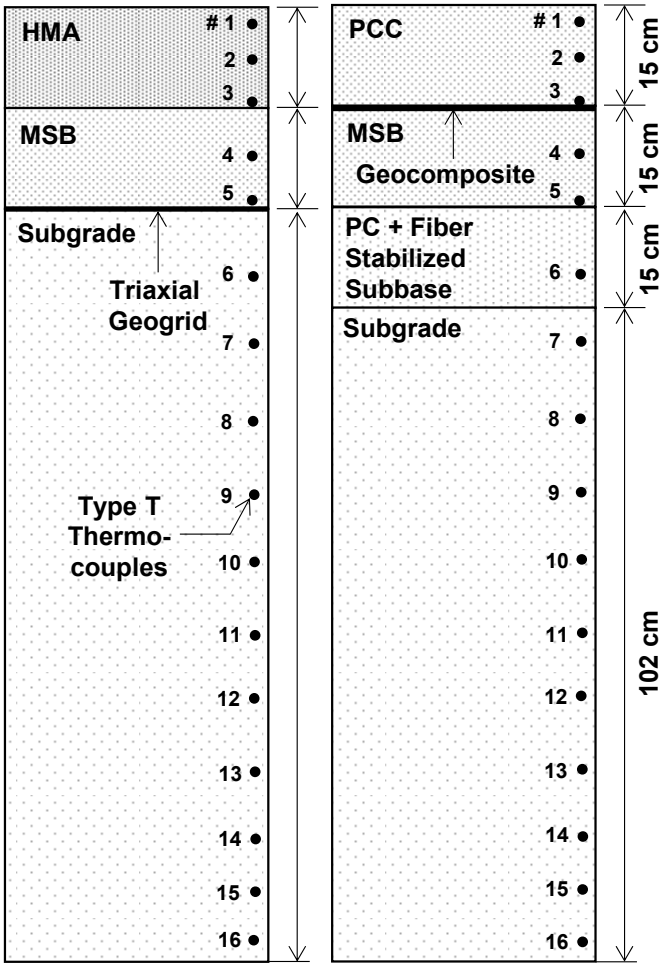

Figure 2.2. Pavement profiles with thermocouples at Expo – 1 (left) and Expo – 2 (right).

Thermocouple temperature sensors were installed at about mile 143.68 on US30 eastbound lane in July 2011. A nominal 25 cm thick jointed plain concrete pavement (JPCP) was placed on a 40 cm thick modified subbase (MSB) that was over the natural existing subgrade. Sensors were installed vertically from about 0.4 m to about 1.6 m below pavement surface. No sensor was installed within the 25 cm thick PCC layer and the upper 15 cm thick MSB layer. All vertical

sensors were located at the center line. A pavement and foundation layer cross-section along with the temperature sensor locations was shown in Johnson (2012).

2.4.2. Frost penetration depth

The number of freeze-thaw cycles with depth calculated for each year from 2013 to 2016 from the temperature monitoring data at both Expo sites are presented in Figure 2.3. The cycles were determined using ±0.5ºC as boundary values, which means temperature dropped below -0.5 ºC and later increased higher than 0.5 ºC was defined as one freeze-thaw cycle. This approach effectively neglected some cycles that the temperature slightly varied around 0 ºC (such as from -0.1 ºC to 0.1 ºC), which may not significantly influence pavement conditions. Freeze-thaw cycles decreased with depth as expected. The number of freeze-thaw cycles in air were between 41 and 65 and decreased to about 3 to 11 cycles near the bottom of the pavement. Although there were differences in the number of freeze-thaw cycles between PCC and HMA layers, the numbers of freeze-thaw cycles became more similar as depth increased. From the bottom of the MSB layer at a depth of about 40 cm, less than 3 cycles were found at both locations. The deepest freeze-thaw cycle during the monitored years was observed between 120 to 140 cm. This finding indicated that the maximum frost penetration was within this range at the Expo sites.

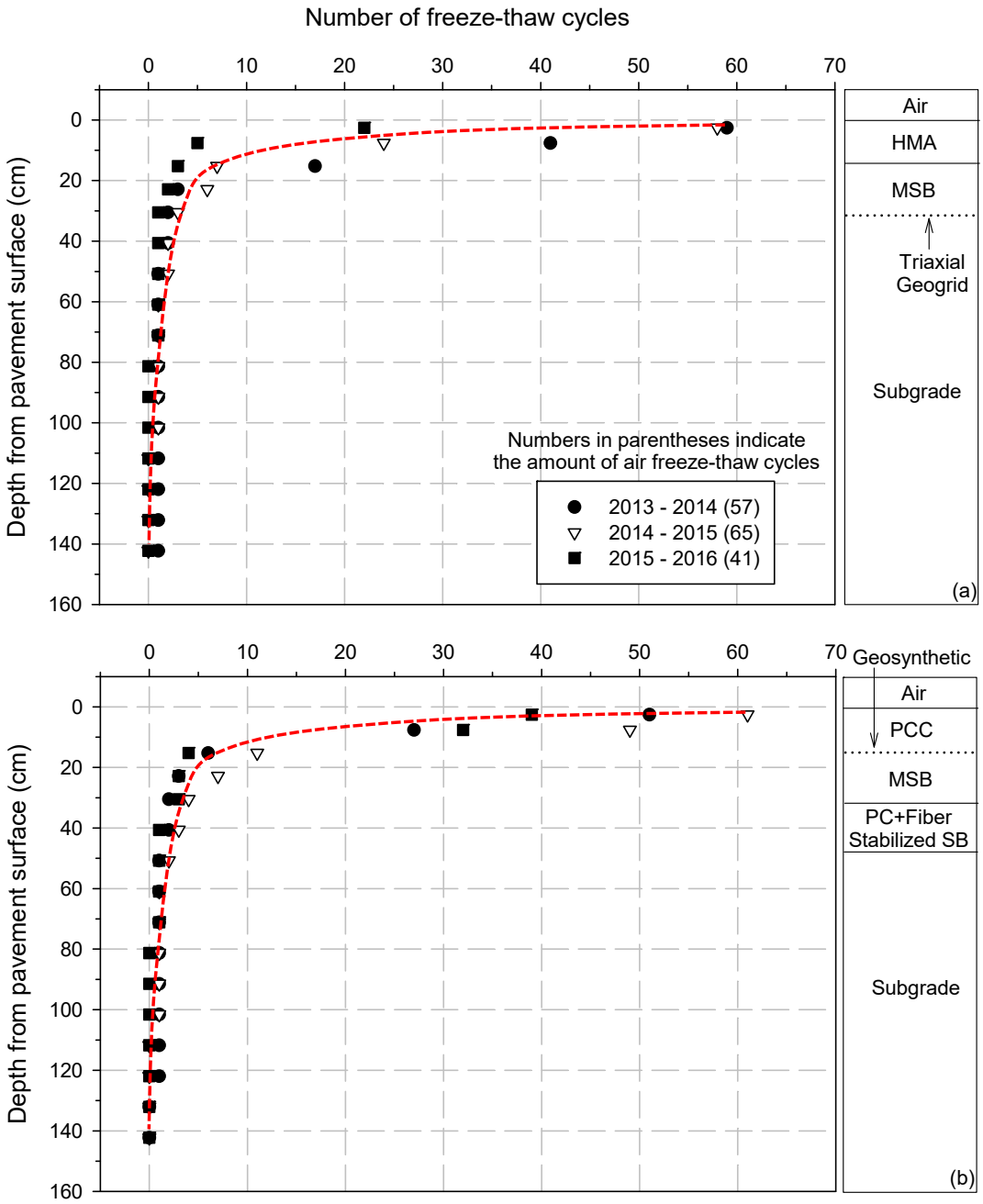

Figure 2.3. Freeze-thaw cycles at depth of (a) Expo – 1 and (b) Expo – 2.

In accordance with the isothermal figure in Andersland and Ladanyi (2004), the dates of 0ºC at each depth were determined during both the freezing and thawing periods. Connecting these 0ºC points provided the estimated isotherm lines (Figure 2.4). The upper areas of the isothermal lines were so called “frost zones”, which indicated the length of freezing periods at different

depths. The lowest point of the isothermal line was the maximum frost penetration of the year. Results in Figure 2.4 show a relatively large frost zone during the 2013–14 winter, two separated medium frost zones during the 2014–15 winter, and a smaller zone for the 2015–16 winter for each street. In general, differences of 2 to 13 cm were found between the maximum frost penetrations at Expo sites for each year. The 2013–14 winter at Expo – 1 presented the largest value of 145 cm for frost penetration. The warmer winter of 2015–16 at Expo sites indicated around 70 cm maximum frost penetration, which was a value within the literature reported range for the 2014–15 winter (DeGaetano et al. 2001).

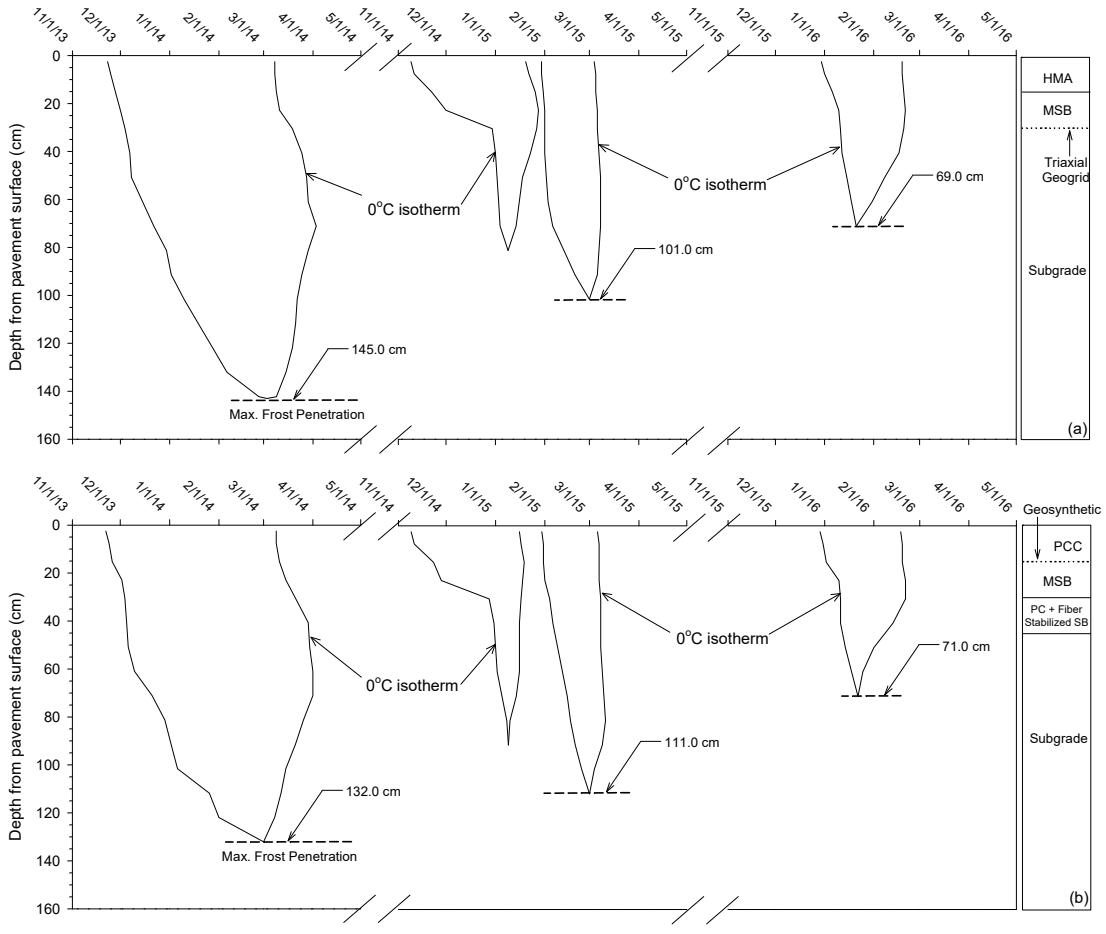

Figure 2.4. Frost zones from 2013 to 2016 at (a) Expo – 1 and (b) Expo – 2.

The maximum frost penetrations from 2011 to 2016 at the US 30 site were also determined based on the in situ measurements. Although the US 30 site was only about 11 km away from the Expo site, significant differences were noticed between the maximum frost penetrations for these locations in the same year (Table 2.3).

Table 2.3. Summary of maximum frost penetration depths at the US 30 and Expo sites.

	US 30 (cm)	Expo – 1 (cm)	Expo – 2 (cm)
2011–12	54	–	–
2012–13	72	–	–
2013–14	102	145	132
2014–15	73	101	111
2015–16	57	69	71

Note: – indicates that data not available.

2.5. Simplified Empirical Correlations

Numerous empirical models have been developed to predict frost penetration with only the freezing index. Most of these models average the soil thermal properties, which indicates that the ground was treated as bare soil with a single layer. Local weather station data provided the air temperature records (RWIS 2016). In this study, the models by Chisholm and Phang (1983) and Rajaei and Baladi (2015) were selected to evaluate the accuracy of applying these models to this project data. The Chisholm and Phang (1983) model (Equation 2.1 in metric units) is based on Ontario weather history, and the Rajaei and Baladi (2015) model (Equation 2.2 for clayey soils and Equation 2.3 for sandy soils) is based on Michigan weather history. Air FI is the only input for frost penetration prediction.

$$X = 4.31\sqrt{1.8FI + 32} - 32.79 \quad (2.1)$$

$$X = 4.0388 \times (1.8FI + 32)^{0.4896} \quad (2.2)$$

$$X = 3.3787 \times (1.8FI + 32)^{0.5423} \quad (2.3)$$

The Frost penetrations of the three locations in this study were estimated with Equations 2.1, 2.2, and 2.3 (Figure 2.5). In comparison with the 11 actual measurements, predicted results showed wide variations. In general, the Rajaei and Baladi (2015) model overestimated actual values, and the Chisholm and Phang (1983) model underestimated actual values. The differences between the penetration results from these two models were around 35 to 50 cm, and it was difficult to develop a particular relationship between FI and the actual frost penetrations. This finding indicated that estimating frost penetrations through these simplified models provided various results. As these models were developed empirically based on local data, many other factors such as soil type, thermal properties, climatic conditions, layer conditions may influence predictions.

Results from this study showed that the frost penetrations were different between two adjacent roads with different pavement surfaces and layer conditions. Also, significant differences were found between frost penetrations between sites with different water conditions. Therefore, it is recommended that improving the frost penetration prediction models still needs numerical analysis based on ground heat transfer. Even though at times the modified Berggren equation applied in PCASE showed estimations approximating the actual measurements, the model ignored the influence of water movement to heat transfer during freezing and thawing, which may essentially affect predicted penetrations (Jury and Horton 2004).

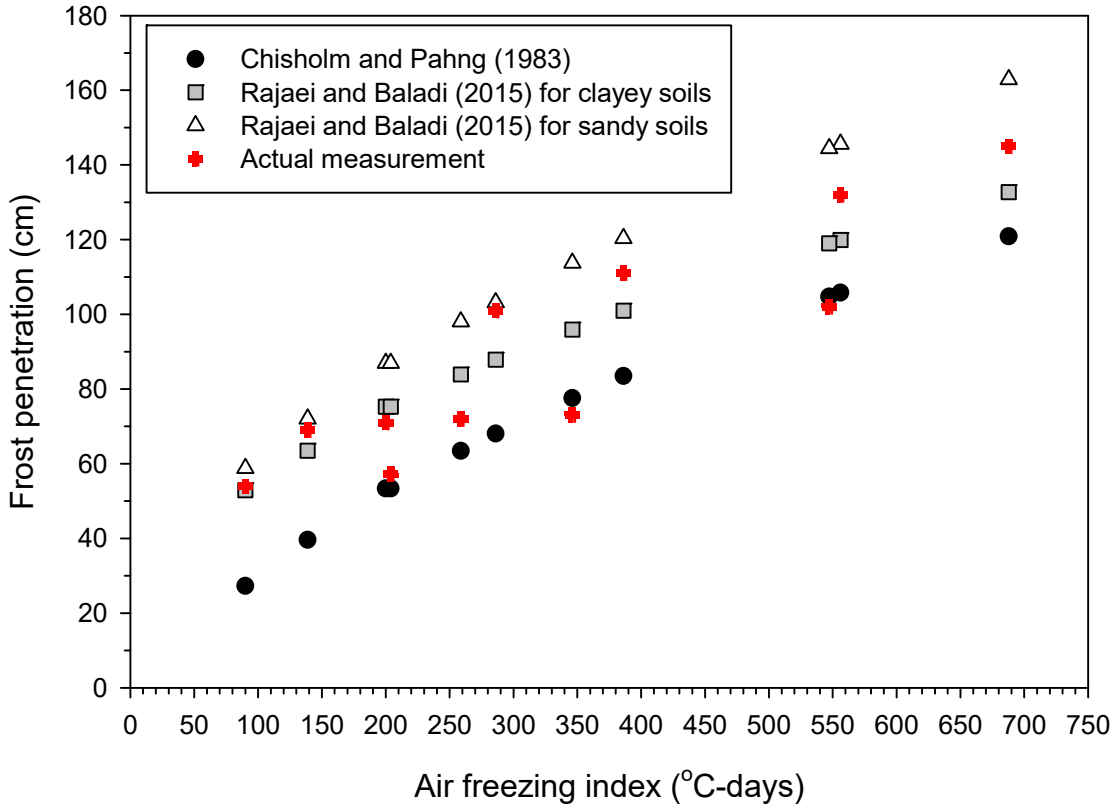

Figure 2.5. Comparisons between results correlated from empirical models and actual measurements.

2.6. Frost Penetration Estimations Using Modified Berggren Equation

A principal objective of this study is to estimate the maximum frost penetration using the modified Berggren model. PCASE is the computer program used to implement the modified Berggren model. Because the modified Berggren model is an energy balance based model, some parameters used in the model can be determined from in situ measurements, but some soil properties used to estimate soil thermal properties must be assumed. The following sections discuss the specific procedures for estimating the frost penetrations in terms of air temperature data and soil properties.

2.6.1. Determination of n-factor & freezing index

Annual air freezing index (FI) was calculated for each test location. At the Expo sites, annual surface FI was calculated from the first subsurface thermocouple data, which were assumed to represent the surface temperature condition. The n-factor is used to relate air FI to surface FI was determined from the measured results. The reason for determining the n-factor was to compare the actual field measurements to the default values that were used in the computer program. Results from the Expo sites showed that the n-factor had a range between 0.41 and 0.72 for the HMA surface, while the value was around 0.6 for the PCC surface (Table 2.4). Because the US 30 site did not have a shallow sensor, the average n value from the Expo PCC surface was used to relate the air FI to the surface FI at the US 30 site.

Table 2.4. Measured n-factor for HMA and PCC pavement surfaces.

	2013–14	2014–15	2015–16	Average
Expo – 1 (HMA)	0.72	0.49	0.41	0.54
Expo – 2 (PCC)	0.59	0.65	0.61	0.62

The air FI and surface FI are summarized in Table 2.5. During the same season, air FI at the different locations had slight differences, however differences between the surface FI values were relatively large. This indicated that the ground surface energy balance was influenced by multiple factors, such as the wind speed, snow cover, and radiation. It was difficult to determine a constant n-factor value for a particular ground surface type. However, as seen from the Stefan equation (see Equation 2.4 in metric units), the n-factor has a significant influence on the calculated results.

Table 2.5. Summary of air and surface freezing index.

Freezing Index	2011–12		2012–13		2013–14		2014–15		2015–16	
(°C-days)	Air	Surface	Air	Surface	Air	Surface	Air	Surface	Air	Surface
US 30	146	90	423	259	892	547	565	346	333	205
Expo – 1	–	–	–	–	948	688	589	286	339	139
Expo – 2	–	–	–	–	948	556	589	386	339	204

Note: – indicates data not available.

$$X = \sqrt{172800 \frac{knFI}{L}} \tag{2.4}$$

where, X is the frost penetration depth, k is soil thermal conductivity, FI is the annual air freezing index, and L is the latent heat.

2.6.2. Predicting multi-layer frost penetration in PCASE

The modified Berggren equation (Equation 2.5) added a factor, λ, into the Stefan equation to account for the volumetric heat. For manual calculations, the new factor λ can be estimated empirically from the thermal ratio (α) and the fusion parameter (μ). The α is a function of mean annual temperature (v_0) and average freezing temperature (v_s), and μ is a function of volumetric heat capacity (C), latent heat (L), and v_s.

$$X = \lambda\sqrt{172800 \frac{knFI}{L}} \tag{2.5}$$

However, for computer calculations such as in PCASE, another method to determine λ is used (Bianchini and Gonzalez, 2012). A transcendental equation in terms of exponential relationships between soil thermal properties (C, k, and L) was used to calculate a constant γ. This constant was originally used to describe the relationship between permafrost soil thawing depth and time (t) (Equation 2.6). As FI is also a time dependent factor (FI is equal to v_s times t), the modified Berggren equation can be converted to Equation 2.8 based on a mathematical relationship between λ and γ (Equation 2.7).

$$X = \gamma\sqrt{t} \tag{2.6}$$

$$\lambda = \gamma\sqrt{\frac{2L}{Cv_s}} \tag{2.7}$$

$$X = \gamma\sqrt{345600\frac{knFI}{Cv_s}} \tag{2.8}$$

After applying the modified factor λ, the modified Berggren equation is considered to overcome the weakness of neglecting sensible heat during ice formation. However, another need is to learn how to apply the modified Berggren equation to solve multi-layer soil conditions, such as the pavement structures in this study. Bianchini and Gonzalez (2012) reported a solution and stated that the fundamental mechanism of the solution was to "compute the required FI for the freezing front to penetrate each layer" in accordance with the work by Zarling et al. (1989). Bianchini and Gonzalez (2012) treated FI as heat energy and calculated the amount of energy (FI) needed to freeze a layer with particular thickness. When the sum of FI for all layers equals the surface FI, the total thickness of all accounted layers represents the freezing front depth, which is the frost penetration. Therefore, Bianchini and Gonzalez (2012) converted Equation 2.2 into a FI expression (Equation 2.9), and modified the equation based on the thermal physics (Equation 2.10).

$$FI = \frac{D^2L}{172800\lambda^2nk} \tag{2.9}$$

$$FI = \frac{DL}{172800\lambda^2n}\left(\sum_{N=1}^{i-1} R_N + \frac{R_i}{2}\right) \tag{2.10}$$

where, D is the layer thickness, L is the layer latent heat, k is thermal conductivity, n is the FI transfer factor, N is the number of layers, and R is the thermal resistance (equal to D divided by k).

In PCASE, the US continent is classified into four typical areas: moist-cold, moist-hot, dry-cold, and dry-moist (Bianchini and Gonzalez, 2012). The PCASE contains a database with air FI collected from weather stations all over the USA. A default value of n-factor for particular

ground surface type was set in the system (0.75 for PCC and 0.7 for ACC), and these values cannot be changed by users. Default and changeable dry unit weights and moisture contents for typical soils were also provided in PCASE for estimating soil thermal properties (Table 2.2). The pavement layer conditions of the Expo sites were input, and default soil properties were applied. Weather stations with similar air FI to locations in this study were selected to calculate the frost penetrations with the PCASE n-factor first. However, because the in situ measured n-factors differ from the default values, weather stations with similar surface FI were then selected for comparison as well. In other words, another approach to estimate the frost penetration based on surface FI in PCASE was performed by avoiding using the default n-factors. The calculated results of frost penetration are summarized in Table 2.6. Results indicated differences between air FI based and surface FI based frost penetration values, primarily due to the different n values. In general, the frost penetration depths based on surface FI were smaller than those based on air FI. The HMA pavement of 2014–15 showed the largest difference of about 23 cm between the two estimations. This finding indicates that the n-factor has significant influence on the modified Berggren equation estimated frost penetrations.

Table 2.6. Summary of PCASE frost penetration results at the Expo site.

Frost penetration based on air FI (cm)			
	2013–14	**2014–15**	**2015–16**
Expo – 1	106.7	85.1	53.3
Expo – 2	116.8	93.9	62.3
Frost penetration based on surface FI (cm)			
	2013–14	**2014–15**	**2015–16**
Expo – 1	109.2	62.2	38.1
Expo – 2	101.6	81.5	55.9

In order to evaluate the estimated frost penetrations from PCASE, a figure was drawn to compare estimates with the actual measurements from the Expo sites (Figure 2.6). Significant

underestimations occurred for PCASE results. For both HMA and PCC pavements, the PCASE results were about 20% lower than the actual measurements. A possible reason for these underestimations might be the foundation layer stabilizations and drainage used at these two pavement sites. For the modified Berggren equation, decreasing the water content results in deeper frost penetration estimates. Stabilizations and drainage systems tend to reduce moisture contents of foundation layers. However, the default soil properties used in PCASE did not change even though the actual stabilization and drainage information was input into the system, which probably resulted in an overestimation of model moisture contents and/or an underestimation of the unit weights.

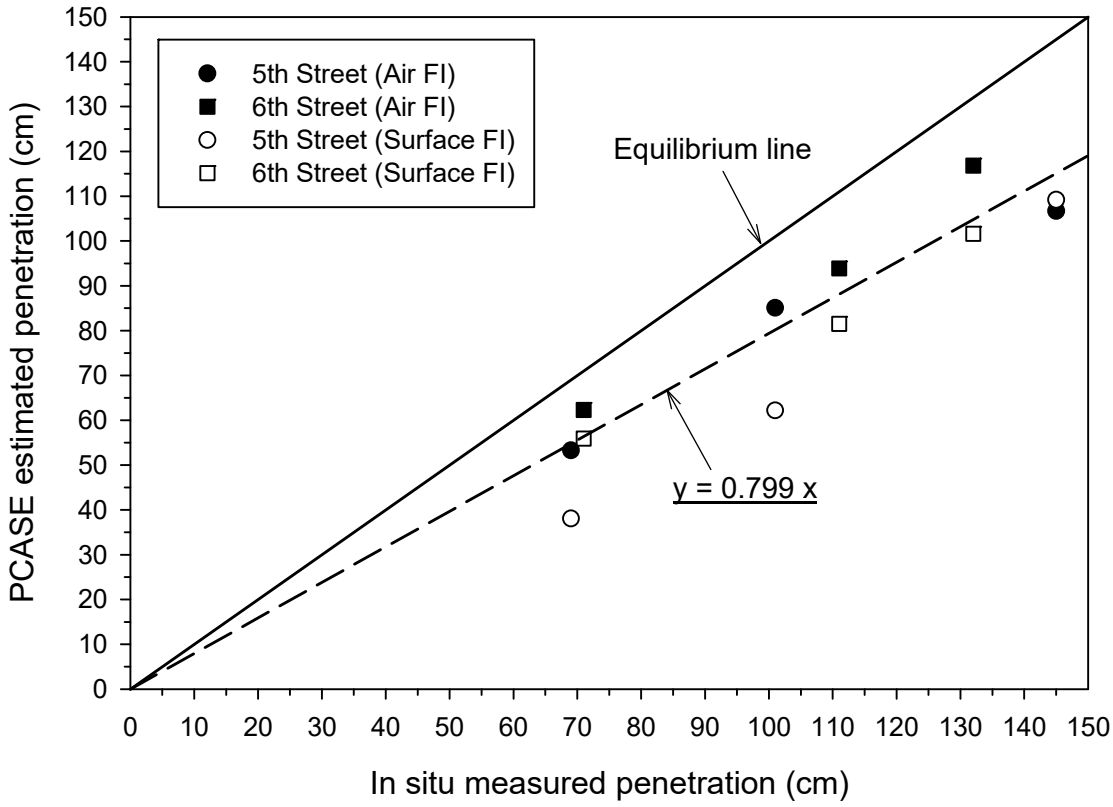

Figure 2.6. Comparison between estimated and measured frost penetrations at the Expo site.

At the US 30 site, no particular treatment or stabilization was applied on the JPCP. Default soil properties were used for this location. Due to the lack of sensor near the pavement surface to estimate surface FI, the average measured n-factor value for the PCC surface of Expo – 2 was used for this location. Differences of 5 to 23 cm are estimated for the air FI and surface FI based results (Table 2.7). However, the estimated frost penetrations were less than 5% different from the in situ measurements at this site (Figure 2.7). The frost penetration depths calculated based on surface FI were similar to actual frost penetration depths. This result indicates that estimations using the measured n-factor value results in higher accuracy than using default n-factor values in PCASE.

Table 2.7. Summary of PCASE frost penetration results at US 30 site.

	2011–12	**2012–13**	**2013–14**	**2014–15**	**2015–16**
Based on air FI (cm)	33.0	73.7	116.8	96.5	68.6
Based on surface FI (cm)	55.8	68.6	102.9	78.7	61.0

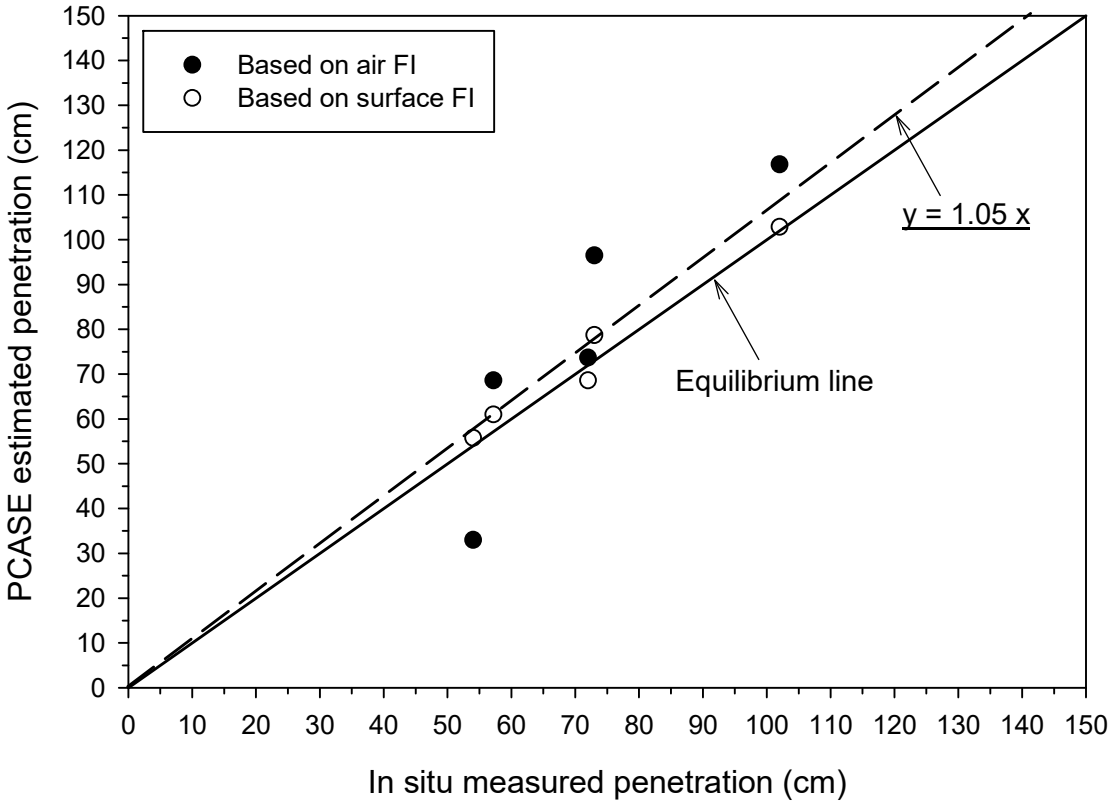

Figure 2.7. Comparison between estimated and measured frost penetrations at US 30 site.

In order to determine if modifications on soil properties can improve PCASE estimation accuracy, the moisture contents and dry unit weights of each soil layer were changed based on laboratory Proctor test results (optimum moisture content and maximum dry unit weight). Some adjusted values were larger and some were smaller than the default values in PCASE. PCASE estimates with adjusted values showed significant improvement on the differences between estimated and measured frost penetrations (Figure 2.8). For the US 30 site, changes in soil properties did not have much influence on the estimations. The estimated results of four of the five seasons maintained high accuracy. For the Expo sites, using either or both air FI and surface FI with modified soil properties provided frost penetration estimates similar to in situ measurements. Besides the n-factor and soil properties, several other factors may also influence the output, such as the unchangeable mean annual temperature and length of the frost season.

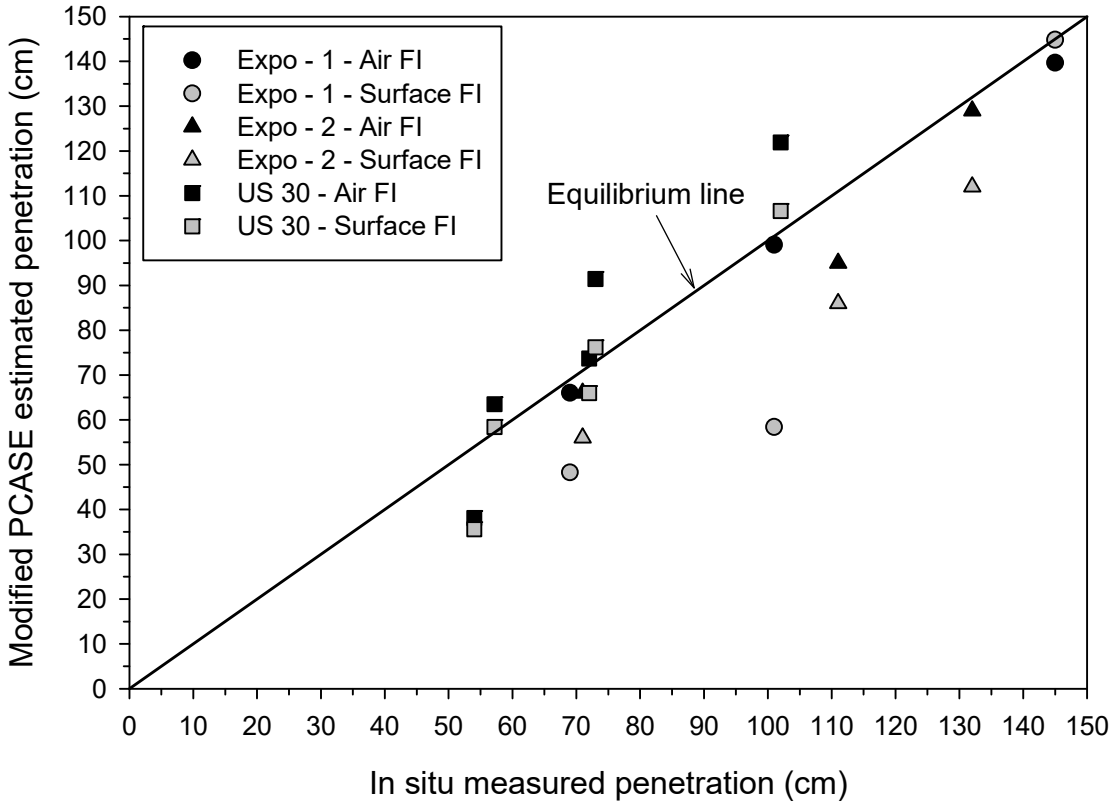

Figure 2.8. Comparison between estimated and measured frost penetrations after modifying soil properties.

2.7.Summary and Conclusions

In this study, pavement and foundation temperatures were recorded at three locations in central Iowa. Air and surface temperatures were used to estimate the seasonal frost penetrations in accordance with three simplified empirical models and the modified Berggren equations applied in PCASE. The estimated results were compared to in situ measurements to evaluate the accuracy of these models. Based on the study findings, the following conclusions have been drawn:

- From field measurements, the maximum frost penetration at central Iowa reached 145 cm. However, during the same winter, locations showed differences between maximum

frost penetrations despite the close distance between tested sites. Different pavement types and foundation conditions influenced the measured frost penetration depths;

- Frost penetration depth estimates with the three simplified empirical equations did not match well the measured frost penetration depths;
- The modified Berggren equation used in PCASE was able to predict frost penetration in multi-layer pavements based on freezing index and soil properties. Using default values for soil properties in PCASE resulted in about 20% underestimation of the frost penetration depths;
- When using tested values for moisture contents and dry unit weights, calculations with the modified Berggren equation in PCASE provided more accurate results of predicted frost penetrations than using default soil properties values. However, the n-factor was found to have a significant influence on the accuracy of estimations, although it is difficult to determine the precise value of n at every specific location. Empirical values of n-factor may not be broadly applicable to each particular site;
- Stabilization and drainage systems utilized in foundation layers may have affected the frost penetration estimations. The possible causes may be that stabilization and drainages lead to changes in soil densities, pore conditions, and water contents;

2.8. Acknowledgments

Research funding was provided from the FHWA DTFH 61-06-H-00011: WO18Pooled Fund Study TPF-5(183) and the Iowa Highway Research Board (TR-677). The support of these agencies is greatly appreciated.

CHAPTER 3. SEASONAL VARIATIONS AND IN SITU ASSESSMENT OF CONCRETE PAVEMENT FOUNDATION MECHANISTIC PROPERTIES

A paper accepted by *International Journal of Pavement Research and Technology*

Yang Zhang, Pavana K.R. Vennapusa, David J. White, and Alex E. Johnson

3.1. Abstract

In cold climates, pavement surface and foundation layers are subjected to seasonal temperature variation and freeze-thaw cycles. The number and duration of freeze-thaw cycles in the foundation layers can significantly influence the pavement performance. Seasonal variation in foundation layers is accounted for in pavement design by empirically adjusting the foundation layer moduli values. This paper presents results from in situ falling weight deflectometer (FWD) and dynamic cone penetrometer (DCP) tests conducted over a two-year period at five sites in Iowa; at one of these sites, temperatures of the foundation layers were continuously monitored during the testing period. FWD testing was conducted to determine the modulus of subgrade reaction (k) values. DCP testing was conducted to estimate California bearing ratio (CBR) values of the subbase and subgrade. Temperature data were analyzed to determine freezing and thawing periods and frost penetrations. Seasonal variations observed in the foundation mechanistic properties were compared with the assumed design values. Empirical relationships between the different mechanistic properties are explored.

3.2. Introduction

Pavements in northern hemisphere are subjected to seasonal temperature variations with freeze-thaw cycles that affect both pavement surfaces and foundation layers. Potential damages from freeze-thaw cycles include frost induced vertical heave, surface cracks, pumping of fines under traffic loading, and loss of support that reduces ride quality. Pavement foundation

mechanistic characteristics such as stiffness and strength are significantly influenced by seasonal temperature variations and therefore have to be properly characterized as it has implications to design, construction, maintenance, and serviceability (Brandl, 2008; Solanki et al., 2013; White et al., 2013).

Various thickness design procedures have been developed since the 1970s for concrete pavement design. PCA (1984) and AASHTO (1993) design procedures are currently the most popularly used methods by the highway agencies in the U.S., while there is increasing interest in implementing the newly developed mechanistic-empirical design guide by AASHTO (2008). While the AASHTO (2008) procedure is a significant advancement over the PCA (1984) and AASHTO (1993) procedures in terms of analyzing the pavement responses, the key design parameter used to characterize foundation layer support is still the modulus of subgrade reaction (*k*) value. Resilient modulus (M_r) value is one of design parameters in AASHTO (1993) and AASHTO (2008), but the M_r value is converted to *k* value using empirical relationships in the design process. AASHTO (1993) provides suggested values for use in design as target M_r values for subgrade in frozen, thawed, and summer conditions. AASHTO (2008) deals with seasonal variations in a much more sophisticated manner based on local climatic modeling data and laboratory test measurements to adjust modulus values for seasonal variations.

The *k* value is determined using a static plate load test, which can be time consuming and expensive to setup. Therefore, various alternative testing methods have been in use by state agencies to determine the *k* value. Deflection tests using falling weight deflectometer (FWD) is a popular choice for determining *k* value based on testing performed on pavement surface layers (Puppala, 2008; AASHTO, 1993; AASHTO, 2008). Dynamic cone penetrometer (DCP) test is another test device that has been recommended in the AASHTO (2008) design guide as a method

to determine California bearing ratio (CBR), which can be empirically correlated to *k* value. Most highway agencies assume *k* values during the design phase either based on experience and historically available data or limited field testing. For rehabilitated pavement designs, agencies in the U.S. typically use FWD testing data on the existing pavements, while for new pavements, CBR or M_r testing is typically performed on samples obtained from the field.

In this study, detailed field testing was conducted with the objective of measuring the seasonal variations in the field *k* values and compare them with what was assumed in the design. This field testing was conducted by using a Kuab FWD and DCP testing on five different pavement test sections in the State of Iowa eight times over a two-year period (July 2010 to July 2012). The pavement test sections varied in age from 6 to 56 years and showed varying level of distresses and ride quality (poor to good) at the time of testing.

Testing was conducted when the foundation layers were in frozen condition (winter), thawed condition, and in equilibrium condition (summer). DCP testing was conducted by drilling a hole in the pavement, and directly testing the foundation layer down to about 2 m below the surface. Both FWD and DCP test results were analyzed to estimate the *k* values and assess the differences in the estimated values. At one of the test sites, temperatures of the foundation layers were continuously monitored during the testing period. FWD testing was conducted to determine the modulus of subgrade reaction (*k*) values. DCP testing was conducted to estimate California bearing ratio (CBR) values of the foundation layers. Temperature data was analyzed to determine freezing and thawing periods and frost penetrations in the foundation layers. Seasonal variations observed in the foundation mechanistic properties were compared with the assumed design values. The findings in this paper will benefit engineers and agencies that design and construct pavements.

3.3. Background

3.3.1. Seasonal freeze-thaw cycles in pavements

Freeze-thaw cycles are common in cold regions and sometimes lead to freezing and thawing related pavement problems. Frost-stiffening and thaw-weakening primarily result from ice forming and melting within the soil. The stiffness and strength of the roadbed material decrease as the phase of the moisture changes from solid to liquid (Janoo and Berg, 1996; Johnson, 2012; Zhang, 2013). Three elements, the freezing front, thawing front, and moisture contents of the pavement layers, primarily influence the mechanistic properties of pavement foundations (Konrad and Roy, 2000). The significant influence of cyclic freezing and thawing on pavement performance means that it is important to investigate freeze-thaw conditions in pavements, such as frost penetration depths, numbers of freeze-thaw cycles, and the duration of freezing and thawing periods.

Hoover et al. (1962) investigated the pavement freeze-thaw conditions over three winters (1957 through 1960) on US Highway 117 in Jasper County, Iowa. Hoover et al. observed seven thawing periods during 1957–1958 winter and nine during 1959–1960 winter. During the 1958–1959 winter, a large continuous frozen zone and several smaller, thawed zones were observed at shallow depths for short time within the frozen zone. Hoover et al. (1962) also estimated the numbers of freeze-thaw cycles based on air temperature data that revealed 11 freeze-thaw cycles. Within the upper 0.4 m of the pavement, annual freeze-thaw cycles decreased from ten to one. The maximum frost penetrations reached around 1.05 m during the three winters.

Andersland and Ladanyi (2004) reported that determining the 0°C isotherm is an approach to analyze temperature variations in pavement focusing on freezing and thawing periods in pavement layers. Frozen and thawed zones versus time can be estimated from isothermal depth.

Determination of this isotherm presents the maximum frost penetrations and the periods that pavements are susceptible to break-up. This period is defined as the time when the upper pavement layers are thawed while the lower layers are still frozen. Thawed water from upper layers cannot drain into lower frozen layers due to the low permeability. In these conditions, the bearing capacity of foundations may significantly decrease, and the upper pavements become more fragile under traffic loads. Andersland and Ladanyi (2004) reported fragile conditions are a problem that pavement engineers need to identify, which is the primary reason why spring load restriction needs to be implemented in seasonal frost regions (Ovik et al., 2000; NDDOT, 2015).

Johnson (2012) estimated the frost penetrations of three locations in Iowa for four winters (2008 through 2012). The first three winters presented 1.1 to 1.4 m maximum frost penetrations, and the 2011–2012 winter presented a lower depth of 0.6 m frost penetrations in average. Johnson (2012) also reported the numbers of freeze–thaw cycles at different depth during the 2010–2011 winter at one of the sites in this study (see Figure 3.1). The upper 0.3 m of the pavement foundation was subjected to approximate 10 to 46 freeze-thaw cycles annually. The number of freeze-thaw cycles decreased to less than three at depths > 0.3 m.

3.3.2. Pavement foundation mechanistic properties

In situ testing to determine foundation layer mechanistic properties is critical for thickness design. The mechanistic properties of pavement foundations, such as the strength and M_r or k of foundation layers, change seasonally due to climatic conditions (Lary et al., 1984; Konrad and Roy, 2000). Pavement design guides take this into consideration (AASHTO, 1993; AASHTO, 2008). For example, AASHTO (1993) suggests adjusting the design M_r of roadbed soil based on the freezing, thawing, and summer durations. AASHTO (1993) provides suggested values for use in design when subgrade is in frozen, thawed, and summer conditions. AASHTO (2008)

deals with seasonal variations in a much more sophisticated manner based on local climatic modeling data and laboratory test measurements to adjust modulus values for seasonal variations.

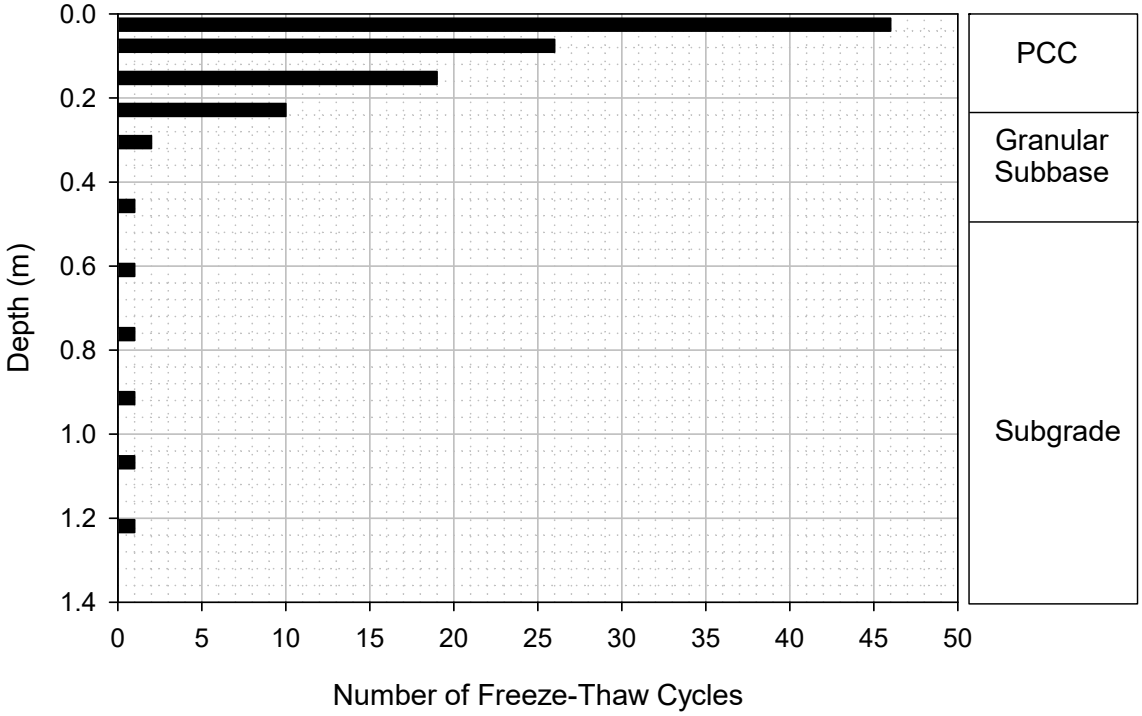

Figure 3.1. Number of freeze-thaw cycles versus depth during winter 2010–2011 at US Highway 218 near Plainfield, Iowa (reproduced from Johnson, 2012).

Janoo and Berg (1998) investigated subsurface properties of PCC pavements at two airfields in Wisconsin, US, during thawing periods by conducting FWD tests to determine the mechanistic properties of the foundation layers. Pavement temperature data indicated that the maximum frost penetrations at the two sites were 2 m and 1.3 m. The basin area (A_T), defined as the area of the basin composed of the deflections and the distances from the sensors to the plate center, was calculated during thawing period to characterize the changes in bearing capacity. During thawing periods, results from three test locations presented that changes in A_T were related to temperature changes as A_T increased with temperature increases. At the end of

thawing, A_T remained constant. Janoo and Berg (1998) reported that the A_T results indicate the recovered foundation bearing capacity decreased by 30–40% at the three sites. The subgrade layer modulus was back calculated using two different methods based on the FWD deflection data. From the beginning to the end of thawing, subgrade modulus determined through both methods decreased by 50–75% at the site with 1.3 m frost penetration and 85% at the site with 2 m frost penetration.

Baladi et al. (2009) reported seasonal changes in pavement subgrade M_r values in the state of Michigan. More than 500 groups of FWD test results, including those conducted in that study and those collected within the previous 20 years, were used to determine layer moduli. The backcalculated *k* values from FWD deflections per empirical AREA method were converted to M_r based on AASHTO (1993). The converted M_r values were also correlated with previous data to consider limitations in applying the AASHTO (1993) conversion process to determine effects on subbase and base layers. Two PCC and one ACC pavement test sections were tested during fall and spring. The results indicated that during thawing, the subgrade M_r under the PCC pavements were 30–50% less than in the fall, but subgrade M_r under the ACC pavement exhibited similar values in both seasons.

Becker et al. (2014) investigated the freeze-thaw performance of stabilized pavement foundations in Iowa from October 2012 to April 2013 by comparing the CBR and elastic modulus in the fall and after the spring thaw. Although several stabilization methods had been used, in comparison with the fall CBR values, the spring CBR of both granular subbase (CBR_{SB}) and subgrade (CBR_{SG}) decreased. Becker et al. reported that the thawed CBR_{SG} was as low as 10% of the values measured during summer/fall. Results of elastic modulus testing indicated the

thawed stiffness of the composite foundation layers decreased by 20–90% compared to values observed in summer/fall.

3.4. Experimental Test Sections and Methods

3.4.1. Test sections

Field tests were conducted at various times during a two-year period (07/2010 to 07/2012) at five test sections in the State of Iowa. Information about the test sites and the pavement condition index (PCI) values reported by Iowa DOT (2014) during the time of testing are summarized in Falling weight deflectometer testing FWD tests were conducted near mid-panel in accordance with ASTM D4694 (2009) using a segmented 300 mm diameter loading plate by applying one seating drop and four loading drops (Figure 3.2a). The applied loads varied from 22 to 75 kN. The peak deflection values measured directly beneath the testing plate (D0) and at several locations away from the testing plate up to about 1.52 m away from the plate, were normalized to 40 kN (9000 lbs.). The FWD deflection basin data was analyzed to determine k values using the AREA4 method described in AASHTO (1993). Table 3.1.

The project sites varied in pavement age from 6 years to 56 years at the time of testing, and the ride quality varied between very poor to good conditions. Four out of the five sections consisted of jointed full depth portland cement concrete (PCC) pavement, while one section consisted of an asphalt overlay over jointed PCC. All sections were underlain by a nominal 254 mm thick granular subbase. Based on the information provided on Iowa DOT (2014), the granular subbase consisted of crushed limestone at four sites.

3.4.2. Falling weight deflectometer testing

FWD tests were conducted near mid-panel in accordance with ASTM D4694 (2009) using a segmented 300 mm diameter loading plate by applying one seating drop and four loading drops

(Figure 3.2a). The applied loads varied from 22 to 75 kN. The peak deflection values measured directly beneath the testing plate (D_0) and at several locations away from the testing plate up to about 1.52 m away from the plate, were normalized to 40 kN (9000 lbs.). The FWD deflection basin data was analyzed to determine *k* values using the $AREA_4$ method described in AASHTO (1993).

Table 3.1. Summary of the project sites.

Project site	Year pavement built	Pavement thickness	Subbase material and thickness	PCI
Fort Dodge	PCC 2005	254 mm	CLS, 254 mm	87 (Good)
Denison	ACC 1987 PCC 1971	114 mm 203 mm	CLS, 254 mm	55 (Fair)
Moville	PCC 1958	254 mm	Information on material type not available, 254 mm	18 (Very Poor to Serious)
Nevada	1992 (west) 1998 (east)	254 mm	CLS, 254 mm	82 (Satisfactory) 91 (Good)
Plainfield*	2002	241 mm	CLS, 254 mm	94 (Good)

Note: CLS indicates crushed limestone; * indicates the pavement temperature was monitored at the site.

The AREA method was first proposed by Hoffman and Thompson (1981) for flexible pavements and has since been applied extensively for concrete pavements (Darter et al. 1995). Since the *k* value determined from FWD test represents a dynamic value, it is referred to here as $k_{FWD\text{-}Dynamic}$. Deflections obtained from four sensors are used in the $AREA_4$ calculation. $AREA_4$ is calculated using Equation 3.1 and has dimensions of length (inches), as it is normalized with deflections under the center of the plate (D_0):

$$AREA_4 = 6 + 12 \times \left(\frac{D_2}{D_0}\right) + 12 \times \left(\frac{D_4}{D_0}\right) + 6 \times \left(\frac{D_5}{D_0}\right) \tag{3.1}$$

where D_0 = deflections measured directly under the plate (inches); D_2 = deflections measured at 305 mm (12 inches) away from the plate center (inches); D_4= deflections measured at 610 mm (24 inches) away from the plate center (inches); and D_5 = deflections measured at 914 mm (36 inches) away from the plate center (inches). AREA method can also be calculated using different sensor configurations and setups, i.e., using deflection data from 3, 5, or 7 sensors and those methods are described in detail in the literature (Stubstad et al. 2006, Smith et al. 2007).

In the early research conducted using the AREA method, the ILLI-SLAB finite element program was used to compute a matrix of maximum deflections at the plate center and the AREA values by varying the subgrade *k*, the modulus of the PCC layer, and the thickness of the slab (ERES Consultants, Inc. 1982). Measurements obtained from FWD tests were then compared with the ILLI-SLAB program results to determine the *k* values through back calculation. Later, in the 1990s to replace the back calculation procedure, Barenberg and Petros (1991) and Ioannides (1990) proposed a forward solution procedure based on Westergaard's solution for loading on an infinite plate. This forward solution presented a unique relationship between AREA value (for a given load and sensor arrangement) and the dense liquid radius of relative stiffness (L) in which subgrade is characterized by the *k* value. The radius of relative stiffness (L) is estimated using Equation 3.2:

$$L = \left[\frac{\ln\left(\frac{x_1 - AREA_4}{x_2}\right)}{x_3}\right]^{x_4} \tag{3.2}$$

where $x_1 = 36$; $x_2 = 1812.279$; $x_3 = -2.559$; $x_4 = 4.387$. It must be noted that the x1 to x4 values vary with the sensor arrangement and these values are only valid for the AREA4 sensor setup. Once the L value is known, the $k_{FWD\text{-}Dynamic}$ value can be estimated using Equation 3.3:

$$k_{FWD-Dynamic}(pci) = \frac{PD_0^*}{D_0 L^2} \tag{3.3}$$

where P = applied load (lb); D_0 = deflection measured at plate center (inches); and D_0* = non-dimensional deflection coefficient calculated using Equation 3.4:

$$D_0^* = a \cdot e^{-be^{-cL}} \tag{3.4}$$

where a = 0.12450; b = 0.14707; and c = 0.07565. It must be noted that these equations and coefficients are valid for an FWD setup with an 11.81 in. diameter plate.

The AREA method assumes the slab and the subgrade are horizontally infinite. This assumption leads to an underestimation of the *k* value. Crovetti (1993) developed the following slab size corrections for a square slab based on finite element analysis conducted using the ILLI-SLAB program, for use in the $k_{FWD\text{-}Dynamic}$:

$$Adjusted\ D_0 = D_0\left(1 - 1.15085e^{-0.71878\left(\frac{L'}{L}\right)^{0.80151}}\right) \tag{3.5}$$

$$Adjusted\ L = L\left(1 - 0.89434e^{-0.61662\left(\frac{L'}{L}\right)^{1.04831}}\right) \tag{3.6}$$

where L′ = slab size (smaller dimension of a rectangular slab, length or width). This procedure also has limitations: (1) it considers only a single slab with no load transfer to adjacent slabs, and (2) it assumes a square slab. The square lab assumption is considered to produce sufficiently accurate results when the smaller dimension of a rectangular slab is assumed as L′ (Darter et al. 1995). There are no established procedures reported to date on correcting for load transfer to adjacent slabs, which remains as a limitation of this method. In this project, $k_{FWD\text{-}Dynamic}$ values corrected for slab size are reported as $k_{FWD\text{-}Dynamic\text{-}Corr}$.

AASHTO (1993) suggests dividing the $k_{FWD\text{-}Dynamic}$ value by a factor of 2 to determine the equivalent $k_{FWD\text{-}Static}$ value. For the analysis conducted in this research project, the $k_{FWD\text{-}Dynamic\text{-}Corr}$ values were divided by 2 and are reported as $k_{FWD\text{-}Static\text{-}Corr}$ values.

3.4.3. Dynamic cone penetrometer testing

DCP tests were performed in accordance with ASTM D6951 (2003) to determine dynamic penetration index (DPI) in units of mm/blow and calculate California bearing ratio (CBR) using Equation 3.7.

$$\text{CBR} = \frac{292}{\text{DPI}^{1.12}} \tag{3.7}$$

Tests were conducted down to a depth of about 2m below pavement surface, by drilling a 20 mm hole in the pavement down to the top of the underlying base layer. The DCP test results are presented as CBR with depth profiles and as point values of CBR_{SB} representative of the subbase layer and CBR_{SG} representative of the top 305 mm of the subgrade. The top 305 mm of the subgrade was selected as the subgrade layer as it is typically the thickness used to scarify and recompact the material during construction. The point data values represent the weighted average CBR within each layer.

All DCP-CBR profiles were also reviewed to determine "weak" layers within the subgrade down to the bottom of the profile. An average CBR of a minimum of 75.6 mm (3 in.) thick layer within the top 1.5 m of subgrade (represented as $CBR_{SG\text{-}Weak}$) was also calculated. The $CBR_{SG\text{-}Weak}$ was determined to assess if weak layer would have influence on the *k* values determined using the FWD test.

The CBR_{SG} and $CBR_{SG\text{-}Weak}$ values were converted to $M_{r\text{-}SG}$ and $M_{r\text{-}SG\text{-}Weak}$ of subgrade, using nomographs provided in AASHTO (1993). AASHTO (1993) uses the following empirical relationship to convert M_r to *k* value, where *k* is in units of kPa/mm and M_r is in units of MPa:

$$k = 2.03\mathrm{M_r} \quad (3.8)$$

Figure 3.2. In situ testing procedures: (a) Kuab FWD setup with 300 mm diameter loading plate and (b) DCP with 2m extension rods.

3.5. Results and Discussions

3.5.1. Seasonal variations in mechanistic properties

Pavement temperature data was continuously (every hour) monitored at the Plainfield test site from surface to about 1.2 m below surface. Using the temperature data, 0° frost isotherms, which form the boundaries of zones of frozen layers were estimated for two winters as shown in Figure 3.3a. Results indicate that the freezing period in 2010-11 lasted for about 3.5 months and in 2011-12 lasted for about 2.5 months. Thawing periods for the two seasons lasted for about 0.3-0.5 months. The maximum frost penetrations based on isotherms were around 1.2 and 0.6 m for 2010-11 and 2011-12 seasons, respectively.

FWD test results obtained from the Plainfield site are shown in Figure 3.3b and Figure 3.3c. The D_0 and $k_{\text{FWD-Static-Corr}}$ varied with variations in ground temperatures, as expected. During frozen conditions, D_0 values were about 45% lower than values before freezing. During the

thawing period, the D_0 values were about the same as the values before freezing. After the thawing period, the D_0 values recovered to levels that were similar to before freezing levels and remained relatively constant in the summer.

During frozen conditions, the $k_{FWD\text{-}Static\text{-}Corr}$ values were nearly twice as higher than the values before freezing (Figure 3.3c). During the thawing period, the $k_{FWD\text{-}Static\text{-}Corr}$ values dropped to the same level as before freezing and remained relatively constant during summer. Under thawing and summer conditions, the measured $k_{FWD\text{-}Static\text{-}Corr}$ values were slightly lower than the Iowa DOT design k value (41 kPa/mm).

The $k_{FWD\text{-}Static\text{-}Corr}$ values from all sites are presented in Figure 3.4, in comparison with the CBR values in the subbase (CBR_{SB}) and subgrade layers (CBR_{SG} and $CBR_{SG\text{-}Weak}$). The full-depth DCP-CBR profiles from the five test sites from three selected testing times are shown in Figure 3.5: February 2011 (frozen state), March 2011 (thawed state), and August 2011 (summer). Average $k_{FWD\text{-}Static\text{-}Corr}$ values from each test site (based on 7 to 10 tests) and CBR_{SB}, CBR_{SG}, and $CBR_{SG\text{-}Weak}$ values are presented as bar charts for measurements obtained in each season (frozen, thawed, and summer) in Figure 3.6, for comparison between test sites and seasons. The Fort Dodge, Denison, Moville, and Nevada test sites are within 200 miles of the Plainfield site and are in the same climatic zone. Due to lack of temperature data from each site, the time of thawing and freezing is assumed to be the same at all sites for analysis in this paper, although some variations are expected between the test sites.

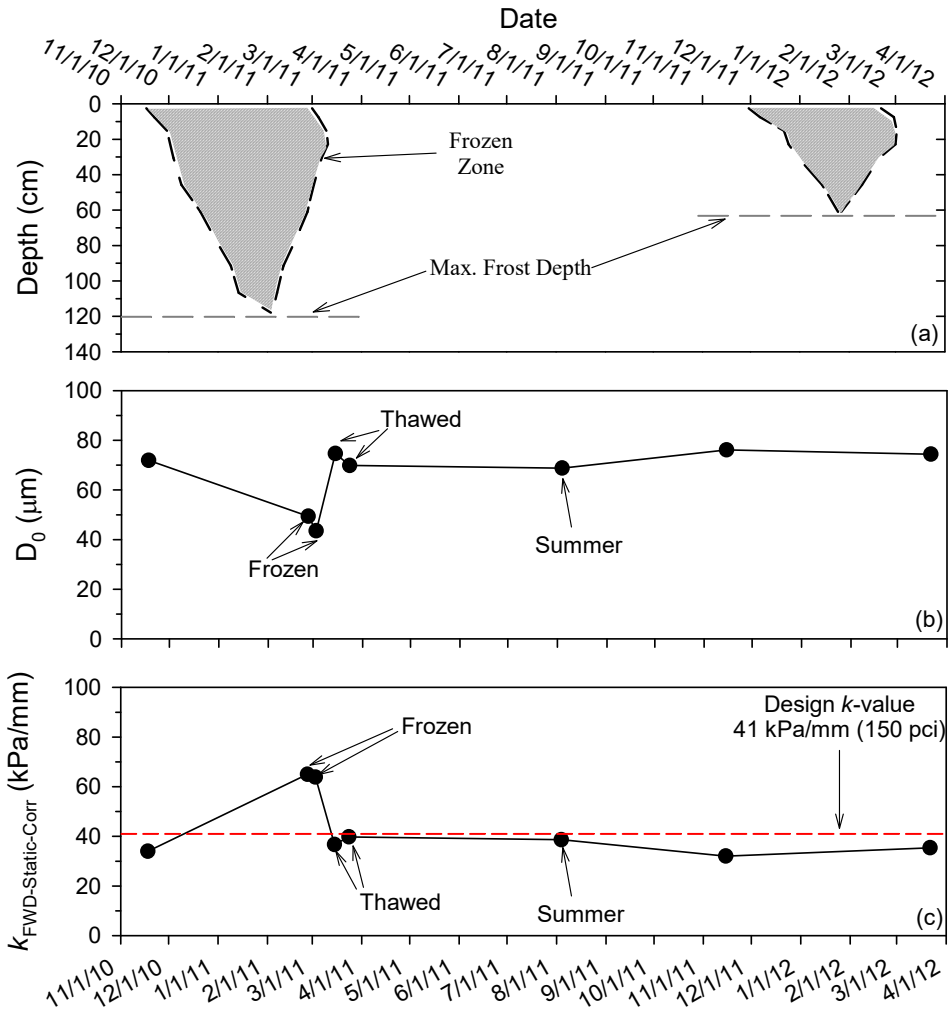

Figure 3.3. (a) 0° isotherm with time, (b) seasonal variations of D_0, and (c) seasonal variations of $k_{FWD\text{-}Static\text{-}Corr}$ at the Plainfield test site.

On average, there was no significant difference in $k_{FWD\text{-}Static\text{-}Corr}$ values obtained in thawed condition and summer at any of the sites. The CBR values also did not show significant differences between thawed condition and summer at most of the sites, except at the Plainfield site where $CBR_{SG\text{-}Weak}$ increased from about 10 in thawed state to about 40 in summer. The $k_{FWD\text{-}Static\text{-}Corr}$ values in frozen condition was about 10% to 56% higher than in summer at four of the five sites. At the Nevada test site, the values were about the same at all testing times. At two of the five sites, the $k_{FWD\text{-}Static\text{-}Corr}$ values were about 1.5 to 2 times lower than the design assumed k value (41 kPa/mm) in thawed condition and in summer.

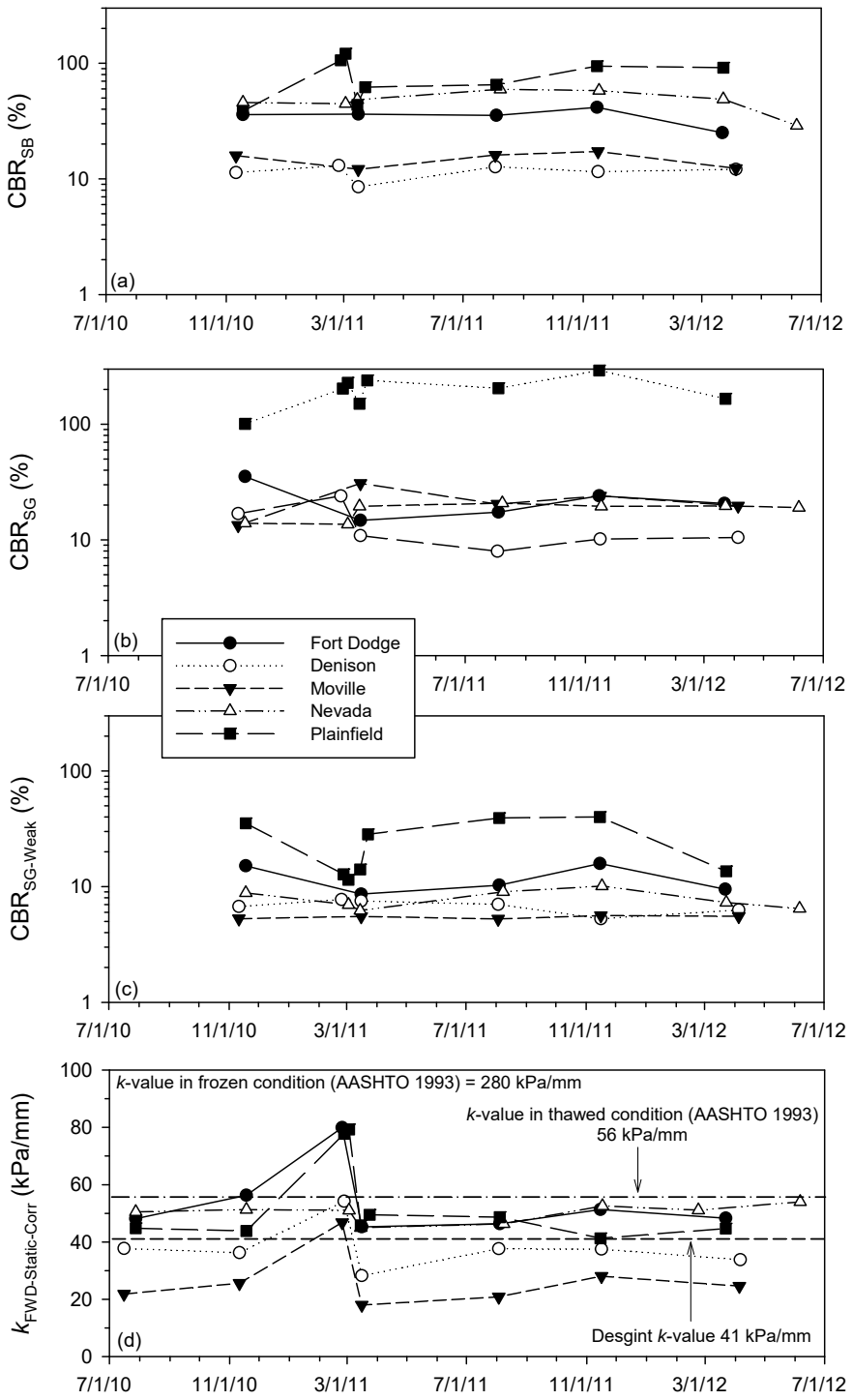

Figure 3.4. Seasonal variations in mechanistic properties at the five test sites: (a) CBR_{SB}, (b) CBR_{SG}, (c) $CBR_{SG\text{-}Weak}$, and (d) $k_{FWD\text{-}Static\text{-}Corr}$.

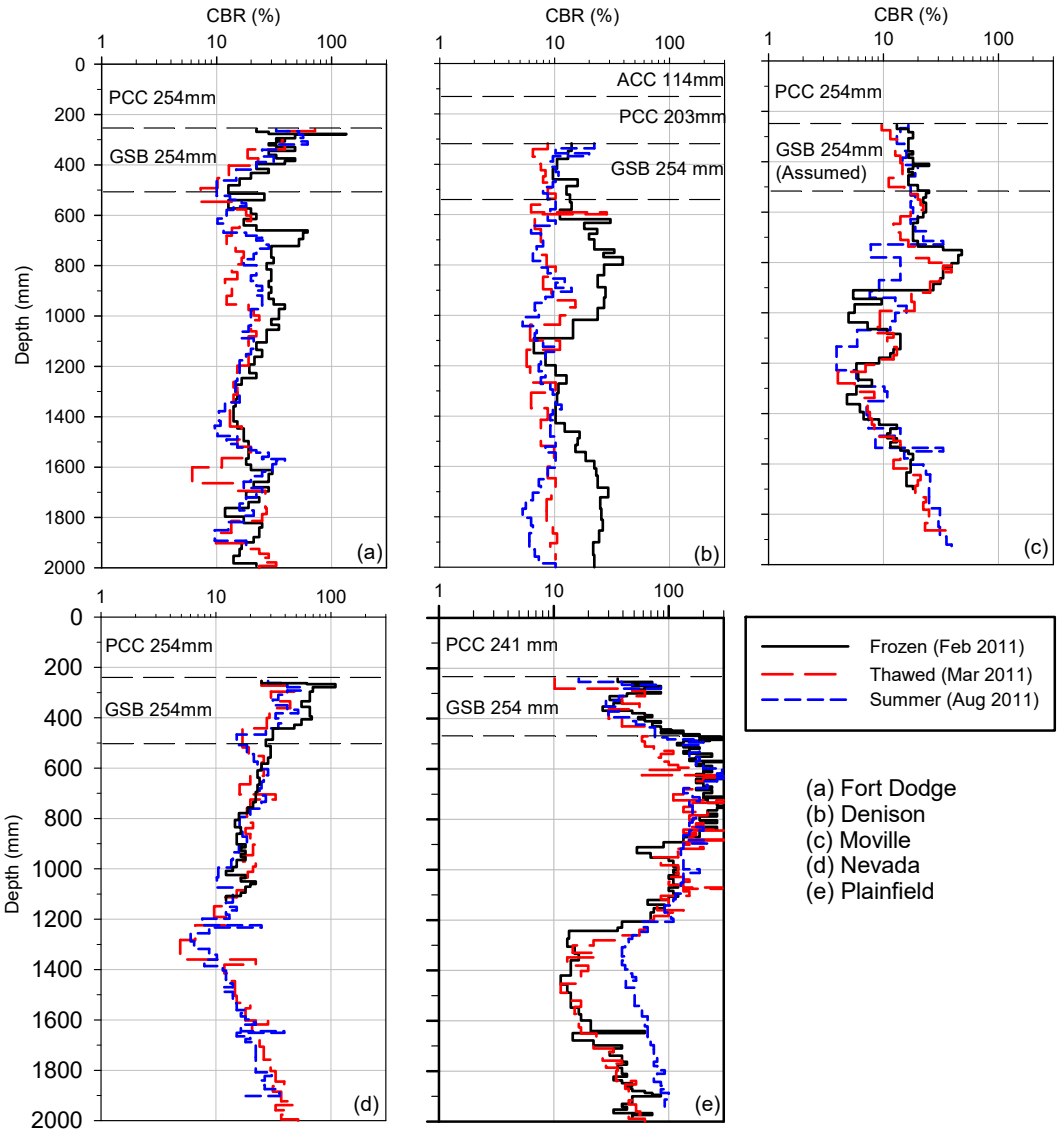

Figure 3.5. DCP-CBR profiles at the five test sites in February (frozen state), March (thawed state), and August (summer).

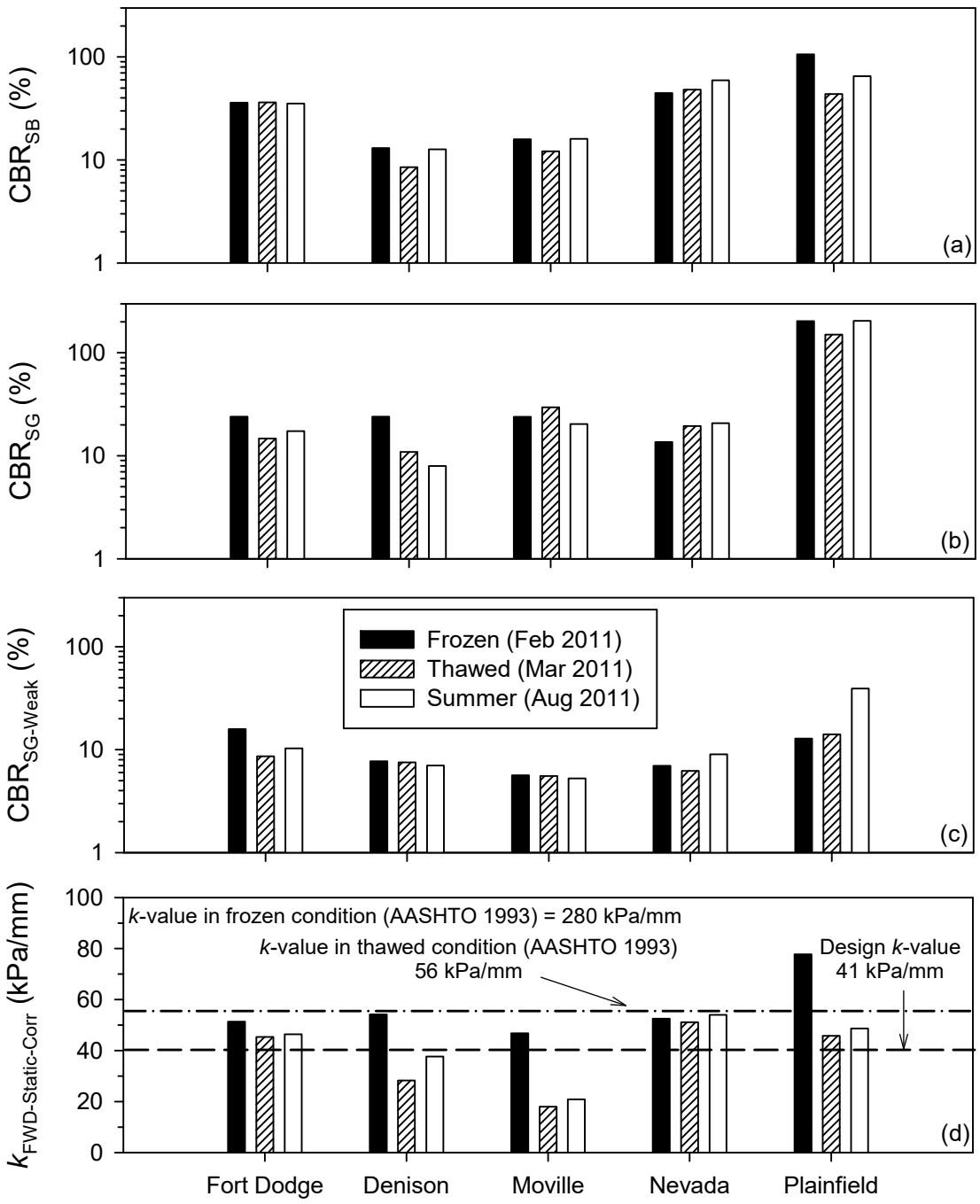

Figure 3.6. Summary of seasonal changes in (a) CBR_{SB}, (b) CBR_{SG}, (c) $CBR_{SG\text{-}Weak}$, and (d) $k_{FWD\text{-}Static\text{-}Corr}$ of each site.

3.5.2. Empirical relationships between *k* and M_r values

CBR data obtained from this study was converted to M_r values based on empirical relationships provided in AASHTO (1993). AASHTO (1993) uses a simple empirical model to convert M_r to *k* for use in design as shown earlier in Equation 8. The *k* values obtained from FWD testing are compared in Figure 3.7 with the M_r values, in reference to the AASHTO empirical model. Both $M_{r\text{-}SG}$ and $M_{r\text{-}SG\text{-}Weak}$ are presented in Figure 3.7.

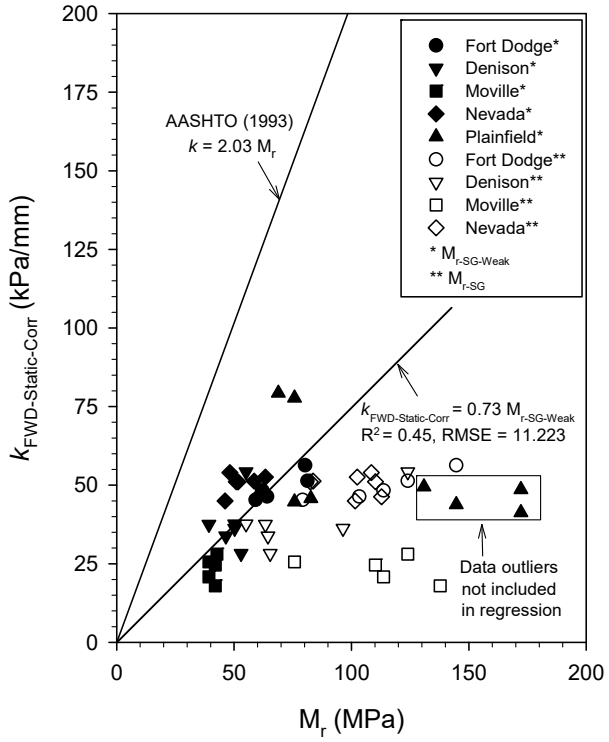

Figure 3.7. Relationship between M_r values determined from CBR and $k_{FWD\text{-}Static\text{-}Corr}$ in comparison with the relationship proposed in AASHTO (1993).

Results indicated that the $M_{r\text{-}SG}$ values were unrealistically high. $M_{r\text{-}SG\text{-}Weak}$ were much lower than the $M_{r\text{-}SG}$ values. A simple linear regression fit was applied to $M_{r\text{-}SG\text{-}Weak}$ versus $k_{FWD\text{-}Static\text{-}Corr}$ results, which yielded a coefficient of determination (R^2) of 0.45 with root mean square error (RMSE) of 11.2 kPa/mm for *k* values. Compared to the linear regression fit in the data, use of the AASHTO model significantly over estimates the *k* values.

It is important for designers and practitioners to recognize these uncertainties in the estimate values when using empirical relationships, and also the differences that exist between the values calculated from the different test methods. Also, it must be noted that k and M_r are stress-dependent parameters and most of the empirical relationships between CBR vs. M_r and M_r vs. k do not properly address this issue.

3.5.3. Mechanistic properties versus pavement performance

The pavement ride quality data available from each test section (PCI) is compared in relationship with pavement age, and in situ test measurements $k_{FWD\text{-}Static\text{-}Corr}$ and $CBR_{SG\text{-}Weak}$ in Figure 3.8 and Figure 3.9, respectively. Relationship between pavement age and PCI showed a strong linear trend with $R^2 > 0.93$. Similar linear regression relationship was documented by White and Vennapusa (2014) based on testing on low volume jointed PCC pavement test sites.

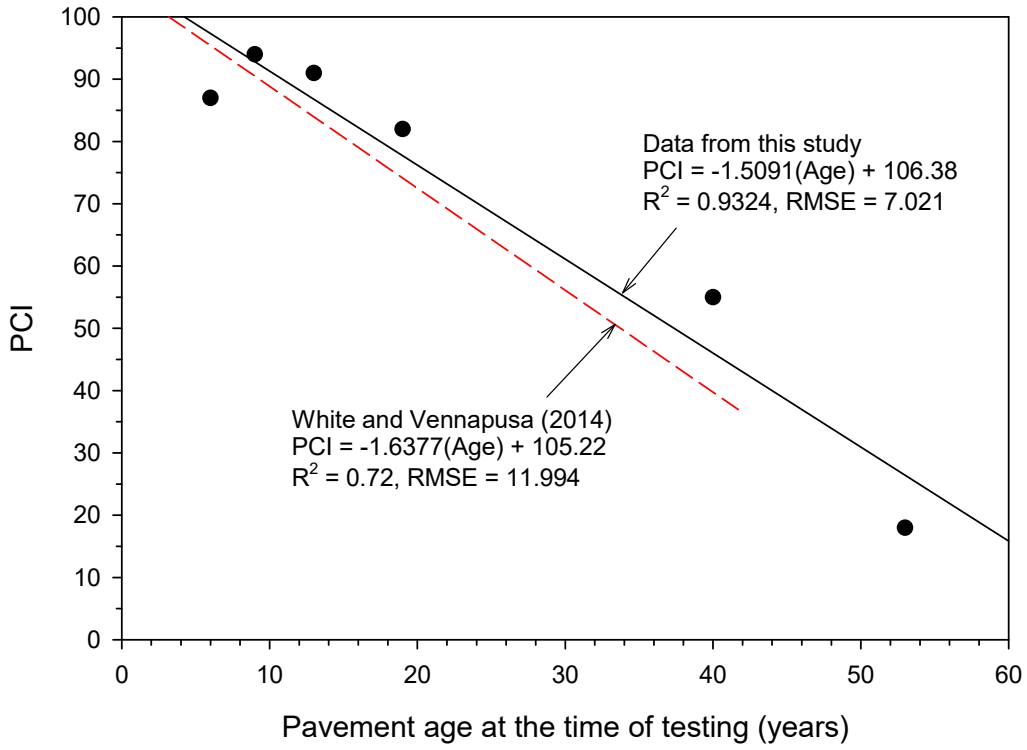

Figure 3.8. PCI versus pavement age.

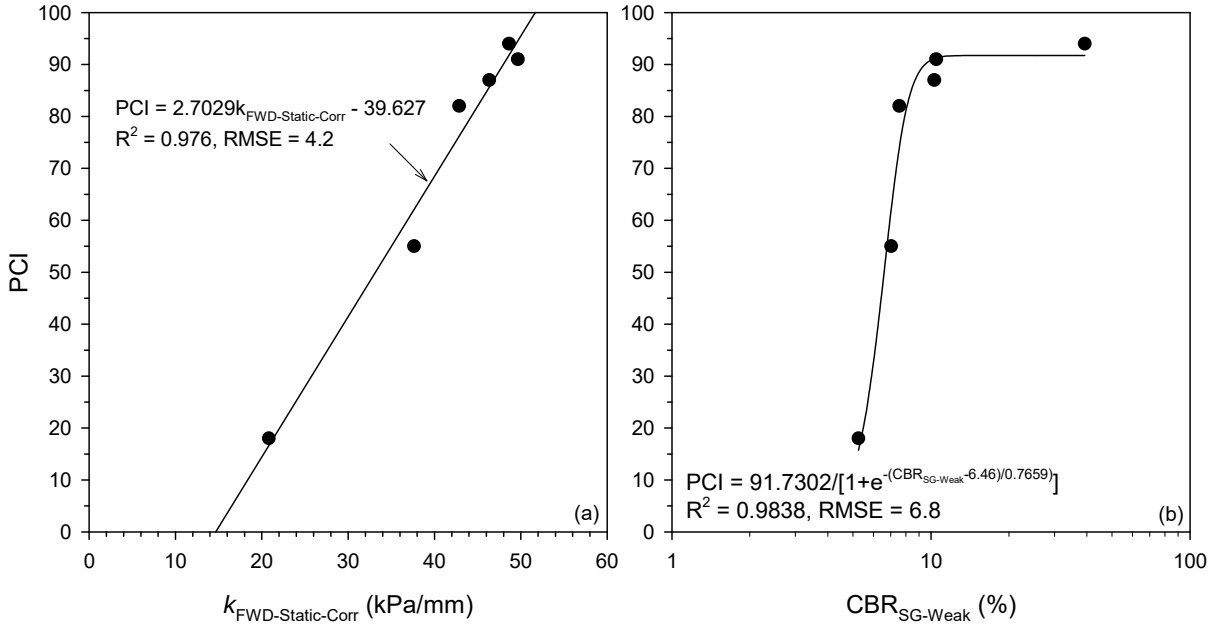

Figure 3.9. PCI versus (a) $k_{FWD-Static-Corr}$ and (b) $CBR_{SG-Weak}$.

The relationship between $k_{FWD-Static-Corr}$ and PCI also yielded a strong linear regression relationship with $R^2 > 0.95$, while the relationship between $CBR_{SG-Weak}$ and PCI yielded a strong non-linear exponential trend with PCI with $R^2 > 0.95$. These trends suggest that higher foundation layer stiffness or strength, provides a better ride quality and that ride quality is also influenced by the pavement age. Additional testing is warranted to further explore these relationships so that designers can have an empirical model that can be used to control the ride quality for a target design age, by controlling the foundation layer stiffness.

3.6.Summary of Key Findings

Following are some key findings from this study:

- On average, there was no significant difference in $k_{FWD-Static-Corr}$ values obtained in thawed condition and summer at any of the sites. The CBR values also did not show significant differences between thawed condition and summer at most of the sites, except at the Plainfield site where $CBR_{SG-Weak}$ increased from about 10 in thawed state to about 40 in

summer. The $k_{FWD\text{-}Static\text{-}Corr}$ values in frozen condition was about 10% to 56% higher than in summer at four of the five sites. At one test site, the values were about the same at all testing times.

- At two of the five sites, the $k_{FWD\text{-}Static\text{-}Corr}$ values were about 1.5 to 2 times lower than the design assumed k value (41 kPa/mm) in thawed condition and in summer.
- Results indicated that the $M_{r\text{-}SG}$ values were unrealistically high when compared with the $k_{FWD\text{-}Static\text{-}Corr}$. $M_{r\text{-}SG\text{-}Weak}$ were much lower than the $M_{r\text{-}SG}$ values. A simple linear regression fit was applied to $M_{r\text{-}SG\text{-}Weak}$ versus $k_{FWD\text{-}Static\text{-}Corr}$ results, which yielded a R^2 of 0.45 with RMSE of 11.2 kPa/mm for k values. Compared to the linear regression fit in the data, use of the AASHTO model significantly over estimates the k values.
- It is important for designers and practitioners to recognize this uncertainty in the estimated values when using empirical relationships, and also the differences that exist between the values calculated from the different test methods. Also, it must be noted that k and M_r are stress-dependent parameters and most of the empirical relationships between CBR vs. M_r and M_r vs. k do not properly address this issue.
- Relationship between pavement age and PCI showed a strong linear trend with $R^2 > 0.93$. Similar linear regression relationship was documented by White and Vennapusa (2014) based on testing on low volume jointed PCC pavement test sites.
- The relationship between $k_{FWD\text{-}Static\text{-}Corr}$ and PCI also yielded a strong linear regression relationship with $R^2 > 0.95$, while the relationship between $CBR_{SG\text{-}Weak}$ and PCI yielded a strong non-linear exponential trend with PCI with $R^2 > 0.95$. These trends suggest that higher foundation layer stiffness or strength, provides a better ride quality and that ride quality is also influenced by the pavement age. Additional testing is warranted to further

explore these relationships so that designers can have an empirical model that can be used to control the ride quality for a target design age, by controlling the foundation layer stiffness.

3.7. Acknowledgments

Research funding was provided from the FHWA DTFH 61-06-H-00011: WO18Pooled Fund Study TPF-5(183) and the Iowa Highway Research Board (TR-677). The support of these agencies is greatly appreciated.

CHAPTER 4. A CASE STUDY OF ASSESSING FROST HEAVE DETERIORATION AT CONCRETE PAVEMENT JOINTS

A paper to be submitted to *Cold Regions Science and Technology*

Yang Zhang, David J. White, Pavana K.R. Vennapusa, Alex E. Johnson, Maxim Prokudin, and Heath H. Gieselman

4.1. Abstract

Frost heave of foundation materials can cause severe joint deterioration in concrete pavements. Sufficient freezing depth, continuous water supply, and frost susceptible geomaterials are the three factors required leading to pavement frost heave. The primary objective of this study is to investigate frost actions at selected deteriorated joints. The longitudinal pavement profiles were estimated by measuring vertical heaves at these transverse joints. Specimens were cored to determine the moisture condition at different layers. The secondary objective of this paper is to evaluate the effect of local climate on pavement structures. Temperature sensors were installed during reconstruction at foundation layers to estimate the frost penetrations, length of freezing and thawing periods, and number of freeze-thaw cycles at depth. The last objective is to evaluate the frost-heave and thaw-weakening susceptibility of the reconstructed foundation materials in laboratory. Results indicate that all three geomaterials were medium frost-heave susceptible, and the soft subgrade showed high thaw-weakening susceptibility.

4.2. Introduction

Pavement deterioration, a universal problem, is primarily related to traffic loading or the environment (Huang, 2004; Simonsen and Isacsson, 1999). In recent decades, research topics in terms of loading-related pavement deterioration have been addressed (Khazanovich and Gotlif,

2003; Owusu-Antwi et al., 1990; Roesler et al., 2015). However, various pavement types, especially roads in cold regions, still exhibit specific deterioration features, such as joint deterioration of jointed plain concrete pavements (JPCP). At this time, climate-related joint deterioration including vertical heaving, spalling, and blow-ups are the main problems to transportation agencies for pavement design, construction, and maintenance (Caltrans, 2015; Hansen and Kang, 2010; Jones et al., 2013).

Most JPCP joint deterioration are typical freeze-thaw related pavement damage (Huang, 2004; Taylor, 2011). Research has shown that concrete freeze-thaw durability is one of the key factors resulting in several types of joint deterioration (Li et al., 2012; Yun and Wu, 2011). However, concrete pavement joint problems still persist (Cho et al., 1998; Gietz, 1979), especially like frost heave at joints during winter. Geomaterial frost heave was noticed as a common problem in civil engineering (Casagrande et al., 1931; Lai et al., 2005; Rui et al., 2016), therefore influences from foundations on pavement performance were then raised and emphasized to address some deterioration problems (Chen et al., 1988; Penner and Eldred, 1985).

Multiple reasons may result in frost heave joint deterioration, which include joint conditions, subsurface permeability, trapped water, geomaterial volume change, and freeze-thaw cycles (Andersland and Ladanyi, 2004; Brandl, 2008; Farnam et al., 2014; Johnson, 2012; Muge et al., 2016; Yang et al., 2006). It was also reported that if subsurface problems are the critical causes for freeze-thaw related deterioration, three factors are necessary: frost penetrations, frost susceptible materials, and water supply (Brandl, 2008; Cassagrande et al., 1931; Chamberlain, 1987; Lai et al., 2012). However, research is limited in exploring the frost actions of deteriorated and newly constructed pavement foundations.

Numerous studies have been conducted to investigate the methods of road maintenance, rehabilitation, or reconstruction due to this type of deterioration. A common approach in Iowa is to resurface the pavement with asphalt cement concrete (ACC) or portland cement concrete (PCC), or reconstruct new roads (Dai et al., 2008; Harrington and Fick, 2014; Marks and Anderson, 1993). In this project, the deteriorated pavements were removed and a new JPCP was reconstructed at the same location. Visual inspections and field testing were conducted in order to evaluating the frost actions near four deteriorated joints on U.S. highway 30 near Ames, IA. Pavement profiles and core specimens of the old pavement were obtained to measure the vertical heave at the joints and moisture contents at different layers. Four-year layer temperature of the new pavement was monitored and assessed to determine the frost penetration and freeze-thaw cycles. In addition, the foundation layer materials of the reconstructed pavements were tested to evaluate the frost-heave and thaw-weakening susceptibility.

4.2.1. Project overview

This project is located on US 30 in Boone County in Iowa (Figure 4.1a), which showed severe pavement distresses between mileposts 139.0 and 147.27 (Figure 4.1b). The existing road consisted of a nominal portland cement concrete layer with asphalt treated base (ATB), which was constructed in 1973, and was resurfaced in 1992 with an ACC overlay. At the four tested joint locations, the thickness of each layer was ACC overlay 76 mm (3 in.), PCC layer 229 mm (9 in.), and ATB 102 mm (4 in.). The existing pavement showed severe surface distresses with reflective cracking and vertical upheave near joints, especially during winter (Figure 4.1c). Initial field investigations by the Iowa Department of Transportation (DOT) reported some related damage to vehicle tires and problems with snowplow blade contact, and the ride quality of the

pavement section was rated as “poor” based on pavement condition index (PCI) ranging between 54 and 56 on a 0-100 scale (IADOT, 2014).

Figure 4.1. Field pictures showing (a) the EB on US 30, (b) joint deterioration with spalling, and (c) vertical heave at joint location.

As part of the reconstruction work that began in summer of 2011, the existing pavement and the asphalt treated base layers were removed and the subgrade was undercut during the reconstruction process to place a nominal 410 mm (16 in.) thick modified subbase over the natural existing subgrade. The modified subbase layer consisted of 150 mm (6 in.) thick RPCC material at the surface underlain by 254 mm (10 in.) thick mixture of RPCC-RAP material. A nominal 254 mm (10 in.) thick jointed plain concrete pavement (JPCP) was placed on the newly constructed foundation layer. Thickness design of the new pavement was conducted by the Iowa DOT according to the PCA (1984) method, by assuming a modulus of subgrade reaction (k) value of 41 kPa/mm (150 pci) for the foundation layer. Iowa DOT rated the ride quality of the new pavement section as “good” based on PCI ranging between 95 and 100 after construction (Iowa DOT, 2014).

4.3. Background

4.3.1. Joint deterioration and subsurface permeability

Studies have shown evidences that the initial step of any frost heave related joint deterioration is concrete material and joint structure distresses, which provides supply and path of water to foundation layers (Dai et al., 2008; Hansen and Kang, 2010). Taylor (2011) investigated concrete pavement joint deterioration, two causes were reported: freezing-related deterioration due to concrete saturation and calcium oxychloride formation. Poor maintenance of sawing equipment or inappropriate sawing practice may result in microcracking that will grow under environmental loading (Taylor, 2011). The onset of most joint deterioration is related to microcracking near the joints that consequently contributes to trapping water. After a period of freeze-thaw cycles, these joint may start to lose material. Freezing-related deterioration is dependent on sufficient moisture trapped in open spaces. In Taylor et al. (2012), two factors were reported that lead to trapped water. One is that joints are not sealed properly, which provides spaces at joints to retain water. Another factor is that the permeability of pavement sub layers is insufficient for water to drain away. Deicing salts and brine may also contribute to pavement deterioration because some salts attract water that keeps the pavement wet. (Jones et al., 2013; Taylor et al., 2012).

Drainage is an essential part of recent pavement design guides (AASHTO, 1993; AASHTO, 2008), because of significant influences on pavement long-term performance. Water retained within pavement structures leads to various kinds of damage (Huang, 2004; Rodden, 2010). Drainable bases have been applied in practice, and the effect of permeability of these constructed drainable layers were investigated (Vennapusa et al., 2006; White et al., 2007).

Zhang et al. (2015) conducted a case study to evaluate the joint performance related to subsurface permeability in a cold region. A borehole permeameter developed by Iowa State University was used to measure the permeability at two locations, one sealed and one unsealed sound joint locations in Iowa. The permeability from these two locations was lower in winter. The results indicated that deteriorated joints can be associated with impermeable base layers, which contribute to the water being trapped in joints. Data showed that freezing resulted in a significant decrease in subsurface permeability. The gradation analysis of the base materials under joints showed that there were more fines materials than at other locations, possibly from dust transported through the joints.

Zhang et al. (2015) collected the base materials from these joints. Laboratory falling head permeability tests were conducted on the materials in frozen and unfrozen conditions. Results showed that the unfrozen permeability (k) decreased from 5 and 15 μm/s to 2 and 6 μm/s when frozen, as the moisture content increased from 0.1% to 9.1%.

4.3.2. Geomaterial frost heave

Frost heave and changes in the stiffness of geomaterials are the most immediate problems caused by freeze-thaw cycles. Frost-heave results from ice lenses formed within the soil during freezing that expand the volume of voids. The overlying pavement surface or upper layer reflects this action as cracks or bulges (Cassagrande et al., 1931; Chamberlain, 1986). Uniform frost heave causes little damage to pavement structures, but differential frost heave weakens pavement foundation layers and increases stress concentrations in the pavement layer.

There are three important factors influencing geomaterial frost heaving, the size and percentage of voids in soil, the size of soil particles, and the water content of soil (Taber 1929). The size and percentage of voids in soil determines the height to which water may be lifted

above the water table by capillary action. The size distributions of soil particles controls the water movement during freezing. The U.S. Army Cold Regions Research Engineering Laboratory (CRREL) and the U.S. Army Corps of Engineers (USACE) proposed a frost susceptibility classification system based on the grain size criteria (US Army, 1965). Previously, the grain size criteria method is a commonly used to determine the frost susceptibility until a five-day laboratory frost-heave and thaw-weakening test was developed with two freeze-thaw cycles by Chamberlain (1987).

Janoo et al. (1997) studied a well-graded sandy material which was used as a pavement subbase layer. The laboratory frost heave tests presented low to medium frost susceptibility for unsaturated condition and high frost susceptibility for the saturated condition. Four computer simulations were also developed. For both simulations with unsaturated conditions, the frost penetration depth reached about halfway into the simulated layer, and the average frost heave value was only around 10 to 15% of the values at the saturated condition (Janoo et al. 1997). Zhang et al. (2016) conducted laboratory freeze-thaw tests on stabilized pavement foundation materials and evaluated the frost susceptibility in accordance with the ASTM D5918(2013) classification system. The test results indicated that the ASTM D5918 (2013) did not specify the frost susceptibility with CBR over 20. A new frost susceptibility rating system was proposed in terms of the negligible thaw-weakening susceptibility with CBR over 100.

4.4. Methods

In the study reported herein, field investigations were conducted though drilling cores from the deteriorated pavement and measuring the vertical heave values near transverse joint locations Testing was conducted on two frost days, February 26, 2010 and March 4, 2010. Core specimens were extracted using diamond rotary bits of 254 mm and 102 mm diameters Figure 4.2a). Air

was used as a drilling medium where needed instead of water lubrication during coring for the purpose of preserving in situ moisture content of the cored specimens. Collected ACC, PCC, and ATB core materials were oven dried to determine their moisture contents (Figure 4.2b, c, and d).Results from core extraction, inspection, and laboratory testing, and vertical heave measurements at transverse joints are presented separately in the following section.

Table 4.1. Selected joint locations, PCI, and test conditions.

No.	Direction	Milepost	PCI	Test date	Air Temp. (oC)
Joint 1	Westbound	143.53	54	2/26/2010	-12
Joint 2	Westbound	143.61	54	2/26/2010	-12
Joint 3	Eastbound	140.79	56	3/4/2010	-4
Joint 4	Eastbound	140.89	56	3/4/2010	-4

Figure 4.2. Core extraction and inspection: (a) drilling core from pavement surface, (b) subsurface concrete specimen, (c) holes with trapped water, (d) broken asphalt concrete specimen, and (e) presented ice lenses.

The vertical heave profiles were measured at locations along the joints (Figure 4.3). Locations were marked 305 mm (12 in.) apart starting at painted edge line and extending 2.4 m (96 in.) the direction towards the longitudinal joint. Once the locations on the selected joints were identified, a marked steel rod was mounted above the marked joint location of interest with ends of the rod extending away from the joint. The rod was mounted on wooden blocks located at each end of the rod to provide a support. The rod was used to establish a reference elevation for making vertical profile measurements between the rod and the pavement. The profile measurements were taken at 25 mm (1 in.) and 50 mm (2 in.) intervals. The measurements were taken using calipers where the distances from the rod down to the point of interest on the pavement were recorded. Collected measurements were normalized with a reference to the lowest measured point identified as a zero level elevation.

Figure 4.3. Measuring vertical heaves at transvers joint locations.

Thermocouple temperature sensors were installed at mile 143.68 on US30 EB lane. Type T thermocouple wires were used to make the sensors. Sensors were installed vertically from about 0.15 m to about 1.2 m below the top of the modified subbase layer. All vertical sensors were located at the center line. A pavement and foundation layer cross-section along with the temperature sensor locations is shown in Figure 4.4. The sensors were connected to a CR5000

Campbell Scientific data logger to record data every 10 minutes. The data logger was charged by a solar panel.

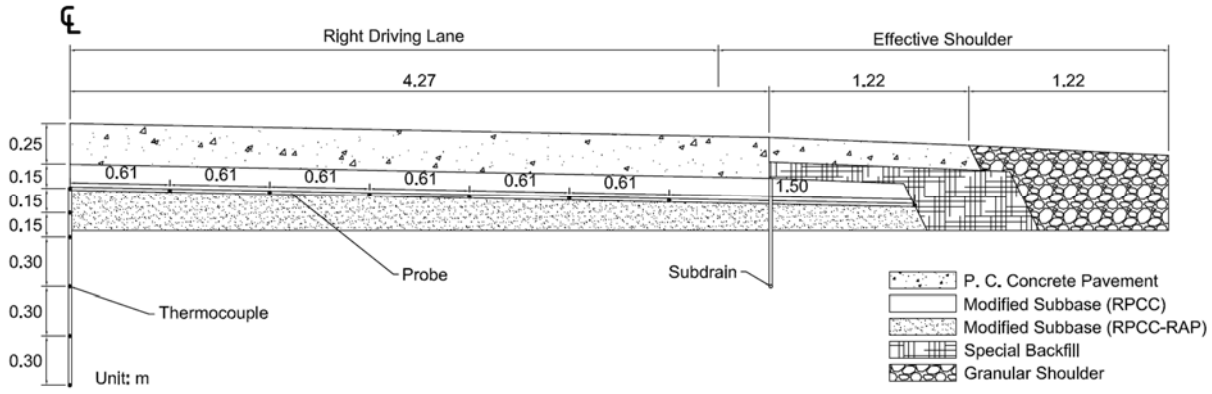

Figure 4.4. Profile of temperature sensor installation.

Laboratory freeze-thaw tests were conducted in accordance with ASTM D5918 (2013). Detailed description of the test equipment is presented in Johnson (2012) and Zhang (2015). A CBR test (ASTM, 2007) was conducted on the two specimens after two freeze-thaw cycles. During freeze-thaw testing, water was continuously supplied to simulate the highest heave potential. The heave rate and the post-test CBR tests were used as the basis for the frost-heave susceptibility classification per ASTM D5918 (2013).

4.5. Results and Discussions

4.5.1. Field investigations on existing pavements

A 102 mm diameter core was drilled at Joint 1. The top ACC overlay was first extracted and then the coring was extended into the underlying PCC layer. An intact PCC layer specimen was difficult to obtain due to weak and deteriorated structures of the concrete (Figure 4.2b). Standing water was observed in the cored 102 mm diameter hole, which might be trapped at the joints (Figure 4.2c). A 254 mm diameter core was drilled at Joint 2. The ACC layer was first extracted and then drilled into the PCC layer. An intact specimen of the ACC layer was also not obtained

due to the fragile structures (Figure 4.2d), but a few micro cracks were observed at the lower PCC pieces. Another 254 mm diameter core was drilled at the middle of the slab panel between miles 143.52 and 143.53. The extraction of the PCC core was unsuccessful, then a 102 mm diameter drill bit was used to extract a smaller diameter specimen in two pieces. The second piece showed the existence of ATB. The PCC core was extracted, and no evidence of free water was observed in the core. However, it was observed that the coring process did result in thawing of the ice lenses in the pavement layers due to heat created by friction. Ice lenses were observed at the ACC and PCC interfaces (Figure 4.2e).

Joint 3 and 4 located in the eastbound lane were cored on March 4, 2010. A 254 mm diameter core was drilled at Joint 3. Standing water was observed in the cored 254 mm diameter hole. A reinforcing dowel was observed in the cavity and was removed. It was observed that the structural integrity of the dowel was intact although surface corrosion existed. A 102 mm diameter core was obtained on the PCC pavement and ATB interface. Standing water was also observed within the ATB layer. The PCC layer specimens obtained from these two joints showed very little structural integrity.

These cored specimens were then sealed and taken back to the laboratory. Averaged oven-dried gravimetric moisture contents of the specimens along with depth are provided in Figure 4.5. The upper part of the ACC overlay showed moisture content less than 3%, while the value of the lower part increased up to 10%. The PCC specimens presented moisture contents between 12.5% and 20.4%, and the moisture content increased with depth. This observation indicated that a large amount of water was trapped at the PCC joint spaces. When deicing salts or brine was sprayed during winter, part of the thawed water from the surface likely infiltrated through the ACC overlay. Ice lenses within the ATB layer indicated that there might be a small amount of

infiltration occurring from the PCC joints to the ATB layer. The micro cracks may contribute to the path of infiltration for the water. That contributed to frost heaving of these geomaterials.

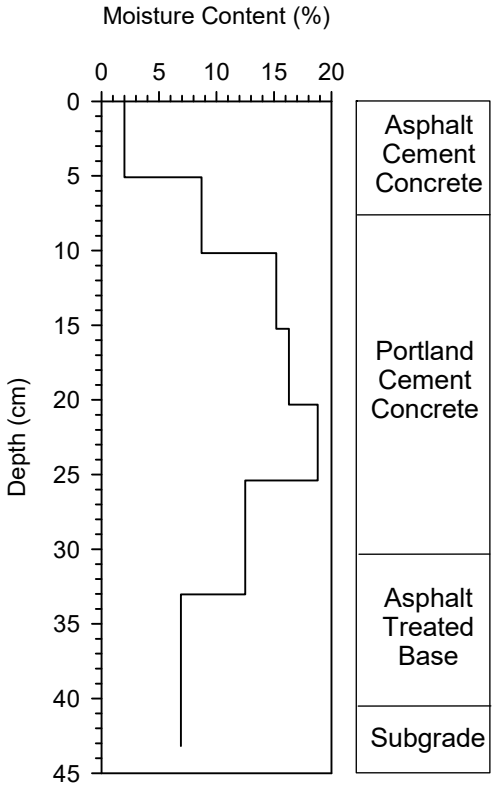

Figure 4.5. Average moisture contents of core specimens at depth.

Vertical heaves at the four transverse joint locations were determined longitudinally. Spatial contour maps of vertical heave measurements are presented in Figure 4.6. At Joint 1 and 3, vertical heaves ranged from 18 mm to 25 mm and from 13 mm to 23. Joint 2 presented significant non-uniform heaves, as the left half lane heaved up to 30 mm while the right part heaved to around 15 mm. At Joint 4 vertical heaves ranging between 25 mm and 38 mm were measured. In comparison, more uniform heaves at Joint 4 also presented relatively greater longitudinal bulge width of 500 mm. The longitudinal width of heaved bulge at the edge (boundary to right shoulder) of Joint 1 was around 760 mm.

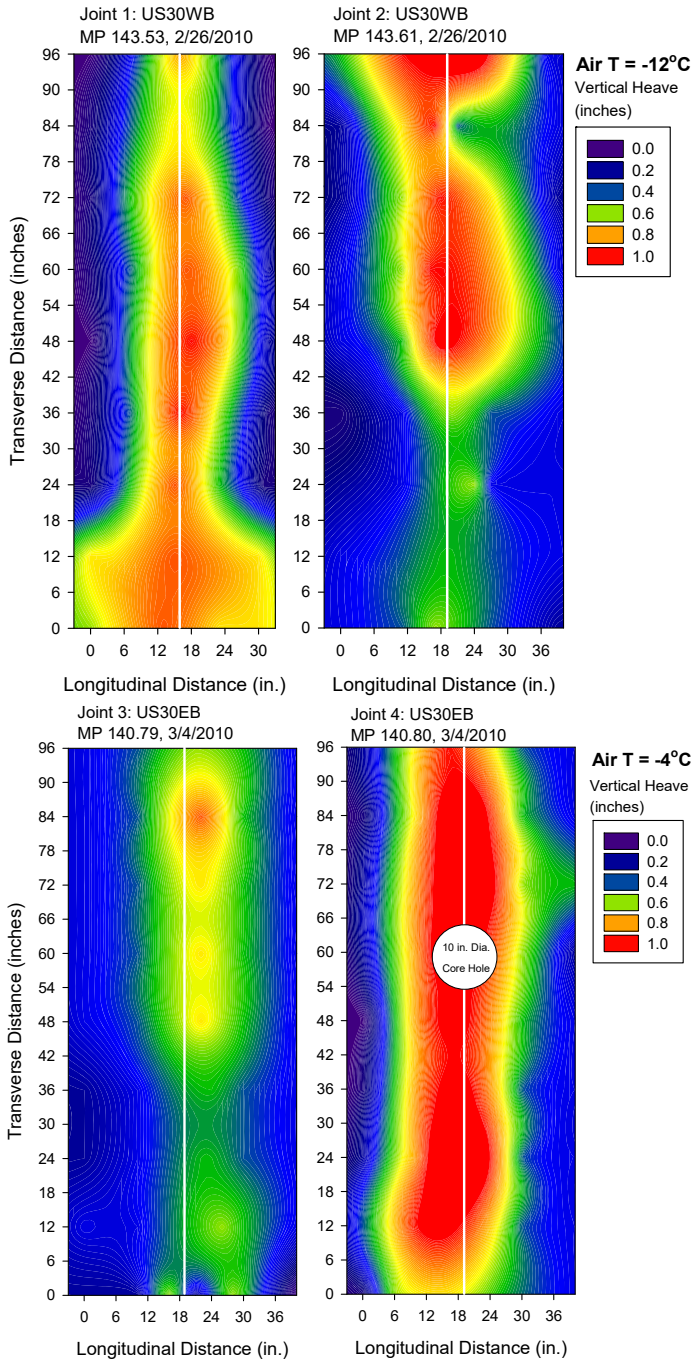

Figure 4.6. Spatial contour plots of joint vertical heave measurements (1 in. =2.54 cm).

4.5.2. Pavement layer temperature

Pavement temperature data was monitored every minute at the test site from pavement surface to about 1.6 m deep. Using the temperature data, 0°C frost isotherms, which form the boundaries of zones of frozen layers were estimated for four winters as shown in Figure 4.7.

Results indicate that the freezing periods in 2011–12 and 2012–13 lasted for about 2.2–2.4 months and in 2013–14 lasted for about 2.6 months. Two separated freezing periods were observed during the 2014–15 winter, while each period lasted about 1 month. Thawing periods for the four seasons showed slight variation, which lasted for about 10 to 25 days. The maximum frost penetration based on isotherms were around 0.58 to 0.75 m for 2011–12, 2012–13, and 2014–15 seasons. The deepest frost penetration was found during 2013–14 winter, which reached 1.05 m.

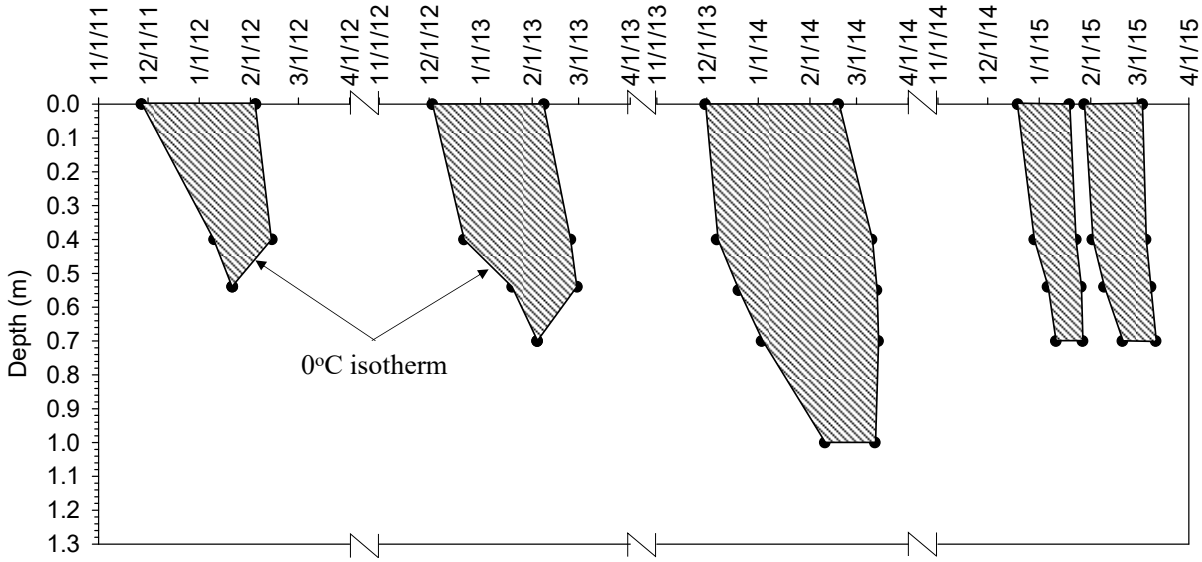

Figure 4.7. Estimated frozen zones (shaded areas) at project site from 2011 to 2015.

The number of freeze-thaw cycles with depth calculated for each year from 2011 to 2015 from the temperature monitoring data near mile 143.68 are presented in Figure 4.8. The cycles were determined using both ±1 and ±0.5°C as boundary values. Freeze-thaw cycles decreased with depth as expected. The number of freeze-thaw cycles at the surface ranged between 59 and 94 cycles and decreased to about 5 to 10 cycles near the bottom of the pavement. The number of cycles decreased to less than 3 at 0.7 m depth and no freeze-thaw cycles were observed at depths greater than 1.1 m during the monitoring period. Frost penetration depth reached around 0.6 to

0.8 m for three winters, while the maximum frost depth of about 1.0 m was observed during 2013–14 winter. These findings match to the results determined from the 0°C isotherm.

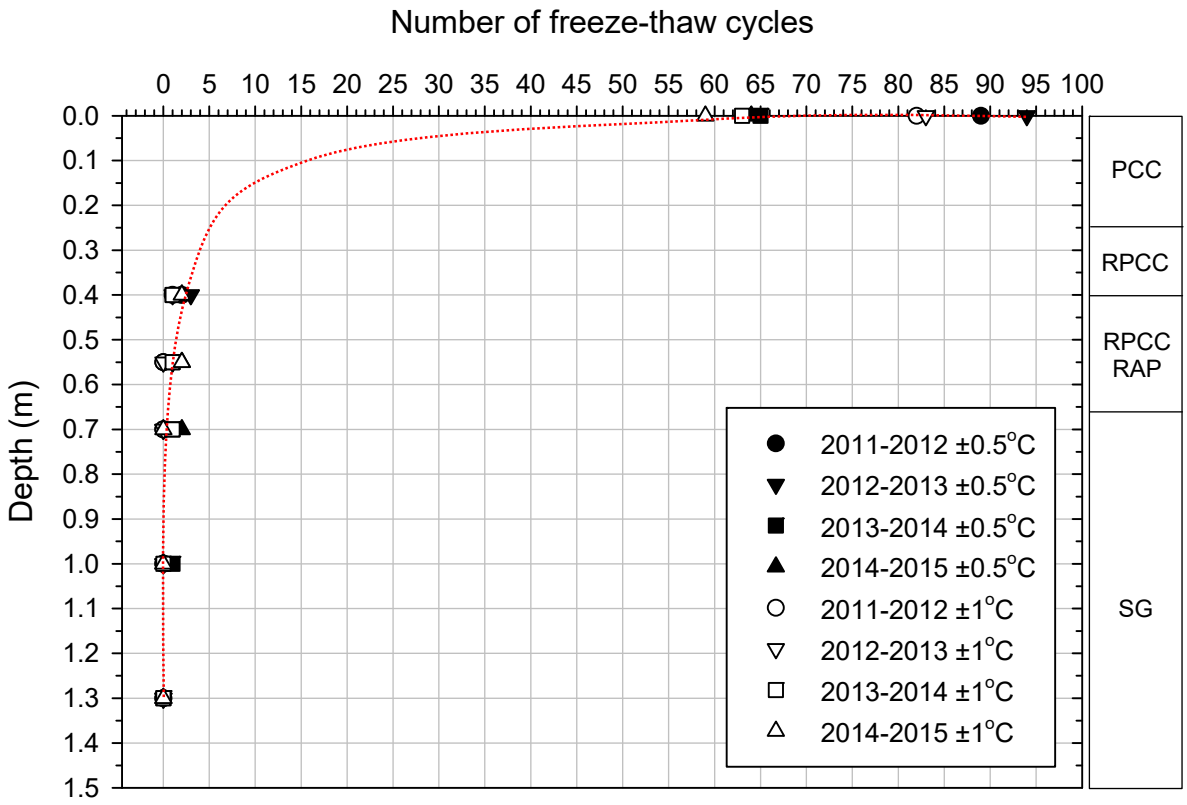

Figure 4.8. Freeze-thaw cycles of winters at depth from 2011 to 2015 using ±0.5 and ±1°C as boundary values.

4.5.3. Frost-heave and thaw-weakening

In order to evaluate the frost-heave and thaw-weakening susceptibility of the geomaterials of the reconstructed pavement foundations, laboratory freeze-thaw and CBR tests were conducted according to ASTM D5918 (2013). Frost-heave rates and the post-test CBR values were used to rate the frost susceptibility of RPCC, RPCC-RAP, and subgrade. The frost-heave versus time plots for the clayey sand subgrade are presented in Figure 4.9. The peak heave values of RPCC and RPCC-RAP were 6–7.5 mm for RPCC and 5–6 mm for RPCC-RAP. It was anticipated that the heave value at the second freeze-thaw cycle is greater than that at the first cycle based on

previous study (Johnson 2012; Zhang et al., 2015), and the larger heave values can be used to determine the consequent heave rate and frost susceptibility. However, RPCC and RPCC-RAP heaved more during the first freezing compared to the second. Therefore, the peak heaves at the first freezing of these two materials were treated as the "governed" values to estimate heave rates. Subgrade materials heaved rather more during the second freezing compared to the first one, which indicates a significant increase in the slope of the heave versus time line. By determining and averaging the slopes of each lines, the "governed" heave rates of RPCC, RPCC-RAP, and subgrade were 8.6, 7.1, and 7.8 mm/day respectively.

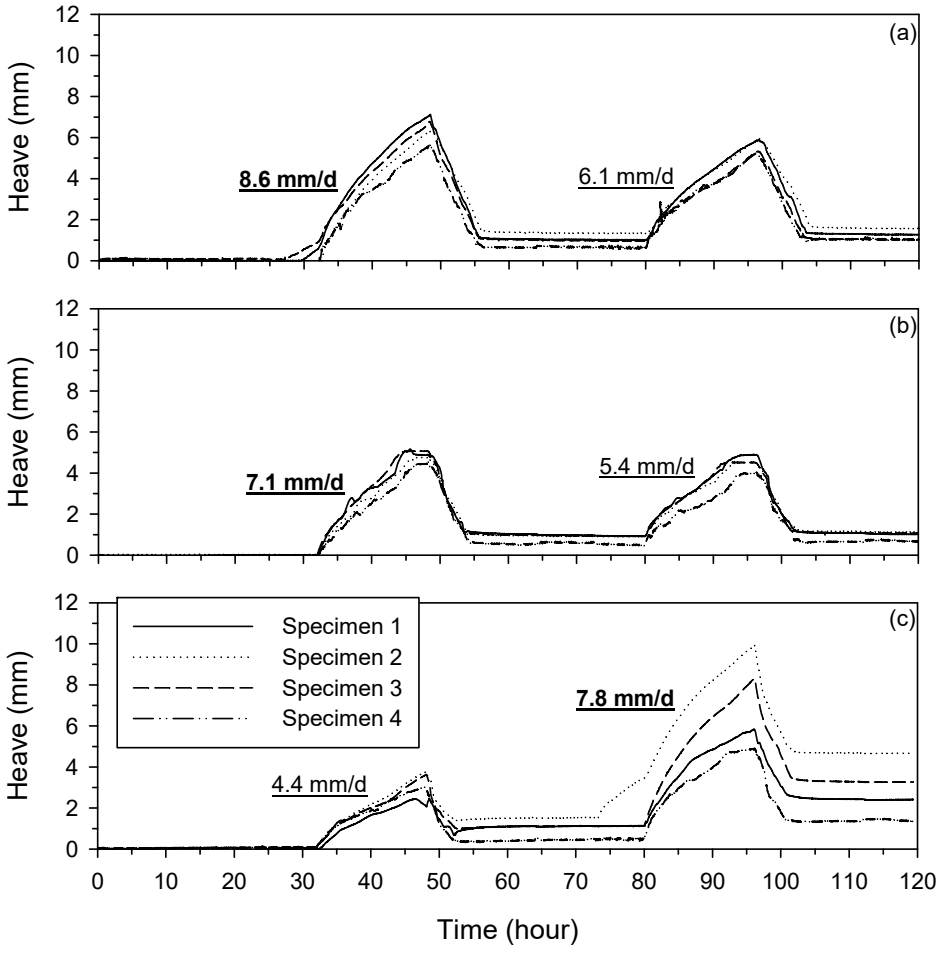

Figure 4.9. Frost heave versus time results of (a) RPCC, (b) RPCC-RAP, and (c) subgrade.

A summary of the material index properties, frost-heave and thaw-weakening test results with CBR testing after freeze-thaw cycles is provided in Table 4.2. Different types of soil presented changes in heave rates and post-test CBR values. Frost-heave susceptibility was rated based on the ASTM D5918 (2013) classification, and thaw-weakening susceptibility was rated based on both ASTM D5918 (2013) and Zhang et al. (2015). Based on the test results, the frost-heave susceptibility of the three materials was medium to high, but the heave rates were close. In ASTM D5918 (2013), the boundary value between medium and high level frost susceptibility was set at 8 mm/day. Three of the four RPCC specimens presented heave rates that can be classified as medium frost-heave susceptibility. The subgrade material was rated as high or very high for thaw-weakening susceptibility probably due to the larger composition of silt and clay, while both RPCC and RPCC-RAP showed very low to negligible thaw-weakening susceptibility.

Table 4.2. Summary of soil index properties and laboratory freeze-thaw test results.

Soil property	Subgrade	RPCC-RAP	RPCC
AASHTO classification	A-6(2)	A-1-a	A-1-a
USCS classification	SC	GP-GM	GP-GM
Gravel (%) (> 4.75 mm)	11.0	51.0	67.0
Sand (%) (4.75 – 0.074 mm)	46.0	43.0	28.0
Silt (%) (0.074 – 0.002 mm)	24.0	4.0	5.0
Clay (%) (≤ 0.002 mm)	19.0	2.0	0.0
Governed frost-heave rate (mm/day)	7.8	7.1	8.6
Post-test CBR (%)	2.7	37.6	33.3
Frost-heave susceptibility (ASTM)	Medium	Medium	High
Thaw-weakening susceptibility (ASTM)	High	Negligible	Negligible
Thaw-weakening susceptibility (Zhang et al., 2016)	Very high	Very low	Very low

Specimens after freeze-thaw testing were cut into six 2.54 cm thick “disks” for measuring the moisture contents at each particular depth of the tested specimens. The moisture content profiles are presented in Figure 4.10. Results showed that the moisture contents of RPCC after testing

increased to 13–14.5% in comparison with 8.5–10% when compacting the specimens. Larger contents of coarse soils may provide more inter-connected voids in RPCC. As water was continuously supplied during the testing, these voids may be filled under the effect of higher water head in water supply. This finding indicates that the RPCC layer may provide a drainage effect in practical engineering. No significant difference was found between the post-test and compaction moisture contents of RPCC-RAP materials. Comparing to RPCC, RPCC-RAP has larger content of sand and clay, and these finer aggregates may fill some voids formed by coarse aggregates and cut off the inter-connected pores. Moisture contents in subgrade materials were about 0 to 2% higher after the freeze-thaw cycles than the compaction moisture contents. In comparison, RPCC and RPCC-RAP showed slight variance between moisture contents at different depth, but the top 1/6 of subgrade specimens showed 2% higher moisture than the lower 5/6 parts. The capillary stress within subgrade specimens may contribute to moving moisture upward.

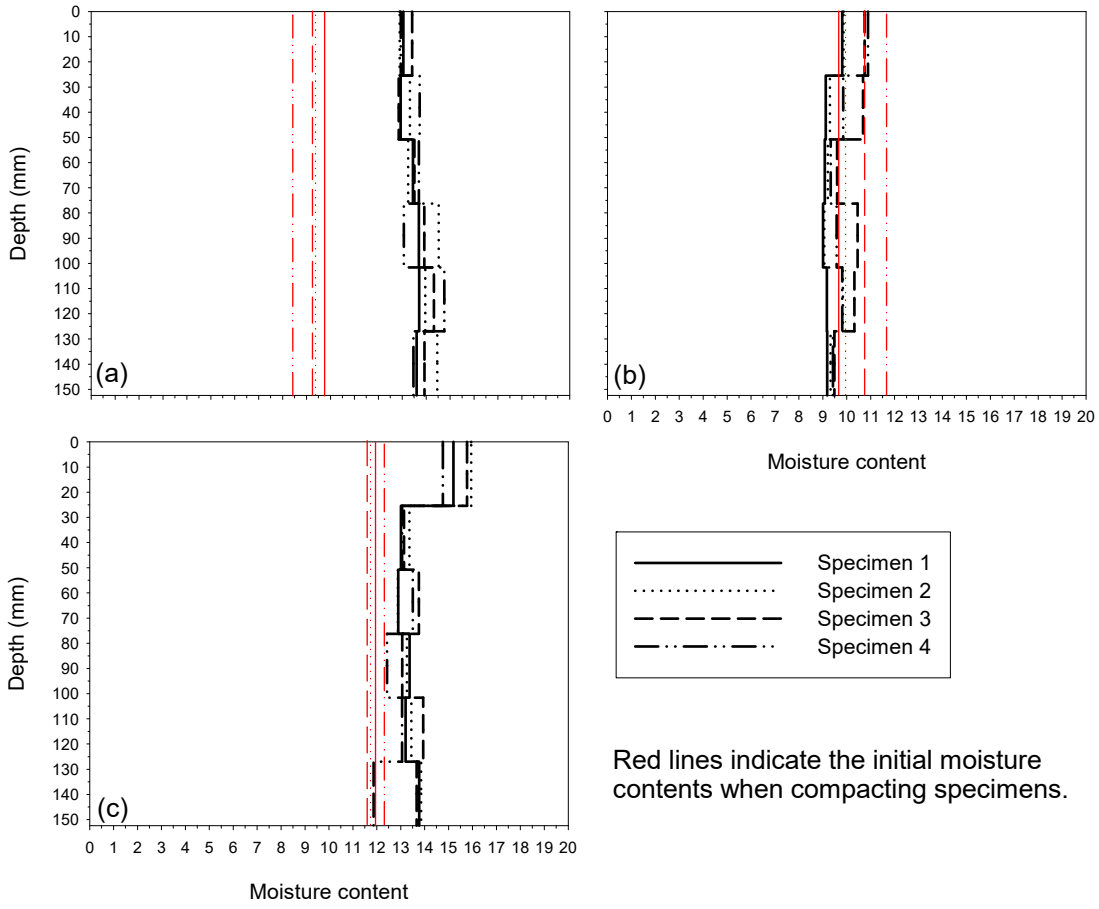

Figure 4.10. Profiles of moisture contents at depth of (a)RPCC, (b) RPCC-RAP, and (c) subgrade.

4.6. Summary and Conclusions

This paper focused on a case study with objectives of evaluating selected deteriorated joints showing frost heaves, the frost penetration and freeze-thaw cycles at the site, and the frost susceptibility of the reconstructed foundation geomaterials. According to the results derived from these tests, key findings are as follows:

- Ice lenses were found at layer interfaces of ACC, PCC, and ATB. ACC overlay and PCC showed weak structures during freezing, and stiff frozen ATB specimens showed low permeability.

- PCC specimens presented significantly higher moisture contents than other layers. This finding indicated that water was trapped at the deteriorated joint spaces at PCC layer. Microcracking on concrete under joints may contribute to water infiltration to lower base and subgrade, which may play the role of supplying water to lower layers for frost heaving.
- Vertical heaves at deteriorated joint locations reached up to 38 mm but showed non-uniformity in the transverse direction. The longitudinal width of the heaved bulge reached up to 760 mm near the shoulder.
- The greatest frost penetration in four monitored years was 1.0 to 1.1 m. A total of 59 to 94 freeze-thaw cycles were counted at the pavement surface, and no freeze-thaw cycle was found for three winters at depths over 0.7 m.
- Local freezing and thawing periods had various lengths. Freezing periods lasted two to three months, and full thawing occurred within 25 days.
- Laboratory freeze-thaw test results indicated that frost-heave and thaw-weakening might be influenced by grain size distribution. All three geomaterials from the reconstructed foundations were medium frost-heave susceptible, and the soft clayey subgrade showed high thaw-weakening susceptibility.
- Water movement after freeze-thaw cycles differed between types of geomaterials, even though the soil classifications were similar. Pore conditions may have critical influences on the amount and direction of water moving during freezing.

4.7. Acknowledgements

This research was conducted under Federal Highway Administration (FHWA) DTFH61-06-H-00011 Work Plan 18 and the FHWA Pooled Fund Study TPF-5(183). The authors would like

to express their gratitude to the National Concrete Pavement Technology (CP Tech) Center, the FHWA, the Iowa Department of Transportation (DOT), and the other pooled fund state partners for their financial support and technical assistance.

CHAPTER 5. ASSESSING STIFFNESS AND SUPPORT CONDITIONS OF RECONSTRUCTED CONCRETE PAVEMENT FOUNDATIONS

A paper to be submitted to *ASCE Journal of Transportation Engineering*

Yang Zhang, Pavana K.R. Vennapusa, David J. White, and Alex E. Johnson

5.1. Abstract

This paper discusses in situ test results assessing the stiffness and support conditions of concrete pavement foundation layers and compares the relationships between these results with previous studies and the design values. Dynamic cone penetrometer (DCP) tests, light weight deflectometer (LWD) tests, and falling weight deflectometer (FWD) tests were conducted either on pavement surface or foundation layers. LWD results indicate that layer stiffness is influenced by aggregate segregations as different fine content distributions. Three methods of obtaining the modulus of subgrade reaction *k* were analyzed. Backcalculated *k* values based on FWD deflection inferred results more close to the design value, while the California bearing ratio (CBR) empirically correlated *k* presented various values differing from the design value. In comparison with previous studies, CBR versus *k* relationships show significant scatter and present significant uncertainty in the predictions. This suggests that improvements are needed on correlating pavement foundation mechanistic parameters.

5.2. Introduction

Various quality control (QC) and quality assurance (QA) testing methods have gained great interests to transportation agencies for determining mechanistic properties of pavement foundations. Stiffness- or strength based QC/QA tests, including falling weight deflectometer (FWD) test, light weight deflectometer (LWD), and dynamic cone penetrometer (DCP) test are a typical approach to evaluate the elastic modulus and bearing strength of foundation layers

(Newcomb and Birgisson, 1999; Konrad and Lachance, 2001; White et al., 2013). Meanwhile, modulus of subgrade reaction (*k*) is a key value that is widely used by the U.S. pavement designers to characterize roadbed support conditions. Some research has been conducted to explore the relationships between these in situ QC/QA testing measurements and the design parameter (Thornton, 1983; Darter et al., 1995; Chen et al., 2005; Vennapusa 2011).

The *k* value is determined using a static plate load test, which can be time consuming and expensive to setup. Therefore, various alternative testing methods have been in use by state agencies to determine the *k* value. Deflection tests using FWD is a popular choice for determining *k* value based on testing performed on pavement surface layers (Puppala, 2008; AASHTO, 1993; AASHTO, 2008). DCP test is another test device that has been recommended in the AASHTO (2008) and ACPA (2012) design guide as a method to determine California bearing ratio (CBR), which can be empirically correlated to *k* value. Most highway agencies assume *k* values during the design phase either based on experience and historically available data or limited field testing. For rehabilitated pavement designs, agencies in the U.S. typically use FWD testing data on the existing pavements, while for new pavements, CBR or M_r testing is typically performed on samples obtained from the field. However, research is limited yet to relate these testing measurements and to further verify if these relationships differ from the existed empirical correlations.

In this study, LWD and DCP tests were conducted on the foundation layer to obtain the stiffness properties of the reconstructed foundations. A few months after the construction was completed, FWD tests were conducted on the pavement surface near mid-panel and joints where the foundation layer testing was previously conducted. Results from FWD and DCP tests were analyzed and compared with the assumed *k* values in pavement thickness design. The

relationship between the *k* values backcalculated from FWD measurements and the resilient modulus correlated from DCP test results was compared to findings from previous studies. The findings from this report should be of significant interest to researchers, practitioners, and agencies who deal with design, construction, and maintenance aspects of PCC pavements.

5.3. Background

5.3.1. Project overview

This project is located on US 30 in Boone County in Iowa and involved removal of the existing old pavement, which showed severe pavement distresses, between mileposts 139.0 and 147.27. The existing pavement showed severe surface distresses with reflective cracking and vertical upheave near joints, especially during winter. Initial field investigations by the Iowa DOT rated the ride quality of the pavement section as "poor" based on pavement condition index (PCI) ranging between 54 and 56 on a 0-100 scale.

As part of the reconstruction work that began in summer of 2011, the existing pavement and the asphalt treated base layers were removed and the subgrade was undercut during the reconstruction process to place a nominal 410 mm (16 in.) thick modified subbase over the natural existing subgrade. The modified subbase layer consisted of 150 mm (6 in.) thick RPCC material at the surface underlain by 254 mm (10 in.) thick mixture of RPCC-RAP material. A nominal 254 mm (10 in.) thick jointed plain concrete pavement (JPCP) was placed on the newly constructed foundation layer. Thickness design of the new pavement was conducted by the Iowa DOT according to the PCA (1984) method, by assuming a modulus of subgrade reaction (k) value of 41 kPa/mm (150 pci) for the foundation layer. The new pavement and foundation layer cross-section is shown in Figure 5.1. Iowa DOT rated the ride quality of the pavement section as "good" based on PCI ranging between 95 and 100 after construction (Iowa DOT, 2014).

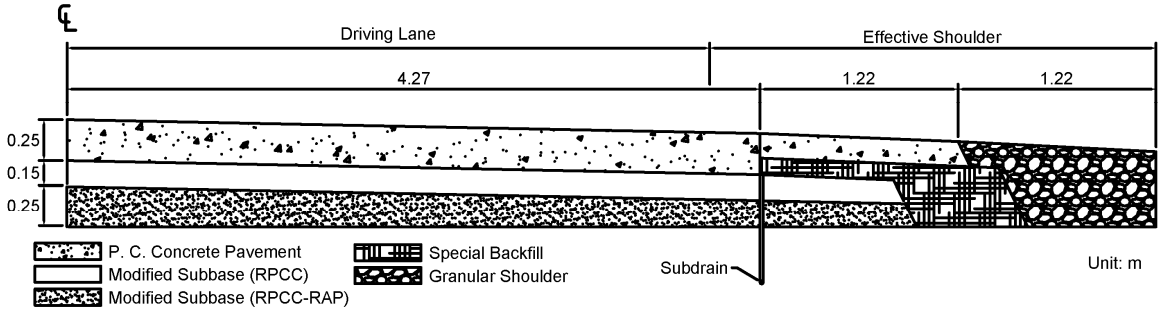

Figure 5.1. The new pavement and foundation layer cross-section of this project.

5.3.2. Literature review

Various thickness design procedures have been developed since the 1970s for concrete pavement design. PCA (1984) and AASHTO (1993) design procedures are currently the most popularly used methods by the highway agencies in the U.S., while there is increasing interest in implementing the newly developed mechanistic-empirical design guide by AASHTO (2008). While the AASHTO (2008) procedure is a significant advancement over the PCA (1984) and AASHTO (1993) procedures in terms of analyzing the pavement responses, the key design parameter used to characterize foundation layer support is still the modulus of subgrade reaction *k* value. Resilient modulus M_r value is one of design parameters in AASHTO (1993) and AASHTO (2008), but the M_r value is converted to *k* value using empirical relationships in the design process. CBR is another widely used value for QC/QA during or after construction. Some direct or indirect correlations between CBR and *k* value were also commonly used. With the objective of comparing the in situ or laboratory measurements to the design parameter values, studies have been conducted to explore the relationships between these mechanistic parameters (Darter et al., 1995; Chen et al., 2005; Barker and Alexander, 2012).

Chen et al. (2005) investigated the correlation between DCP measurements and moduli of pavement foundation layers. The layer moduli were determined by backcalculating FWD deflection measurements using a computer program. The output DCP measurement was

penetration rate (PR) with unit of mm per blow (dynamic penetration index in this study). A total of 198 test locations on asphalt concrete pavements were selected to conduct both DCP and FWD tests. Test locations were with various granular subbase thickness and pavement conditions. A previous study also by Chen et al. (2001) has reported that PR values change as DCP is performed on pavement surface or directly on foundation layers, due to the loading from the surface layer. Modification coefficients were proposed in that study to transfer PR values between surface and foundation testing measurements respectively for subbase and subgrade. A correlation equation was presented in Chen et al. (2005) to estimate layer moduli based on PR for both subbase and subgrade. The equation raised from this study did not significantly differ from the conventional correlation, the Powell's model (Powell et al., 1984). It was found that the difference between these two correlations varied as the PR changes. When the PR was smaller than 10 mm/blow, the difference was over 10 % and it reduced to about 1.7% when the PR reached 80 mm/blow.

Ping and Sheng (2011) conducted a study investigating the correlation relationship between the *k* and M_r of local pavement subgrade soils. The *k* values in this study were obtained by conducting in situ static plate load tests directly on the subgrade layer. Two methods, laboratory triaxial testing and simulated cyclic plate load testing, were applied in this study to measure the soil M_r. Comparing testing results based on strains measured at the middle half of the specimens, the M_r measured from triaxial testing was close to the values measured from simulated testing. However, test results based on the specimen full strains indicated that the triaxial M_r differed from the simulated M_r, and difference between these two values increased as the M_r increases. Ping and Sheng (2011) also reported the findings by correlating the laboratory triaxial M_r and in situ static plate load *k*. The conversion equation from M_r to *k* was close to the AASHTO

correlation relationship which considers the subgrade is linearly elastic, as the conversion factor was 2.25 in comparison with the AASHTO recommended value of 2.03 (in metric units).

Barker and Alexander (2012) reviewed the existing correlations for estimating *k* and effective *k* that considers the influence from subbase thickness. Several linear relationships between *k* and CBR were summarized in this study. The most important uncertainty focused on the conversion factor between these two parameters. In general, this factor varied from 6.5 to 20 (transferring CBR to *k*). Baker and Alexander (2012) also provided a detailed procedure of theoretically calculating *k* from CBR, which uses the Young's modulus, E, as a medium parameter. The result showed that 6.5 is the number theoretically be used for the conversion. No later study has reported any number lower than 6.5. Baker and Alexander (2012) then conducted plate load tests to directly measure the in situ *k* values and compared to the CBR values. Based on results from that study and existing correlations, the values of the conversion factor can be classified into two parts. Non-granular materials presented a conversion factor approaching 20, and this factor for granular materials approaches to the theoretical number 6.5.

5.4. Methods

Laboratory freeze-thaw tests were conducted in accordance with ASTM D5918 (2013). Detailed description of the test equipment is presented in Johnson (2012) and Zhang (2015). A CBR test was conducted on two specimens prior freeze-thaw cycles and the other two specimens was subjected to two freeze-thaw cycles and then tested for CBR. The heave rate and the post-test CBR tests are used as the basis for the frost-heave susceptibility classification per ASTM D5918 (2013). The DCP, LWD, and FWD testing methods used in this study was described in this section. The procedures of determining *k* values from various field measurements were also discussed here.

5.4.1. Dynamic cone penetrometer testing

DCP tests (Figure 5.2a) were performed in accordance with ASTM D6951 (2003) to determine dynamic penetration index (DPI) in units of mm/blow and calculate CBR using Equation 5.1.

$$CBR = \frac{292}{DPI^{1.12}} \tag{5.1}$$

Tests were conducted down to a depth of about 2 m below pavement surface, by drilling a 20 mm hole in the pavement down to the top of the underlying base layer. The DCP test results are presented as CBR with depth profiles and as point values of CBR_{SB} representative of the subbase layer and CBR_{SG} representative of the top 305 mm of the subgrade. The top 305 mm of the subgrade was selected as the subgrade layer as it is typically the thickness used to scarify and recompact the material during construction. The point data values represent the weighted average CBR within each layer.

All DCP-CBR profiles were also reviewed to determine "weak" layers within the subgrade down to the bottom of the profile. An average CBR of a minimum of 75.6 mm (3 in.) thick layer within the top 1.5 m of subgrade (represented as $CBR_{SG\text{-}Weak}$) was also calculated. The $CBR_{SG\text{-}Weak}$ was determined to assess if weak layer would have influence on the *k* values determined using the FWD test.

The CBR_{SG} and $CBR_{SG\text{-}Weak}$ values were converted to $M_{r\text{-}SG}$ and $M_{r\text{-}SG\text{-}Weak}$ of subgrade, using nomographs provided in AASHTO (1993). AASHTO (1993) uses the following empirical relationship to convert M_r to *k* value (Equation 5.2), where *k* is in units of kPa/mm and M_r is in units of MPa:

$$k = 2.3M_r \tag{5.2}$$

5.4.2. Zorn light weight deflectometer testing

Zorn LWD tests (Figure 5.2b) were performed on subbase and subgrade layers to determine elastic modulus. The LWD was set up with 300 mm diameter plate and 71 cm drop height. The tests were performed following manufacturer recommendations (Zorn 2003) and the elastic modulus values were determined using Equation 5.3:

$$E = \frac{(1-\eta^2)\sigma_0 r}{D_0} \times F \tag{5.3}$$

where E = elastic modulus (MPa); D_0 = measured deflection under the plate (mm); η = Poisson's ratio (0.4); σ_0 = applied stress (MPa); r = radius of the plate (mm); and F = shape factor depending on stress distribution (assumed as 8/3) (Vennapusa and White 2009).

5.4.3. Falling weight deflectometer testing

FWD tests (Figure 5.2c) were conducted near mid-panel in accordance with ASTM D4694 (2009) using a segmented 300 mm diameter loading plate by applying one seating drop and four loading drops. The applied loads varied from 22 to 75 kN The peak deflection values measured directly beneath the testing plate (D_0) and at several locations away from the testing plate up to about 1.52 m away from the plate, were normalized to 40 kN (9000 lbs.).

The FWD deflection basin data was analyzed to determine peak deflections under the loading plate (D_0), load transfer efficiency (LTE) near joints, and zero-load intercept (I) values. Tests conducted at the center were used to determine *k* values and I values.

LTE values were determined by placing the FWD loading plate close to the joint and positioning a deflection sensor on the unloaded panel about 305 mm away from the plate to measure D_1 and using Equation 5.4:

$$LTE(\%) = \frac{D_1}{D_0} \times 100 \tag{5.4}$$

I values are determined by plotting applied load measurements on the x-axis and corresponding deflection measurements on the y-axis, and plotting a best fit linear regression line. The intersection of this line on the y-axis referred to as the I-value. McCracken (2008) have reported I = 0.05 mm (2 mil) as a critical value for void detection.

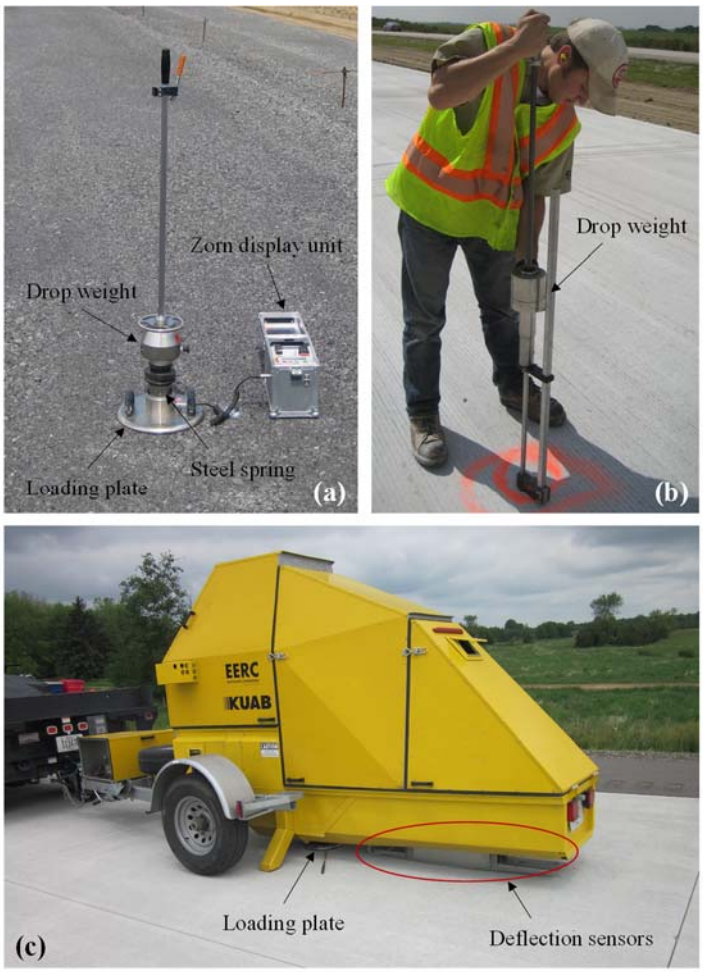

Figure 5.2. In situ testing equipment used in this study: (a) Zorn LWD, (b) DCP, and (c) Kuab FWD.

5.4.4. Determination of *k* values

Subgrade *k* values were determined directly from field measurements using FWD testing, empirical relationships from DCP test measurements, and empirical relationships from laboratory measurements. All of these values are compared in this report with reference to the design assumed value. The *k* values determined using different procedures and the notations are listed below:

- $k_{FWD\text{-}Static\text{-}Corr}$ – determined from the FWD test and corrected for slab size.
- $k_{AASHTO(1993)}$ – determined using Equation 8, where M_r is determined from CBR_{SG} or $CBR_{SG\text{-}Weak}$ using charts provided in AASHTO (1993)
- $k_{PCA(1984)}$ – determined from CBR using charts provided in PCA (1984)

The FWD deflection basin data was analyzed to determine *k* values using the $AREA_4$ method described in AASHTO (1993). The AREA method was first proposed by Hoffman and Thompson (1981) for flexible pavements and has since been applied extensively for concrete pavements (Darter et al. 1995). Since the *k* value determined from FWD test represents a dynamic value, it is referred to here as $k_{FWD\text{-}Dynamic}$. Deflections obtained from four sensors are used in the $AREA_4$ calculation. $AREA_4$ is calculated using Equation 5.5 and has dimensions of length (inches), as it is normalized with deflections under the center of the plate (D_0):

$$AREA_4 = 6 + 12 \times \left(\frac{D_2}{D_0}\right) + 12 \times \left(\frac{D_4}{D_0}\right) + 6 \times \left(\frac{D_5}{D_0}\right) \tag{5.5}$$

where D_0 = deflections measured directly under the plate (inches); D_2 = deflections measured at 305 mm (12 inches) away from the plate center (inches); D_4= deflections measured at 610 mm (24 inches) away from the plate center (inches); and D_5 = deflections measured at 914 mm (36 inches) away from the plate center (inches). AREA method can also be calculated using

different sensor configurations and setups, i.e., using deflection data from 3, 5, or 7 sensors and those methods are described in detail in the literature (Stubstad et al. 2006, Smith et al. 2007).

In the early research conducted using the AREA method, the ILLI-SLAB finite element program was used to compute a matrix of maximum deflections at the plate center and the AREA values by varying the subgrade *k*, the modulus of the PCC layer, and the thickness of the slab (ERES Consultants, Inc. 1982). Measurements obtained from FWD tests were then compared with the ILLI-SLAB program results to determine the *k* values through back calculation. Later, in the 1990s to replace the back calculation procedure, Barenberg and Petros (1991) and Ioannides (1990) proposed a forward solution procedure based on Westergaard's solution for loading on an infinite plate. This forward solution presented a unique relationship between AREA value (for a given load and sensor arrangement) and the dense liquid radius of relative stiffness (L) in which subgrade is characterized by the *k* value. The radius of relative stiffness (L) is estimated using Equation 5.6:

$$L = \left[\frac{\ln\left(\frac{x_1 - AREA_4}{x_2} \right)}{x_3} \right]^{x_4} \tag{5.6}$$

where $x_1 = 36$; $x_2 = 1812.279$; $x_3 = -2.559$; $x_4 = 4.387$. It must be noted that the x1 to x4 values vary with the sensor arrangement and these values are only valid for the AREA4 sensor setup. Once the L value is known, the $k_{FWD\text{-}Dynamic}$ value can be estimated using Equation 5.7:

$$k_{FWD-Dynamic}(pci) = \frac{PD_0^*}{D_0 L^2} \tag{5.7}$$

where P = applied load (lb); D_0 = deflection measured at plate center (inches); and D_0* = non-dimensional deflection coefficient calculated using Equation 5.8:

$$D_0^* = a \cdot e^{-be^{-cL}} \tag{5.8}$$

where a = 0.12450; b = 0.14707; and c = 0.07565. It must be noted that these equations and coefficients are valid for an FWD setup with an 11.81 in. diameter plate.

The AREA method assumes the slab and the subgrade are horizontally infinite. This assumption leads to an underestimation of the *k* value. Crovetti (1993) developed the following slab size corrections for a square slab based on finite element analysis conducted using the ILLI-SLAB program, for use in the $k_{\text{FWD-Dynamic}}$:

$$Adjusted\ D_0 = D_0(1 - 1.15085e^{-0.71878(\frac{L'}{L})^{0.80151}}) \tag{5.9}$$

$$Adjusted\ L = L(1 - 0.89434e^{-0.61662(\frac{L'}{L})^{1.04881}}) \tag{5.10}$$

where L′ = slab size (smaller dimension of a rectangular slab, length or width). This procedure also has limitations: (1) it considers only a single slab with no load transfer to adjacent slabs, and (2) it assumes a square slab. The square lab assumption is considered to produce sufficiently accurate results when the smaller dimension of a rectangular slab is assumed as L′ (Darter et al. 1995). There are no established procedures reported to date on correcting for load transfer to adjacent slabs, which remains as a limitation of this method. In this project, $k_{\text{FWD-Dynamic}}$ values corrected for slab size are reported as $k_{\text{FWD-Dynamic-Corr}}$.

AASHTO (1993) suggests dividing the $k_{\text{FWD-Dynamic}}$ value by a factor of 2 to determine the equivalent $k_{\text{FWD-Static}}$ value. For the analysis conducted in this research project, the $k_{\text{FWD-Dynamic-Corr}}$ values were divided by 2 and are reported as $k_{\text{FWD-Static-Corr}}$ values.

5.5. Test Results and Analysis

5.5.1. Laboratory freeze-thaw and CBR tests

In order to evaluate the bearing capacity of foundation layers, two groups of laboratory CBR tests were conducted on regular specimens and specimens experienced two freeze-thaw cycles.

Test results summarized in Table 5.1 show the CBR values without freeze-thaw cycles (pre-test CBR) and CBR values after two 8-hour freeze-thaw cycles (post-test CBR). For the purpose of evaluating the impact of fines content on aggregate strength, modified RPCC material was tested.

Table 5.1. Summary of CBR and freeze-thaw tests results.

Material	USCS	Pre-test CBR (%)	Post-test CBR (%)
Subgrade	SC	8.4	2.7
RPCC-RAP subbase	GP-GM	40.6	37.6
RPCC subbase	GM	70.3	33.3
RPCC subbase (half of fines removed)	GP	49.4	39.2
RPCC subbase (all fines removed)	GP	47.0	35.5

Note: – indicates data not available.

The natural subgrade shows the lower bearing capacity both with or without freeze-thaw, in comparison with the two subbase layer materials. Freeze-thaw cycles present significant influence on CBR values except for slight influence to RPCC-RAP. Though RPCC show CBR value over 70 on regular specimens, it decreased around 53% after freeze-thaw testing, which is close to the pre- and post-test CBR of RPCC-RAP. RPCC specimens modified by removing half or all fines were then tested and compared to the regular specimens. The pre-test CBR values reduced around 30% when half of fines were removed and 42% when all fines were removed. The results indicate that fines content has significant influence on aggregate strength. However, the CBR values of specimens with various fines content settled to similar level after freeze-thaw cycles.

5.5.2. In situ stiffness and strength tests

In situ DCP and LWD tests were conducted on the foundation layers and FWD tests were conducted on the pavement layer.

Elastic modulus of RPCC layer were determined based on LWD results. Figure 5.3 shows the E_{LWD} values of 40 longitudinal test points starting at Sta. 1394.20 with 20 test locations in each of the left and right lanes over a 105 m distance along the center of each lane. In addition, 32 tests were conducted at Sta. 1394.60 transversely across the full pavement width. Results indicated the E_{LWD} varied between 11 and 79 MPa in the longitudinal direction and between 19 and 100 MPa in the transverse direction. In total of 72 tests, the average E_{LWD} was about 56.2 MPa. LWD tests were conducted transversely to capture the variability observed at the surface with aggregate segregation. Figure 5.4 is the top view of RPCC layer on left and right lanes. The two lanes can be observed with different fines contents. E_{LWD} values on the right lane were comparatively higher than in the left lane. As can be seen in Figure 5.3 and Figure 5.4, higher moduli values were in areas with more fines content. This result matches to the finding from the laboratory CBR tests.

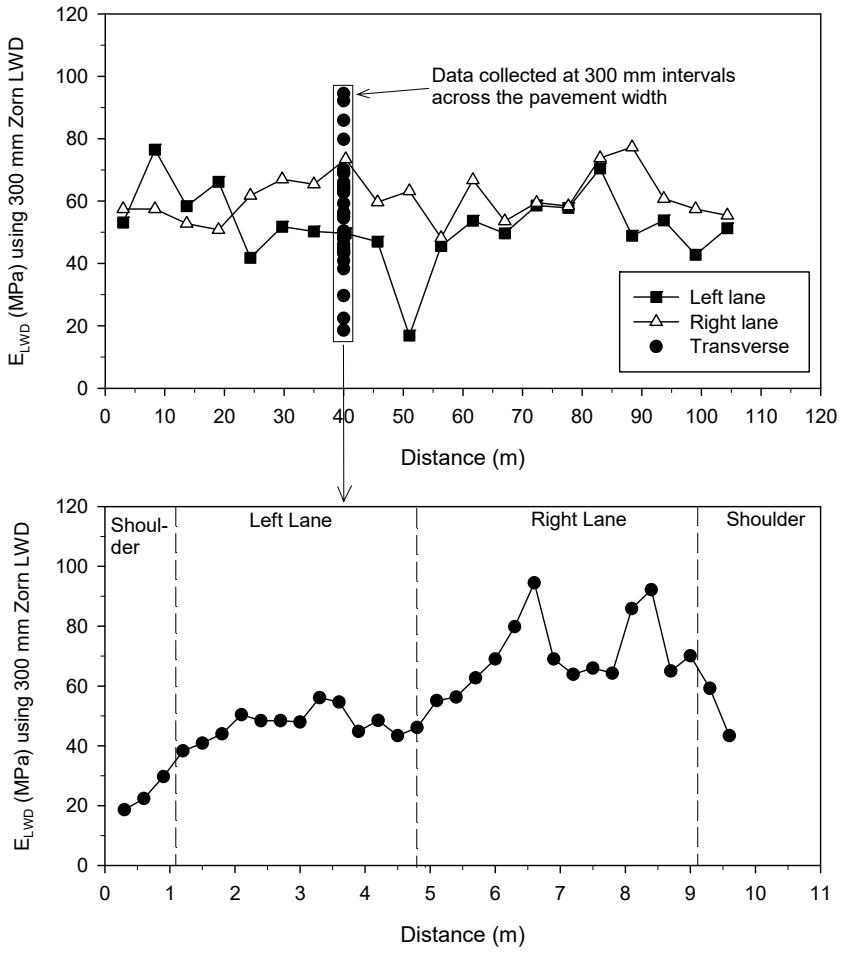

Figure 5.3. LWD dynamic modulus of longitudinal and transverse measurements.

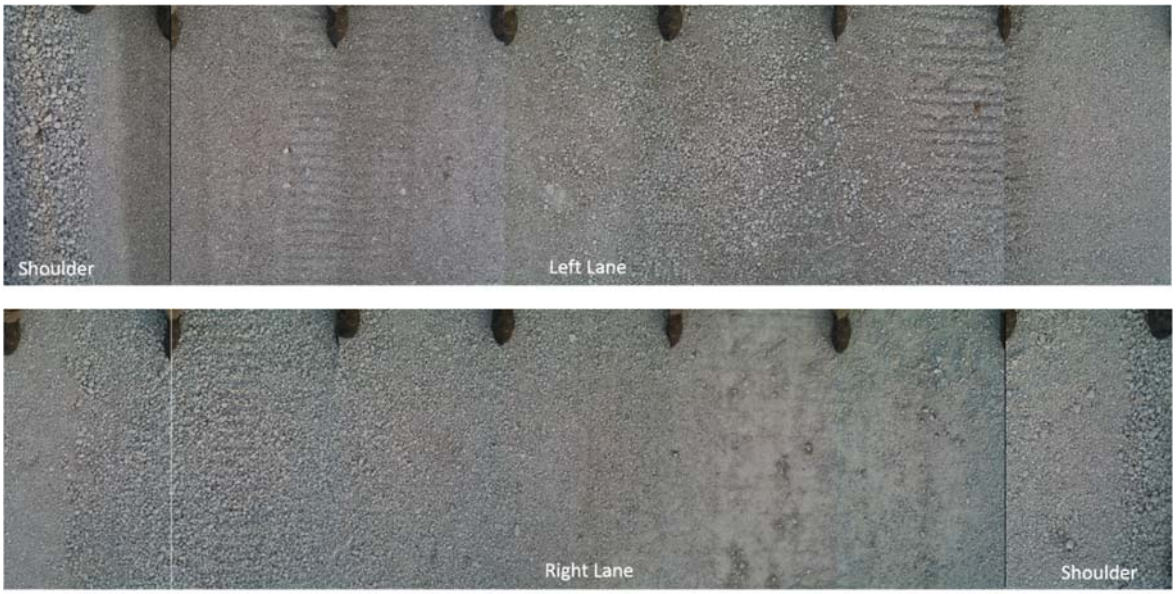

Figure 5.4. RPCC modified subbase layer surface from left lane shoulder (top) to right lane shoulder (bottom).

DCP tests were conducted at 20 test locations, with 10 locations each in the left and right lanes over a 100 m distance along the center lane. The DCP-CBR and cumulative blows with depth profiles for left and right lanes are presented in Figure 5.5. CBR values of each layer at each test location are plotted with distance in Figure 5.6. CBR values were lower in the top 150 mm of RPCC modified subbase layer than that in the bottom 250 mm of RPCC-RAP modified subbase layer. The average CBR of the RPCC modified subbase layer was about 11 and the average CBR of the RPCC-RAP layer was about 69, though the laboratory tests showed 70% higher CBR values of RPCC than RPCC-RAP. The subgrade was significantly variable in CBR and the average value for the top 300 mm was about 14. The $CBR_{SG\text{-}Weak}$ was about 7, which stands for the average value a minimum of 75.6 mm (3 in.) thick “weak” layer within the top 1.5 m of subgrade.

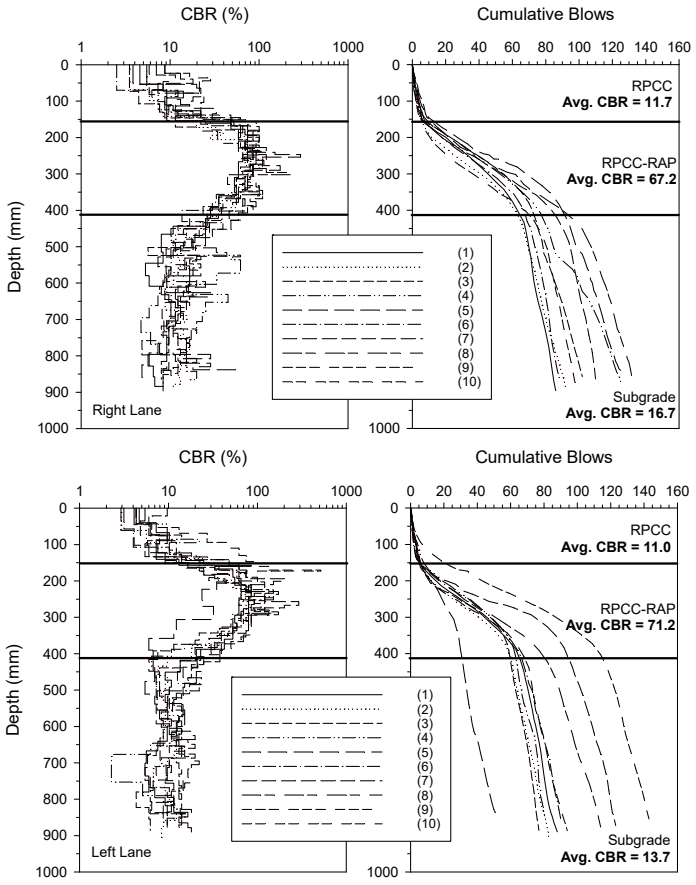

Figure 5.5. DCP-CBR and cumulative blows with depth profiles.

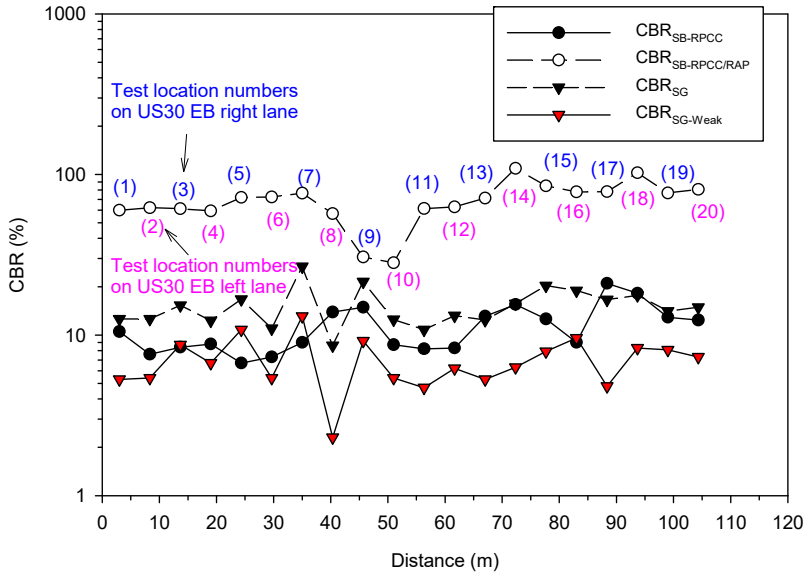

Figure 5.6. Layer CBR values at each test location.

FWD tests were conducted on the pavement surface after construction. Tests were conducted near the mid-panel for D_0 and I and at joints for D_0, I, and LTE (Figure 5.7). The D_0 did not varied significantly but presented significant difference between the measurements at mid-panel and at joints. It ranged from 0.07 to 0.08 mm at mid-panel and 0.09 to 0.11 mm at joints. I-values kept within a relatively small range between -2 to +5 μm. Based on AASHTO (1993), no void was detected either at joints or mid-panel. An average value of approximate 97% indicated excellent load transfer ability at joints.

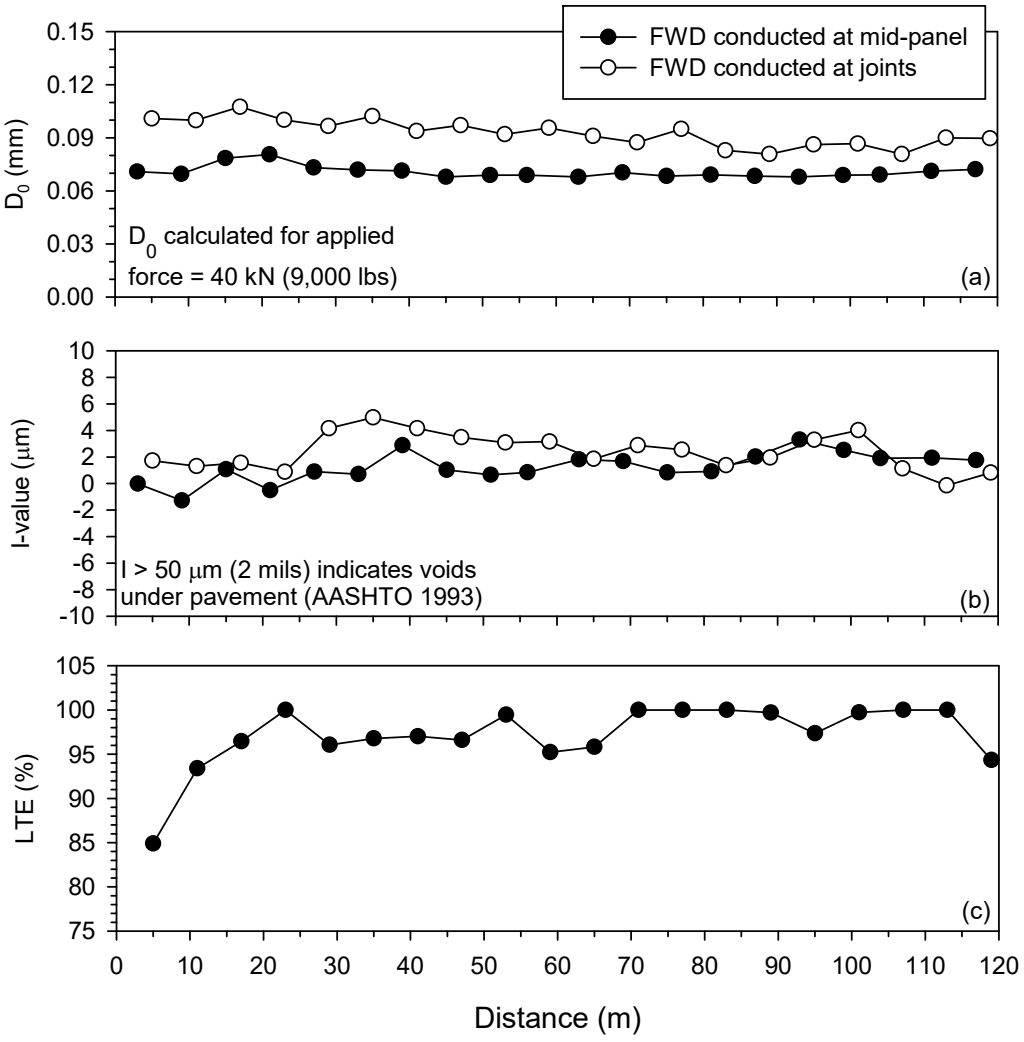

Figure 5.7. FWD test results of (a) D_0, (b) I value, and (c) LTE at each test location.

5.5.3. Comparison of *k* values with target design values

The *k* values along with distance obtained from FWD test, and using the PCA and AASHTO procedures using CBR-*k* correlations are summarized in Figure 5.8. Both CBR_{SG} and $CBR_{SG\text{-}Weak}$ were used in calculating the *k* values using the PCA and AASHTO procedures. The average $k_{FWD\text{-}Static\text{-}Corr}$ was about 37.1 kPa/mm with relatively small variety (7% COV), while $k_{AASHTO(1993)}$ showed a large variety between 40 to 160 kPa based on $CBR_{SG\text{-}Weak}$ and 120 to 260 kPa based on CBR_{SG}.

The average *k* values determined from the three procedures are also presented as bar charts in Figure 5.9. The results showed that the *k* values determined from the FWD test showed the lowest values, and were closer to the assumed design *k* value. On average, the average $k_{FWD\text{-}Static\text{-}Corr}$ value was about 0.95 times the design *k* value. The $k_{PCA(1984)}$ calculated based on $CBR_{SG\text{-}Weak}$ were also closer to the assumed design *k* value. The average $k_{PCA(1984)}$ calculated based on CBR_{SG} was about 1.4 times higher than the design *k* value. The *k* values calculated using the empirical relationships between CBR and *k* from AASHTO (1993) produced the highest values. The average $k_{AASHTO(1993)}$ was about 2 to 4 times higher than the design *k* value.

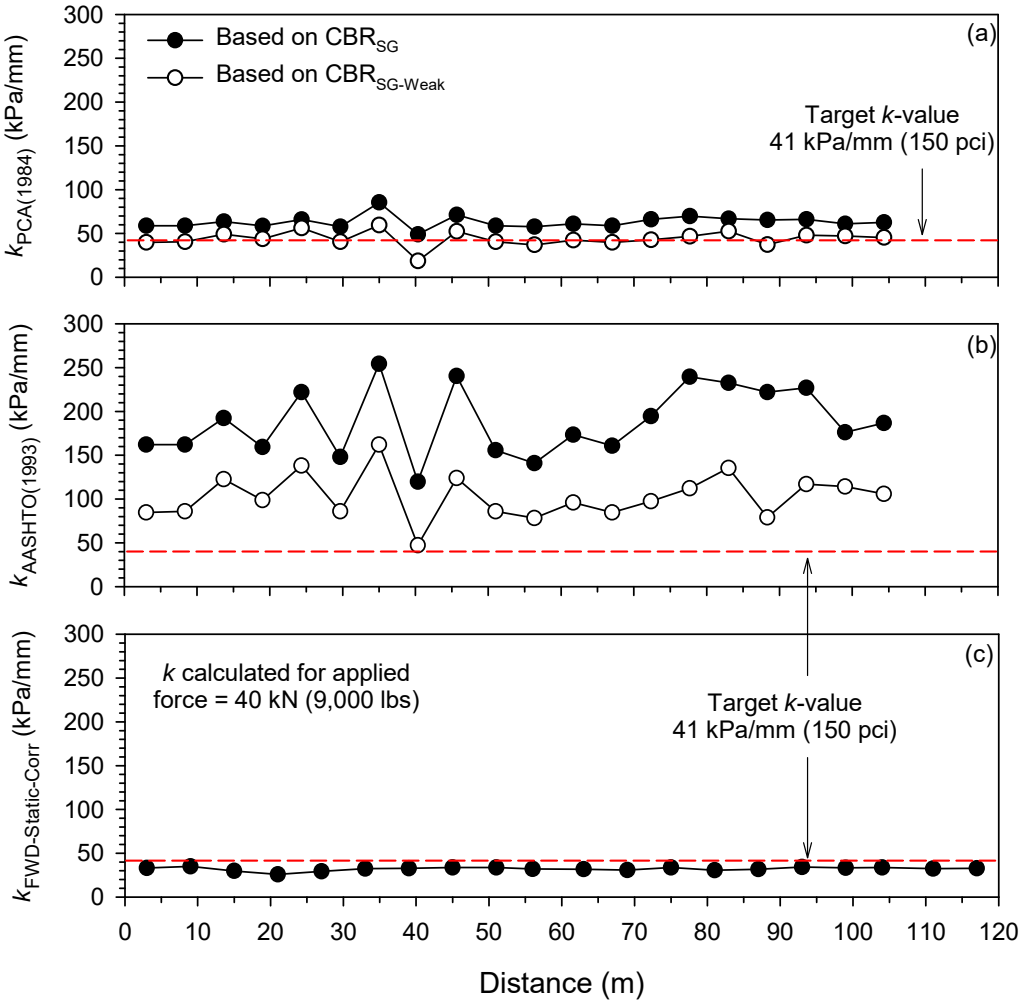

Figure 5.8. Estimated *k* values based on different methods.

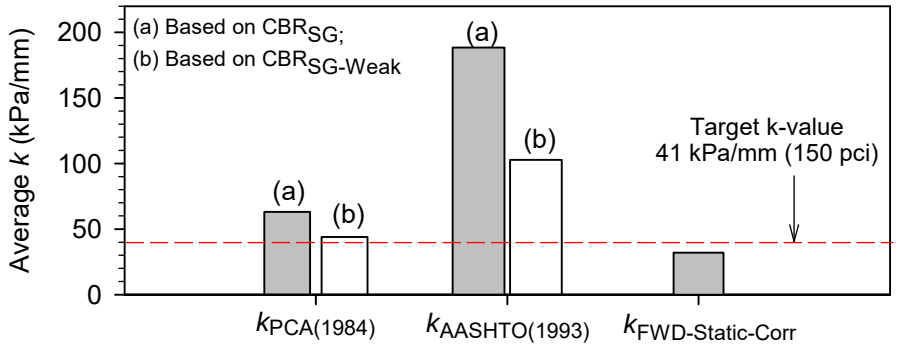

Figure 5.9. Bar chart comparing the design target *k* value with measured and estimated *k* values from field measurements.

Relationships and data published in the literature are compared with $k_{FWD\text{-}Static\text{-}Corr}$ and CBR_{SG} values in Figure 5.10a and with $CBR_{SG\text{-}Weak}$ values in Figure 5.10b. $CBR_{SG\text{-}Weak}$ values are in line with published relationships, but CBR_{SG} values are not. Nevertheless, CBR versus *k* relationships show significant scatter and present significant uncertainty in the predictions. The authors estimated the upper and lower bounds and mid-range based on the published relationships from 5 literatures or design manuals. Data published in the literature fell into the area below the mid-range except for several data points from Darter et al. (1995). Corresponding to CBR_{SG}, Data from White and Vennapusa (2014), White et al. (2016), and this project all fell significantly below the lower bound. The CBRSG-Weak data points primarily fell near the lower bound when CBR value is less than 20.

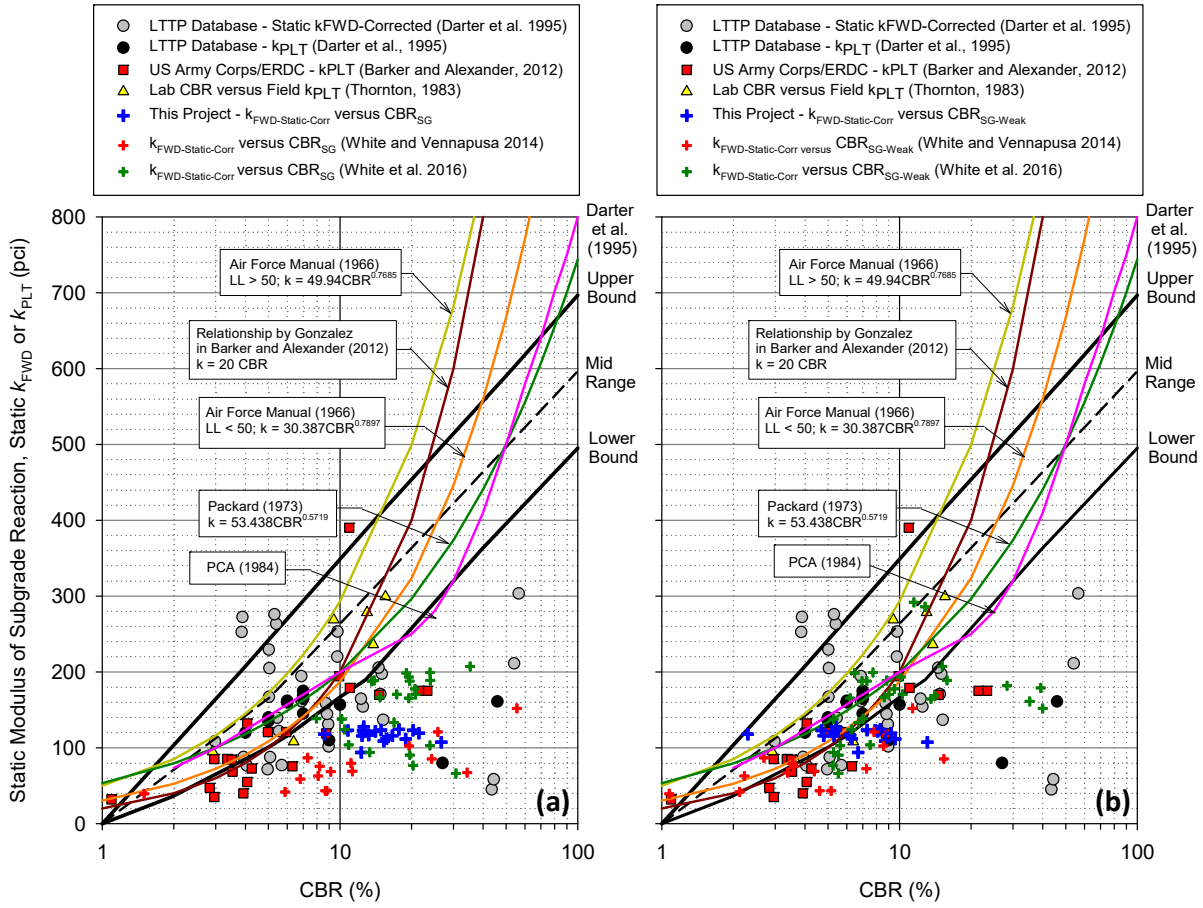

Figure 5.10. Average $k_{FWD\text{-}Static\text{-}Corr}$ versus (a) average CBR_{SG} and (b) average $CBR_{SG\text{-}Weak}$ compared with relationships published in the literature (1 pci = 0.27 kPa/mm).

5.6. Summary and Key Conclusions

This paper discusses the stiffness and support conditions of constructed pavement foundation layers. Results from this project were compared with the data reported in literatures and also the target design values. and The key findings in this pare are as follows:

- The laboratory CBR testing showed that materials with lower fines content provided lower bearing capacity. However, the CBR values may reduce to a similar level after experiencing freezing and thawing damage.
- Aggregate segregation showed significant influence on subbase layer elastic modulus. Higher moduli values were observed in areas with high fines content.

- The k values determined from the FWD deflection basin data showed the lowest values. The $k_{PCA(1984)}$ calculated based on $CBR_{SG\text{-}Weak}$ and the $k_{FWD\text{-}Static\text{-}Corr}$ were relatively closer to the assumed design k value.
- The k values calculated using the empirical relationships between CBR and k from AASHTO (1993) produced the highest values. The average $k_{AASHTO(1993)}$ was about 2 to 4 times higher than the design k value with a wide variety.
- The $k_{FWD\text{-}Static\text{-}Corr}$ versus $CBR_{SG\text{-}Weak}$ results are in line with previously published relationships, but $k_{FWD\text{-}Static\text{-}Corr}$ versus CBR_{SG} results are not. Nevertheless, CBR versus k relationships show significant scatter and present significant uncertainty in the predictions.

5.7. Acknowledgements

This research was conducted under Federal Highway Administration (FHWA) DTFH61-06-H-00011 Work Plan 18 and the FHWA Pooled Fund Study TPF-5(183). The authors would like to express their gratitude to the National Concrete Pavement Technology (CP Tech) Center, the FHWA, the Iowa Department of Transportation (DOT), and the other pooled fund state partners for their financial support and technical assistance.

CHAPTER 6. COMPARISON OF PAVEMENT SLAB STABILIZATION USING CEMENTITIOUS GROUT AND INJECTED POLYURETHANE FOAM

A paper published on *ASCE Journal of Performance of Constructed Facilities*

Pavana K.R. Vennapusa, Yang Zhang, and David J. White

6.1. Abstract

This paper reviews the current status of slab stabilization specifications and describes in situ test results and statistical analysis comparing injected polyurethane foam and cementitious grout for a deteriorating jointed concrete pavement supported on open-graded aggregate subbase. The stabilization was performed to improve support conditions by filling voids, reducing deflections under loading, and improving load transfer efficiency (LTE) near joints and cracks. Falling weight deflectometer (FWD) tests and faulting measurements were obtained before and after stabilization. LTE measurements indicated statistically significant improvement near cracks and joints in both sections. Deflections under loading showed statistically significant improvements only near cracks (and not near joints) in the injected foam section and only near joints (and not near cracks) in the cementitious grout section. Faulting reduced by about 2 to 5 mm after injected foam stabilization and 0.5 mm to 2 mm after cementitious grout stabilization, while the maximum allowable slab movement during stabilization was 1.3 mm. Although improvements were evident in FWD measurements after both stabilization methods, faulting reductions indicate slab movements that are greater than allowed. This suggests a need for improved process control with vertical movement during the stabilization process, particularly with the injected foam stabilization method.

6.2. Introduction

Development of new technologies that rehabilitate in-service pavements suffering from premature distress is a challenge facing the transportation industry. Many highway agencies are now evaluating different rehabilitation techniques that can potentially provide cost-effective and rapid solutions. Slab stabilization, also referred to as undersealing, is a commonly used rehabilitation procedure for portland cement concrete (PCC) pavements that suffer from faulting and transverse cracking. The purpose of slab stabilization is to fill voids beneath the slab thus minimizing deflections under loading. By controlling deflection, deflection-related distresses are reduced (FHWA 2005). Cementitious grout is the most common material used for slab stabilization (ACPA 1994). The use of injected expanding polyurethane foam is increasingly being used as an alternative to grout, primarily because of the shortened construction time, reduced materials/equipment requirements, and less labor (Abu al-Eis and LaBarca 2007, Barron 2004, Chen et al. 2008, Gaspard and Zhang 2010, Priddy et al. 2010, Vennapusa and White 2014). Currently, a few state agencies (Missouri and New Jersey) have included high density polyurethane (HDP) foam technology as part of their standard specifications for slab stabilization (MoDOT 2009b; NJDOT 2007a). Concerns over the benefits to long-term pavement performance and ride quality, however (Chen et al. 2009, Gaspard and Zhang 2010, Vennapusa and White 2014), have slowed use of slab stabilization technologies. To the authors' knowledge, field performance comparisons between cementitious grout and injected foam stabilization methods have not been well documented.

This paper presents results of in situ test results and statistical analysis on jointed PCC pavement test sections where injected HDP foam and cementitious grout were used for slab stabilization to stop premature deterioration. The test sections are located on US Highway 422 in

Pennsylvania, where a 9.7 km four-lane divided highway was rehabilitated. The pavement showed premature distresses with mid-panel cracking and faulting which progressively increased due to lack of adequate support attributed to the underlying open-graded stone (OGS) subbase layer (Vennapusa and White 2014). The Pennsylvania Department of Transportation (Penn DOT) initiated a rehabilitation strategy that primarily involved injecting high density polyurethane (HDP) foam. A control section (160 m long) was stabilized using cementitious grout for performance comparison. The purpose of the stabilization was to: (1) stabilize the open-graded subbase layer, (2) reduce deflections under loading, and (3) improve load transfer efficiency (LTE) near joints and cracks. At selected locations, full-depth patching and dowel bar retrofitting was performed after the stabilization.

In situ testing was conducted before and after stabilization/dowel bar retrofitting using falling weight deflectometer (FWD) to measure deflections under loading, LTE, and deflection basin parameters. Faulting measurements were obtained before and after treatment to assess slab movements due to stabilization. Results presented in this paper provide new experimental evidence of the field performance with comparisons of HDP foam and cementitious grout.

6.3. Background

Voids beneath concrete pavement slabs cause loss of support and lead to distresses such as transverse cracking, faulting, and corner breaks. These distresses lead to poor ride quality. Slab stabilization involves injecting durable materials into the voids. The main purpose of slab stabilization process is to reduce deflections under loading and *not* to lift pavements (FHWA 2005). Slab jacking is another similar rehabilitation process used to vertically lift faulted slabs (Del Val 1981; Taha et al. 1994). Slab jacking is a common technique used to fill voids beneath faulted bridge approach pavement slabs (see White et al. 2007).

A summary of the current state highway agency specifications for slab stabilization and slab jacking using cementitious grout and HDP foam is provided in Table 6.1 and Table 6.2, respectively. Many agencies use cementitious grouts as they are readily available within reasonable distance for most projects (ACPA 1994). Out of the 7 state agency specifications reviewed, only 2 agencies currently allow HDP foam for slab stabilization, but all 7 allow HDP foam for slab jacking applications. The foam injection method has been gaining popularity for slab stabilization applications because of its advantages with faster setting times and strength gains compared to cementitious grouts (Abu al-Eis and LaBarca 2007; Barron 2004; Chen et al. 2008; Gaspard and Zhang 2010). When cementitious grouts are used, the traffic delay times typically vary from several hours to three days depending on how fast the grout achieves its strength (Table 6.1). The traffic delay time is typically < 1 hr when injected foam is used (Table 6.2).

In the following, material properties and mix design of cementitious grouts and HDP foam, the construction quality control and testing, and a review of previous studies documenting the field performance of the two materials are described.

Table 6.1. Summary of cementitious grout in state DOT specifications.

State	Reference	Application	Materials	Mix Design	Requirements	Slab Movement	Testing	Traffic Delay
AL	ALDOT (2012a)	Slab jacking	Type I or III PC, $CaCl_2$, FA, air entraining additives or chemical admixtures, LD, FS.	The following mix design proportions (by volume) are specified: 80% FA + 20% PC; 50% LD + 30% FA + 20% PC; 80% LD + 20% PC; 20% FS + 50% FA + 20% PC; 50% FS + 30% FA + 20% PC; 50% FS + 30% LD + 20% PC.	PP: ≤ 1.5 MPa ET: 18–25 s	± 6 mm of the final grade	4.5m long straight edge is used to verify that the final grade is within ± 6 mm.	Minimum of 3 hrs. For Type III cement, delay should be greater than the initial set time.
	ALDOT (2012b)	Slab stabilization			PP: ≤ 1.5 MPa ET: 14–22 s	≤ 1 mm	A rubber-tired 90 kN single axle load is used to check if slab movement under loading < 0.8 mm. Increase in IRI values after stabilization should be < 10 mm/km.	
CA	Caltrans (2010a)	Slab stabilization	PC, class C/F FA, chemical admixtures and $CaCl_2$ (optional).	2.4–2.7 parts FA to 1 part PC by weight.	7-day CS: ≥ 5.2 MPa ET: 10–16 s PP: ≤ 1.0 MPa	≤ 1.3 mm	Not specified	
	Caltrans (2010b)	Slab jacking			ET: 16–26 s PP: ≤ 1.4 MPa	± 3 mm of the final grade		
IA	Iowa DOT (2012)	Slab stabilization	Type I PC, class C FA.	1 part by volume of Type I PC and 3 parts by volume of class C FA.	ET: 10–16 s Initial PP: ≤ 0.15 MPa PP: ≤ 0.05 MPa	≤ 2.5 mm	Not specified	Delay time should be greater than the initial set time (6 hours at 4°C and 4 hours at 10°C).
KS	KDOT (2015)	Slab stabilization	Type I or II PC, FA, air entraining or chemical admixtures (optional).	≥ 25% by volume of PC and ≥ 50% by volume of FA.	ET: 9–15 s 7-day CS: ≥ 4.1 MPa PP: sustained 1.0 MPa	≤ 3.2 mm	FWD test is used to determine the effectiveness of the undersealing operation through voids under the slabs.	Not Specified
LA	Louisiana DOTD (2006)	Slab stabilization and slab jacking	Type I PC, FA, Powdered ammonium sulphonate.	1 part PC and 3 parts FA by volume and powdered ammonium lignin sulphonate at 0.5 to 1.5% by weight of PC.	ET: 12–18 s for undersealing and 15–26 s for slab jacking PP: ≤ 1.4 MPa.	± 3 mm of the final grade	Not specified	At least 1 hour after pumping operations.
MO	MHATC (1999)	Slab stabilization	Type I, II or III PC, FA.	≥ 1 part PC by volume to 3 parts FA.	7-day CS: ≥ 4.1 MPa ET: 10–16 s Initial PP: 1.380 MPa PP: ≤ 0.69 MPa (0.205 to 0.345 MPa)	≤ 3 mm	FWD test is used for void detection and undersealing verification. Requires $\Delta_L \leq 0.38$ mm or $(\Delta_A - \Delta_L) \leq 0.25$ mm.	Three hours after the end of pumping operations, and after all drill holes are plugged.

Table 6.1. Summary of cementitious grout in state DOT specifications (continued).

State	Reference	Application	Materials	Mix Design	Requirements	Slab Movement	Testing	Traffic Delay
NJ	NJDOT (2007a; 2007b)	Slab stabilization	Type I, II, III PC, FA chemical admixtures.	1 part PC to 3 parts FA. Use admixtures if needed.	7-day CS: ≥ 4.1 MPa ET: 9–16 s PP: ≤ 0.4 MPa	≤ 2.5 mm	Deflection test is needed to verify if the deflection value is less than 0.25 mm.	At least one hour after initial set.
OK	OKDOT (2009)	Slab stabilization	PC, FA, air/chemical/corrosion-inhibiting/latex emulsion admixtures.	A mix design showing the CS, ET, VC, and initial set time needs to be reviewed and approval by the Engineer.	7-day CS: ≥ 5.5 MPa ET: 10–16 s Pumping head: 1.54 m^3/hr	0.825 mm–0.925 mm	A standard Benkelman Beam is used to monitor excessive lifting of pavement or rising of the adjacent shoulders.	3 calendar days or directed by the Resident Engineer.
PA	Penn DOT (2011)	Slab stabilization	PC, pozzolan (class C/ F/FA, ground granulated blast furnace slag, silica fume)	1 part PC to 3 parts of pozzolan by volume and admixtures if required.	7-day CS: ≥ 4.8 MPa ET: 10–15 s PP: ≤ 1.4 MPa VC: -2.5–10% Initial set time: 1–6 hr	≤ 1.3 mm	A vehicle having a dual-tire single axle with an 80 kN single axle load is used to detect if slab corner deflection ≤ 0.5 mm and joint efficiency ≥ 65%.	At least 12 hours after completing grouting operations.
SD	SDDOT (2004a)	Slab stabilization	Type I or II PC, class C FA.	1 part PC to 3 parts FA.	7-day CS: ≥ 4.1 MPa ET: 9–15 s PP: ≤ 0.4 MPa	≤ 3 mm	FWD test or a single axle truck needs to be used to determine if the deflection is in excess of 0.25 mm.	Not specified
	SDDOT (2004b)	Slab jacking			7-day CS: ≥ 4.1 MPa Initial ET: 9–15 s ET: 16–36 s PP: ≤ 1.4 MPa	± 6 mm of the final grade	A laser leveling unit is used to ensure if the concrete is raised to an even plane and to the required elevation.	
UT	UDOT (2012)	Slab jacking	Hydraulic cement, fine aggregate, other ingredients.	Packaged dry, hydraulic-cement grout (non-shrink) by manufacturer.	7-day CS: ≥ 24 MPa 28-day CS: ≥ 34 MPa Early age VC: ≤ 4% Hardened VC: ≤ 0.3%	± 3.2 mm of the final grade	Not specified	

Note: PC–portland cement, FA–fly ash, LD– limestone dust, FS–fine sand, PP–pumping pressure, ET–efflux time, CS–compressive strength, Δ_L–the average of three normalized deflections on leave side, Δ_A–the average of three normalized deflections on approach side.

Table 6.2. Summary of HDP in state DOT specifications.

State	Reference	Application	Requirements	Slab Movement	Testing	Traffic Delay
MO	MoDOT (2009a)	Slab stabilization	Density: ≥ 64 ± 8 kg/m^3 CS: ≥ 0.55 MPa TS: ≥ 0.62 MPa VC: ≤ 5% CR: ≤ 15 min. for 90% CS	≤ 3 mm	FWD test is used for void detection and undersealing verification. $\Delta_L \leq 0.38$ mm or $(\Delta_A-\Delta_L) \leq 0.25$ mm.	At least 30 min after ceasing pumping operations.
	MoDOT (2009b)	Slab jacking		≤ 3 mm of the final grade		Three hours after the end of pumping operations, and after all drill holes are plugged.
NJ	NJDOT (2007a; 2007b)	Slab stabilization and slab jacking	Density: 90.5–94.5 kg/m^3 CS: 0.45- 0.66 MPa TS:0.48–0.69 MPa VC: 5% to 11% for humid 28-day, -0.1% to -0.9% for 5-day freezing SS: 0.28–0.59 MPa Close cell %: 85%–95% CR: ≤ 15 min. for 90% CS	≤ 2.5 mm for undersealing and ± 6.4 mm of the final grade for slab jacking	Deflection test is needed to verify if the deflection value is less than 0.25 mm.	At least one hour after initial set.
NC	NCDOT (2008)	Slab jacking	Density: 48–67.3 kg/m^3 CS: ≥ 0.28 MPa	± 6.4 mm of the final grade	A tight string line is used to monitor and verify elevations for slab lengths of 15.24 m or less.	Not specified
OH	Ohio DOT (2007)	Slab jacking	Density: ≥ 48 kg/m^3 TS: ≥ 0.28 MPa CS: ≥ 0.28 MPa VC: -0.6%–4% Water absorption: ≤ 2.0% volume	± 5 mm of the final grade.	Use a tight string or laser level to monitor and verify elevations.	Not specified
PA	Penn DOT (2010)	Slab jacking	Density: ≥ 64 kg/m^3 CS: ≥ 0.41 MPa TS: ≥ 0.48 MPa SS: ≥ 0.28 MPa Close cell content: ≥ 85%	± 1.3 mm of the final grade	Deflection test is performed to check if slab corner deflection ≤ 0.5 mm and joint efficiency ≥ 80% at least 24 hours after injection.	At least 30 min after injection.
SD	SDDOT (2004b)	Slab jacking	Free rise density: 48–51 kg/m^3 CS: ≥ 0.28 MPa CR: ≤ 15 min. for 90% CS	± 6 mm of the final grade	A laser leveling unit is used to ensure if the concrete is raised to an even plane and to the required elevation.	Not specified
UT	UTDOT (2012)	Slab jacking	Density: 60.9–68.9 kg/m^3 TS: ≥ 0.55 MPa Elongation: ≤ 5.1% CS: ≥ 0.41 MPa CR: ≤ 15 min. for 100% CS	± 3.2 mm of the final grade	Not specified	

Note: CS–compressive strength, TS–tensile strength, VC–volume change, SS–shear strength, CR–curing rate, Δ_L–the average of three normalized deflections on leave side, Δ_A–the average of three normalized deflections on approach side.

6.3.1. Material properties and mix design

The materials and mix designs used in cementitious grouts vary between agencies. Most commonly used materials in the mixture are portland cement (type I or II or III) and pozzalonic material such as fly ash (class C or F). Pozzalonic materials have spherical shape fine particles which enhances the flow properties of the mixture. Other materials also considered in the mix design for cementitious grouts are $CaCl_2$, lime dust, silica fume, ammonium sulphonate, and blast furnace slag. The maximum pumping pressure (PP), efflux time (ET) range, and minimum compressive strength required are typically included in the specifications, as summarized in Table 6.1.

The HDP foam used for pavement rehabilitation is a closed cell rigid hydrophobic foam with nominal densities ranging from about 56 to 240 kg/m^3 (Priddy et al. 2010; Priddy and Newman 2010; Yu et al. 2013). These types of foams are referred to as HDP foams, while low density polyurethane foams comprise of densities less than 56 kg/m^3 (Priddy and Newman 2010). The HDP foam is primarily made of two liquid chemicals: (a) a blend of polyol comprising polyether-polyol and catalysts, and (b) water and isocyanate desmador (Brewer et al. 1994). These chemicals combine under heat to form a strong lightweight foam-like substance. When the two chemicals are injected together under pressure, a rapid chemical reaction occurs and causes the polyurethane foam to rapidly expand. The various material properties that are included in the specifications for HDP foam are summarized in Table 6.2.

6.3.2. Construction and testing procedures

As part of testing prior to construction, FHWA (2005) recommends conducting field deflection testing using a FWD or a loaded truck or ground penetrating radar (GPR) scanning to detect areas of voids that need stabilization.

Once the stabilization areas are determined, the construction process involves drilling holes, injecting foam/grout, and conducting QC/QA testing to control slab movements. A pattern of one to three holes, that are placed close enough to achieve flow of grout from one hole to the other, is typically used (FHWA 2005). An optimum hole pattern can be determined based on field trials. The holes are drilled to the bottom of the concrete slab or to the bottom of the subbase layer if the subbase layer needs stabilization (FHWA 2005).

Monitoring pavement slab movement is a critical part of QC during the injection process. For slab stabilization applications, slab movement is restricted to a specified maximum value, which varies between DOT agencies from 1 to 3 mm (see Table 6.1 and Table 6.2). For slab jacking applications, slab movement is controlled by raising slabs to a uniform or original grade within a minimum specified tolerance, which varied between ±2.5 and ±6.4 mm. Verification of slab movement is accomplished using a string level or a laser level or a straight edge. Deflection testing after stabilization is specified by some agencies using FWD or Benkelman beam and a loaded truck to verify a reduction in pavement deflections, voids have been filled, and LTE across joints or stabilized cracks has been improved. International roughness index (IRI) testing is specified in ALDOT (2012a; 2012b) with a requirement of <10 mm/km after slab stabilization.

6.3.3. Previous performance monitoring studies

Although cementitious grouting has been widely used for pavement rehabilitation applications, to the authors' knowledge, very limited performance monitoring data has been reported in the literature.

Taha et al. (1994) reported performance results from two slab stabilization projects (to fill voids beneath slabs) using cementitious grout on undoweled jointed PCC pavements (originally constructed in 1971) in comparison with nearby unstabilized sections. The grout used was a

mixture one part cement to three parts fly ash by volume with a minimum 4.1 MPa (600 psi) 7-day compressive strength. On one project, slab stabilization was performed in 1987. A field survey conducted six years after stabilization indicated an average joint faulting of 2.5 mm in stabilized sections as compared to 4.8 mm average faulting unstabilized sections. FWD test results showed average corner deflections of 0.53 mm and LTE of 79% in stabilized sections, while average corner deflections were 0.64 mm and LTE was 45% in unstabilized sections. On the other project, stabilization was performed in 1989. No significant faulting was observed about five years after stabilization, but an average faulting of about 3.2 mm was observed in the unstabilized sections. FWD tests showed an average corner delfection of 0.69 mm and and LTE of 39% in stabilized sections and an average corner deflection of 1.07 mm and LTE of 23% in unstabilized sections. Taha et al. (1994) concluded that while cementitious grout for slab stabilization is an effective method for void filling beneath the slabs and short-term improvement in performance, it does not fully prevent future faulting or significantly improve long-term performance. They also indicated that injecting cementitious grout is effective if joint faulting is < 5.1 mm (0.2 in.).

Ni and Cheng (2011) reported FWD and GPR test results before and after stabilization using cementitious grout on an airport runway pavement consisting of jointed PCC pavement. The grout consisted of 7% portland cement by weight with 0.8 water-cement ratio. Their GPR results indicated that the number of voids and the area voids present reduced after grouting, although the voids were not completely filled. The calculated zero load deflections (deflection intercept) and peak deflections from FWD testing also reduced after stabilization.

Recent studies have reported field performance results on HDP foam stabilized concrete pavements with mixed conclusions in terms of the observed improvements (Chen and Scullion

2007; Chen et al. 2009; Chen et al. 2008; Crawley et al. 1996; Gaspard and Morvant 2004; Gaspard and Zhang 2010; Opland and Barnhart 1995; Vennapusa and White 2014).

Opland and Barnhart (1995) conducted IRI and FWD tests before and after slab stabilization using HDP foam on concrete pavements supported on open-graded drainage course layers. They found that ride quality, LTE at joints and cracks, and peak deflections under FWD loads were improved shortly after stabilization, particulary in sites with previous severe cracks. However, , they reported differential frost heave in sections reative to the adjacent lane that were not stabilized and attribted this to the lower thermal conductivity of the foam. They also reported that the performance of the test sections within the one-year trial period varied significantly and in some cases had returned to pre-stabilization conditions.

Crawley et al. (1996) reported field observations and test results from a jointed PCC slab stabilization project using HDP foam to repair faulted joints and transverse cracks. Their observations indicated that, after stabilization, the joint LTE increased and maximum deflections under loading decreased. They also found that the injection process produced new voids under the panels, but re-injection mitigated the problem.

Gaspart and Morvant (2004) and Gaspard and Zhang (2010) reported FWD and ride quality tests on continuously reinforced PCC and jointed PCC pavements, before and after injecting HDP foam for filling slab voids and leveling slabs. Their results indicated that foam injection successfully filled voids beneath the pavements, but did not improve ride quality. They also found that LTE at joints was not improved after stabilization.

Chen and Won (2008) and Chen et al. (2009) documented field observations from projects in Texas where PCC pavement faulting was repaired using HDP foam injection. They reported that the foam injection process raised panels and reduce faulting during stabilization, but did not

provide long-term improvement. Chen and Scullion (2007) conducted a GPR survey on a five year old HDP stabilized pavement section in Texas and found voids beneath the pavement that contributed to further cracks and faulting.

6.4. Project Overview, Rehabilitation Process, and Test Sections

6.4.1. Project overview

The test area is located on US Highway 422 in Indiana, Pennsylvania. The jointed PCC pavement was originally built in 1995 with a nominal 280 mm thick PCC over 100 mm thick OGS subbase layer consisting of crushed limestone, 100 mm thick well-graded subbase also consisting of crushed limestone, and variable subgrade consisting of residual clay, shale, and sandstone rock. Samples collected from multiple locations during the rehabilitation process indicated the classification of the subbase layer material varied from poorly-graded gravel to silty gravel to well-graded gravel according to the Unified Soil Classification System (USCS), with fines content (passing the #200 sieve) varying between 3 and 8 percent. The underlying well-graded subbase layer classified as silty gravel to poorly graded gravel according to the USCS, with fines content varying between 8 and 14 percent.

The PCC panels were approximately 3.7 m wide x 6.1 m long. The pavement started showing distresses in early 2000s with mid-panel cracking (Figure 6.1a) that progressively increased (Terry Kerr, personal communication, October 1, 2009). Penn DOT conducted IRI testing from 2005 to 2009, which indicated a progressively decreasing ride quality (Vennapusa and White 2014). Based on FWD testing at over 1500 test locations which included joints and cracks, 300 panels were selected for slab stabilization. The FWD testing procedure and the criteria for selecting panels for stabilization is explained in detail in Vennapusa and White (2014). In brief, tests were conducted by applying a 40 kN load and measuring deflections directly beneath the

plate (D_0) and on the unloaded panel (D_1) about 305 mm away from the center of the plate. LTE was calculated as the ratio of D_1 and D_0. Additional loads were applied varying from 40 to 71 kN to measure corresponding deflections and determine zero-load deflections (or intercept value; calculations are discussed later in the paper). Joints and cracks that do not meet the criteria of D_0 < 0.5 mm under a 40 kN applied load, joint LTE > 65%, and Intercept < 0.076 mm, were selected for stabilization.

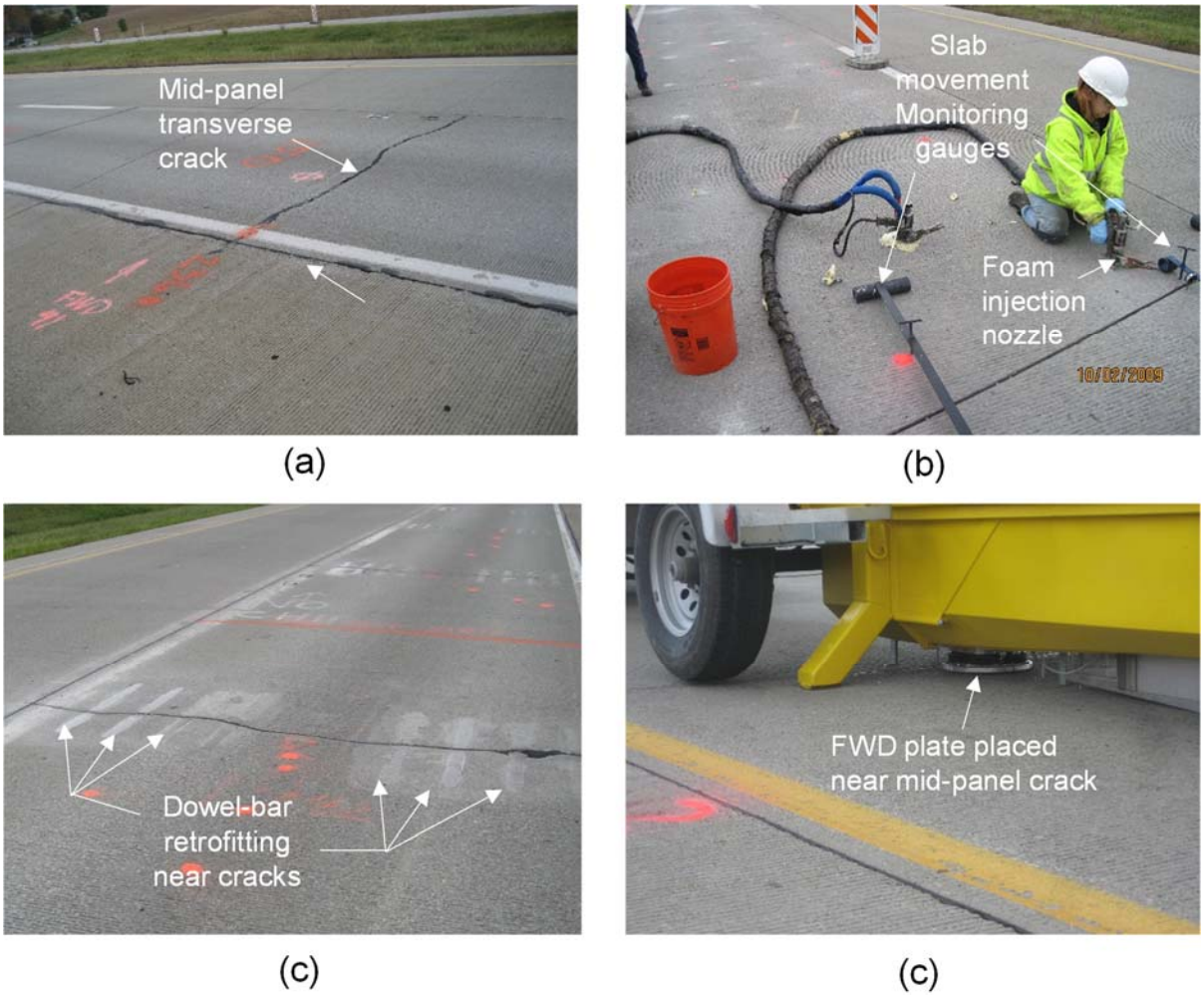

Figure 6.1. Field photos showing (a) mid panel cracks on the pavement; (b) HDP injection process; (c) crack location after stabilization and dowel bar retrofitting; and (d) FWD testing near cracks.

6.4.2. Rehabilitation process

Penn DOT designed the rehabilitation process to include injected HDP foam under the pavement surface and dowel bar retrofitting (Figure 6.1c) or patching at selected locations. A 160 m control section was selected for cementitious grout stabilization for comparison with the HDP method. The foam stabilization process was carried out between September 29 and November 10, 2009, and was followed by dowel bar retrofitting and concrete patching on selected panels between March 31 and July 20, 2010. Cementitious grout stabilization was carried out in May 2010 and was shortly followed by dowel bar retrofitting on all cracked panels.

The foam stabilization process involved four steps: (1) drilling a series of 9.5 mm diameter holes in the PCC layer extending at least 50 mm into the underlying base layer in a triangular spatial pattern on each panel (at 8 to 9 locations), (2) inserting a plastic sleeve in each hole to mate with the injection nozzle, and (3) injecting the HDP foam under pressure into the hole (Figure 6.1b). Mechanical deflection measurement gauges were used to monitor the panel lifting process by using the adjacent stabilized pavement panels or the shoulder as a reference. Based on the information provided by the manufacturer, the foam was injected at a maximum flow rate of about 272 kg/min and a maximum pressure of about 378 kPa. The density of the HDP ranged between 80 kg/m^3 and 128 kg/m^3, and the shear strength ranged between 682 and 876 kPa. The material had a reaction time of < 1 min and a curing time of < 15 min. Reaction time refers to the time to react and cause the material to expand, while curing time refers to the time for the foam to achieve its ultimate density and strength (Gaspard and Zhang, 2010).

Cementitious grout stabilization was performed in accordance with Pennsylvania standard specification for Slab Stabilization (Penn DOT 2011). Per specification, one part cement to two

parts fly ash pozzolon by volume was used in preparing the grout. Slab movement was monitored during the injection process by the contractor as part of their QC program.

6.4.3. Test sections

The HDP foam stabilized test section was about 220 m long with thirty five pavement panels. Nine panels were selected for testing, of which seven showed mid-panel cracks. After foam stabilization, two cracked panels were repaired with full-depth patching while the remaining five panels were repaired with dowel bar retrofitting. Full depth patching and dowel-bar retrofitting repair work was done in May 2010. In situ tests were conducted in October 2009 shortly before and after stabilization, in November 2009, and in July 2010.

The cementitious grout stabilized test section was about 150 m long with twenty three pavement panels. Ten panels were selected for testing, of which four showed mid-panel cracks. All cracked panels were repaired with dowel-bar retrofitting in May 2010. Tests were conducted in October 2009 before stabilization and in July 2010 after stabilization and dowel-bar retrofitting.

In situ testing included FWD testing (Figure 6.1d) and fault measurements at cracks and shoulders were obtained before and after stabilization. The test methods and data analysis are described in the following section of the paper. FWD tests were conducted at mid-panel, near crack, and near joint.

6.5. In Situ Testing and Data Analysis Methods

6.5.1. Falling weight deflectometer

FWD tests were conducted in accordance with ASTM D4694 (ASTM 2009) using a segmented 300 mm diameter loading plate by applying one seating drop and four loading drops. The applied loads varied from 22 to 75 kN. The deflection values at each test location were

normalized to 40 kN. FWD tests were conducted near mid-panel (i.e., between the two joints or between the joint and the crack on a panel), joints, and transverse cracks.

The FWD deflection basin data was analyzed to determine peak deflections under the loading plate (D_0), surface curvature index (SCI), base damage index (BDI), base curvature index (BCI), area factor (AF), load transfer efficiency (LTE) near joints and cracks, and zero-load intercept (I) values.

The SCI, BDI, BCI, and AF measurements are referred to as deflection basin parameters and are determined using the following equations:

$$\text{SCI (mm)} = D_0 - D_2 \tag{6.1}$$

$$\text{BDI (mm)} = D_2 - D_4 \tag{6.2}$$

$$\text{BCI (mm)} = D_4 - D_5 \tag{6.3}$$

$$\text{AF (mm)} = \frac{152.4 \times (D_0 + 2D_2 + 2D_4 + D_5)}{D_0} \tag{6.4}$$

where, D_0 = peak deflection measured directly beneath the plate, D_2 = peak deflection measured at 305 mm away from the plate center, D_4 = peak deflection measured at 510 mm away from the plate centre, and D_5 = peak deflection measured at 914 mm away from the plate centre.

According to Horak (1987), the SCI parameter provides a measure of the strength/ stiffness of the upper portion (base layers) of the pavement foundation layers (Horak 1987). Similarly, BDI represents layers between 300 mm and 600 mm depth (base and subbase layers) and BCI represents layers between 600 mm and 900 mm depth (subgrade layers) from the surface (Kilareski and Anani 1982). The AF is primarily the normalized (with D_0) area under the

deflection basin curve up to sensor D_5 (AASHTO 1993). The AF has been used to characterize variations in the foundation layer material properties by some researchers (e.g., Stubstad 2002). Comparatively, lower SCI or BDI or BCI or AF values indicate better support conditions (Horak 1987).

LTE values were determined by placing the FWD loading plate close to the joint/crack and positioning a deflection sensor on the unloaded panel about 305 mm away from the plate to measure D_1 and using Equation 6.5:

$$LTE(\%) = \frac{D_1}{D_0} \times 100 \tag{6.5}$$

I values are determined by plotting applied load measurements on the x-axis and corresponding deflection measurements on the y-axis, and plotting a best fit linear regression line. The intersection of this line on the y-axis referred to as the I-value. According to Penn DOT (2005), I > 0.076 mm indicates that there is a void underneath the pavement. Others have reported I = 0.05 mm (2 mil) as a critical value for void detection (McCracken 2008).

6.5.2. Field Survey

Faulting was observed near mid-panel cracks and near shoulder/panel interface (due to panel settlement). Faulting was measured using a ruler at 8 to 10 locations along the width of the panel and along the crack to determine average crack faulting (CF). Similarly, faulting was measured at the shoulder at 8 to 10 locations along the length of the panel to determine average shoulder faulting (SF).

6.5.3. Statistical Analysis

Student *t*-test analysis (Ott and Longnecker 2001) was conducted to assess differences between before and after stabilization and between the two stabilization methods, using the following equations:

$$t = \frac{\mu_0 - \mu_1}{s_p \sqrt{\frac{1}{n_0} + \frac{1}{n_1}}} \tag{6.6}$$

where,

$$S_p = \sqrt{\frac{(n_0 - 1) \times s_0^2 + (n_1 - 1) \times s_1^2}{n_0 + n_1 - 2}} \tag{6.7}$$

n_0 and n_1 = number of measurements obtained before and after stabilization, respectively; S_p = pooled standard deviation; and s_0 and s_1 = standard deviation of measurements obtained before and after stabilization or on cementitious grout and HDP foam stabilized sections, respectively.

The observed *t*-values were compared with the minimum t-value for a one-tailed test with degree of freedom (df) = $n_0 + n_1 - 2$, for 95% confidence level (i.e., $\alpha = 0.05$). When comparing measurements from before and after stabilization or from the two stabilization methods, if the *t*-values were greater than the minimum *t*-value, then it was concluded that there is sufficient evidence that the measurements were statistically different.

6.6. Performance Test Results and Discussion

The CF and SF results and FWD test results are presented as box plots in Figure 6.2 to Figure 6.6. The results are presented separately for measurements near cracks, joints, and mid-way

between joint and crack. The boundaries of the box plots indicate the 25th and 75th percentiles, and the error bars indicate the 10th and 90th percentiles. The solid thin line in the box indicates the median, and the solid thick line in the box indicates the mean. Data points (circles) outside the error bars are statistical outliers.

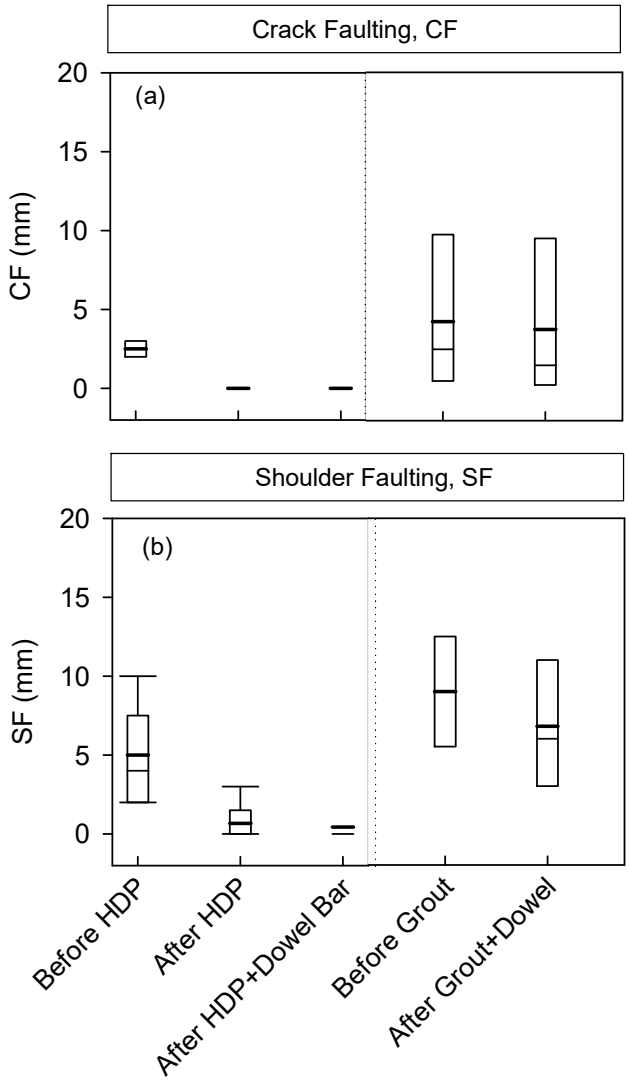

Figure 6.2. Box plots of (a) crack faulting and (b) shoulder faulting, before and after HDP/grout stabilization and dowel bar retrofitting at cracks.

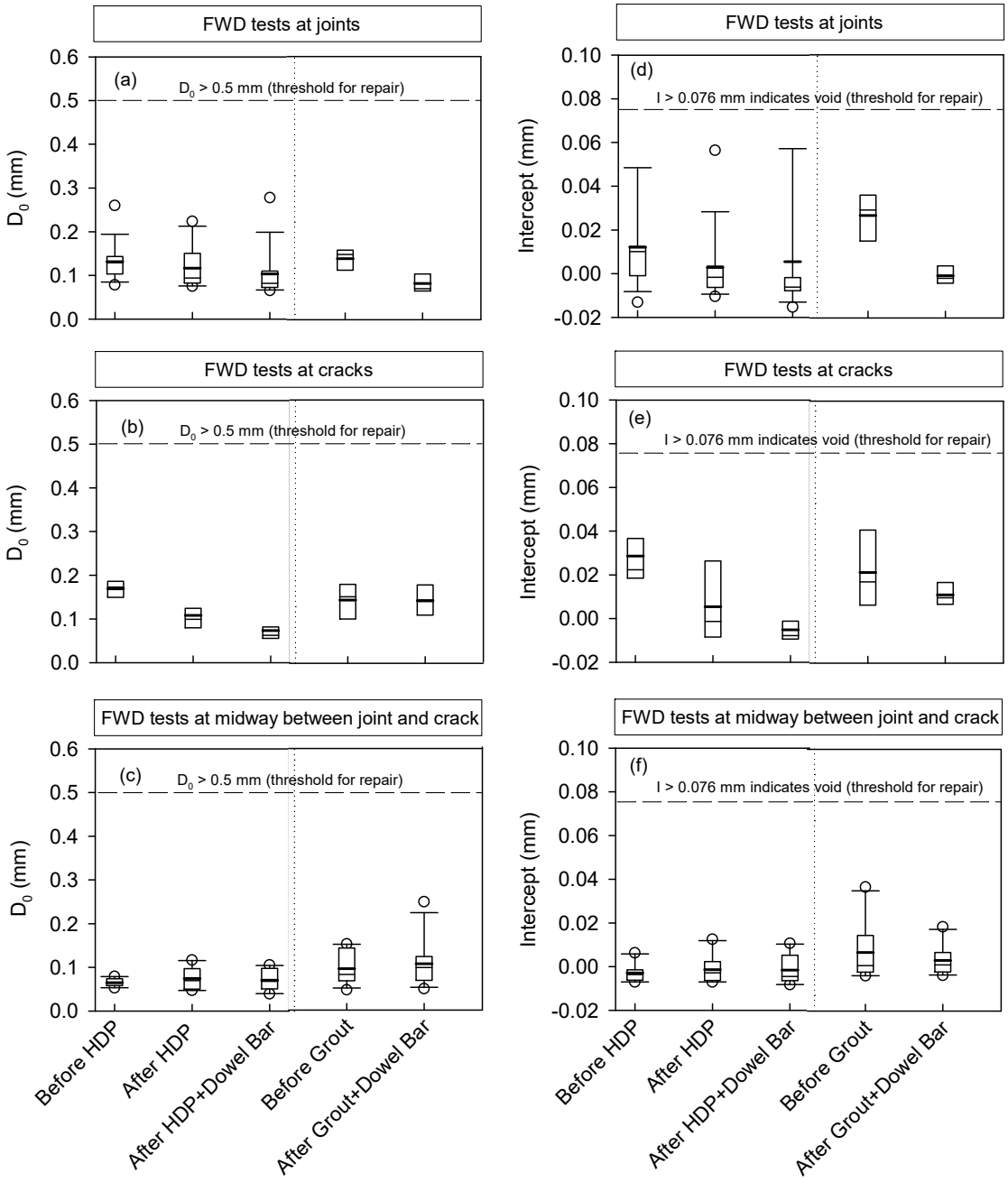

Figure 6.3. Box plots of (a) D_0 at joints; (b) D_0 at cracks; (c) D_0 at midway between joint and crack; (d) intercept at joints; (e) intercept at cracks; (f) intercept at midway of joint and crack, before and after HDP/grout stabilization and dowel bar retrofitting at cracks.

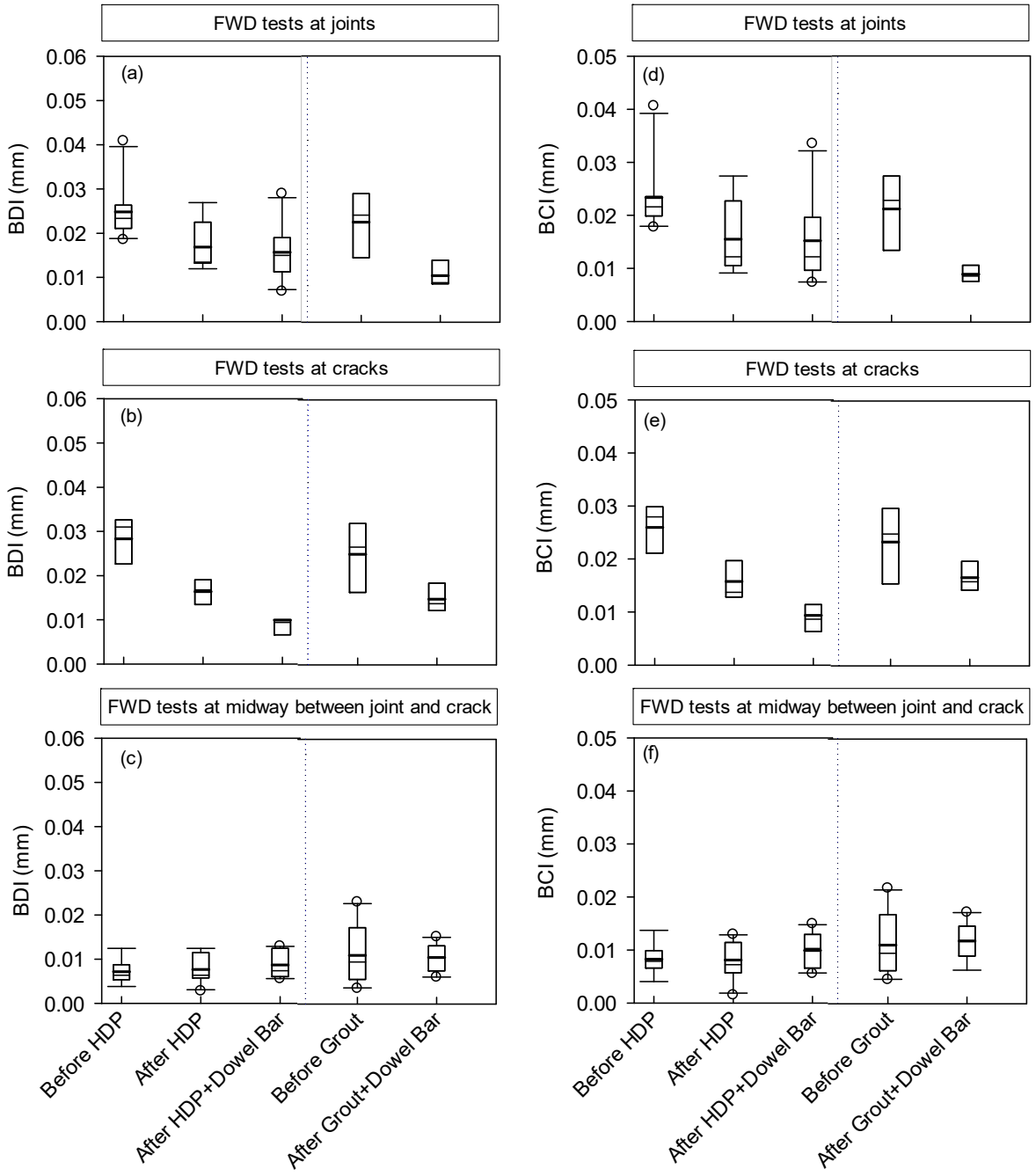

Figure 6.4. Box plots of (a) BDI at joints; (b) BDI at cracks; (c) BDI at midway between joint and crack; (d) BCI at joints; (e) BCI at cracks; (f) BCI at midway of joint and crack, before and after HDP/grout stabilization and dowel bar retrofitting at cracks.

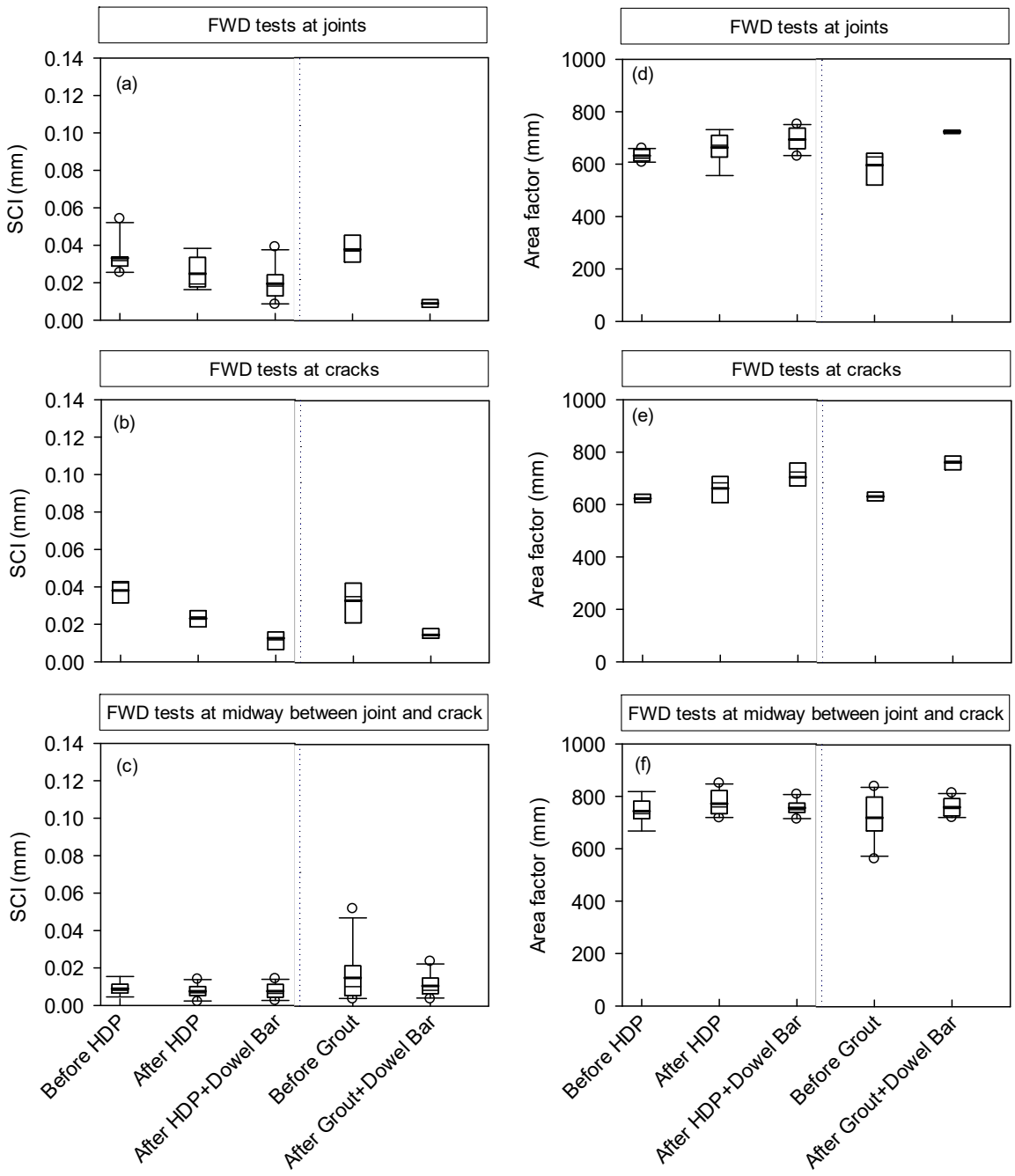

Figure 6.5. Box plots of (a) SCI at joints; (b) SCI at cracks; (c) SCI at midway between joint and crack; (d) area factor at joints; (e) area factor at cracks; (f) area factor at midway of joint and crack, before and after HDP/grout stabilization and dowel bar retrofitting at cracks.

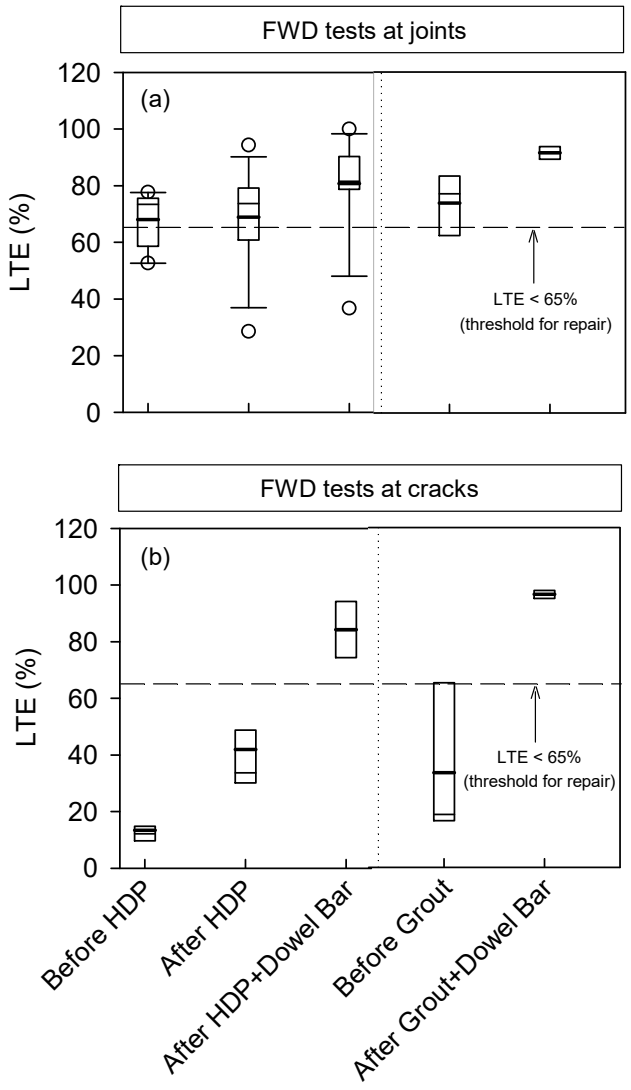

Figure 6.6. Box plots of (a) LTE at joints and (b) LTE at cracks, before and after HDP/grout stabilization and dowel bar retrofitting at cracks.

Statistical analysis results comparing before and after stabilization test results for the two methods are provided in Table 6.3, and comparing results between the grout and HDP test sections are provided in Table 6.4. The *t*-values that are greater than the minimum *t*-value are highlighted in the tables. The comparisons have been separated for measurements obtained near joints, cracks, and at mid-panel.

Table 6.3. Results of statistical analysis comparing before and after stabilization test results.

Parameter and Location		Before or after stabilization[1]	HDP				Cementitious Grout			
			Mean	COV (%)	*t*-value	P_r	Mean	COV (%)	*t*-value	P_r
D_0 (µm)	Joints	Before	132	31	1.64	0.111	139	17	5.02	<0.001
		After	104	56			82	25		
	Cracks	Before	169	18	5.97	<0.001	142	30	0.046	0.965
		After	73	39			140	26		
	Midway	Before	65	13	-0.72	0.483	89	38	-0.20	0.846
		After	71	34			91	29		
I (µm)	Joints	Before	12	213	0.56	0.580	27	47	5.86	<0.001
		After	6	709			-1	-516		
	Cracks	Before	27	66	4.50	<0.001	22	86	1.06	0.329
		After	-5	-125			11	48		
	Midway	Before	-3	-142	<0.01	0.997	7	189	0.803	0.433
		After	-3	-434			3	209		
SCI (µm)	Joints	Before	33	24	3.65	0.002	38	19	6.71	0.003
		After	19	46			9	22		
	Cracks	Before	38	17	6.70	<0.001	33	34	3.11	0.021
		After	13	53			15	23		
	Midway	Before	9	37	1.34	0.198	16	93	1.33	0.202
		After	7	50			10	45		
BDI (µm)	Joints	Before	25	25	3.30	0.004	23	33	2.62	0.059
		After	16	39			10	29		
	Cracks	Before	28	19	6.60	<0.001	25	33	2.27	0.064
		After	10	42			15	23		
	Midway	Before	7	36	-1.21	0.243	11	61	0.218	0.830
		After	9	34			11	30		
BCI (µm)	Joints	Before	23	28	2.52	0.021	21	34	2.92	0.043
		After	15	52			9	17		
	Cracks	Before	26	19	6.72	<0.001	23	33	1.65	0.151
		After	9	40			17	18		
	Midway	Before	8	33	-1.20	0.248	11	54	-0.35	0.727
		After	10	33			12	32		
AF (µm)	Joints	Before	632	4	-4.11	<0.001	596	11	-3.31	0.030
		After	694	6			724	1		
	Cracks	Before	623	2	-3.04	0.012	634	3	-7.86	<0.001
		After	704	8			765	4		
	Midway	Before	743	6	-0.68	0.503	722	11	-1.44	0.167
		After	755	4			762	4		
LTE (%)	Joints	Before	68	14	-2.39	0.026	74	18	-3.65	0.003
		After	81	19			92	3		
	Cracks	Before	13	41	-15.25	<0.001	33	94	-3.99	0.007
		After	84	13			97	2		

Notes: Highlighted cells indicate values that are statistically significant; number of tests on HDP stabilized sections: at joints = 16, at cracks = 7, at midway = 10; number of tests of cementitious grout stabilized sections: at joints = 8, at cracks = 4, at midway = 10. [1] *Before* indicates before construction and *after* indicates after dowel bar retrofitting.

Table 6.4. Results of statistical analysis comparing HDP and grout stabilization methods.

Parameter and Location		Stabilization method	Before stabilization				After stabilization			
			Mean	COV (%)	*t*-value	P_r	Mean	COV (%)	*t*-value	P_r
D_0 (µm)	Joints	HDP	132	31	-0.48	0.636	104	17	1.04	0.308
		Grout	139	56			82	25		
	Cracks	HDP	169	18	1.25	0.245	73	30	-3.41	0.008
		Grout	142	39			140	26		
	Midway	HDP	65	13	-2.18	0.043	71	38	-1.83	0.083
		Grout	87	34			91	29		
I (µm)	Joints	HDP	12	213	-1.51	0.145	6	47	0.45	0.659
		Grout	27	709			-1	-516		
	Cracks	HDP	27	66	0.60	0.561	-5	86	-4.23	0.002
		Grout	22	-125			11	48		
	Midway	HDP	-3	-142	-2.27	0.036	-2	189	-1.58	0.131
		Grout	7	-434			3	209		
SCI (µm)	Joints	HDP	33	24	-0.94	0.366	19	19	1.94	0.079
		Grout	38	46			9	22		
	Cracks	HDP	38	17	0.87	0.413	13	34	-0.60	0.563
		Grout	33	53			15	23		
	Midway	HDP	9	37	-1.40	0.181	8	93	-1.07	0.299
		Grout	16	50			10	45		
BDI (µm)	Joints	HDP	25	25	0.54	0.599	16	33	1.39	0.193
		Grout	23	39			10	29		
	Cracks	HDP	28	19	0.72	0.498	10	33	-1.99	0.078
		Grout	25	42			15	23		
	Midway	HDP	7	36	-1.63	0.122	9	61	-1.36	0.193
		Grout	11	34			11	30		
BCI (µm)	Joints	HDP	21	28	0.07	0.949	15	34	1.33	0.210
		Grout	21	52			9	17		
	Cracks	HDP	26	19	0.62	0.553	9	33	-3.34	0.009
		Grout	23	40			17	18		
	Midway	HDP	8	33	-1.29	0.213	10	54	-1.23	0.234
		Grout	11	33			12	32		
AF (µm)	Joints	HDP	632	4	1.58	0.142	694	11	-1.21	0.253
		Grout	596	6			724	1		
	Cracks	HDP	623	2	-1.01	0.345	704	3	-1.95	0.083
		Grout	634	8			765	4		
	Midway	HDP	743	6	0.69	0.500	755	11	-0.47	0.647
		Grout	722	4			762	4		
LTE (%)	Joints	HDP	68	14	-1.12	0.277	81	19	-1.91	0.073
		Grout	74	24			92	3		
	Cracks	HDP	13	41	-1.71	0.121	84	13	-2.27	0.058
		Grout	33	47			97	2		

Notes: Highlighted cells indicate values that are statistically significant; number of tests on HDP stabilized sections: at joints = 16, at cracks = 7, at midway = 10; number of tests of cementitious grout stabilized sections: at joints = 8, at cracks = 4, at midway = 10. [1] *Before* indicates before construction and *after* indicates after dowel bar retrofitting.

Faulting measurements (Figure 6.2) indicated that slabs were raised after HDP foam stabilization while less slab movement was measured after cementitious grout stabilization. On average, faulting reduced by about 2.5 mm near cracks and by about 4.6 mm near shoulder pavement, after HDP foam injection. Within the cementitious grout section, faulting was reduced on average by about 0.5 mm near cracks and by about 2.2 mm near the shoulder pavement. Per Penn DOT (2010), a maximum slab movement of 1.3 mm is allowed during slab stabilization (see Table 6.1).

Statistical *t*-test results on FWD measurements before stabilization indicated no statistically significant differences between the two test sections, with the exception of D_0 and I measurements at the mid-panel (Table 6.4). It is important to have the two sections with similar conditions so that the comparison after stabilization is not biased.

Analysis of FWD measurements revealed differences between the two stabilization methods (Figure 6.2 to Figure 6.6 and Table 6.3). In the HDP stabilized section, all FWD measurement parameters indicated statistically significant improvement near cracks. Near joints, SCI, BDI, BCI, AF, and LTE measurements showed improvement, but D_0 and I measurements did not. In the cementitious grout stabilized section, however, D_0 and I measurements did not show improvement near cracks but showed improvement near joints. All the remaining FWD measurement parameters showed improvement near joints and cracks (except BCI near cracks). No statistically significant improvement was determined in measurements obtained at the mid-panel, for both stabilization methods.

In both sections the BCI parameter showed improvement. As explained earlier, BCI represents strength/stiffness properties of the subgrade layer (at 600 mm to 900 mm depth below

surface), which was not expected here as stabilization occurred at the PCC and subbase layer interface and top portions of the subbase layer.

Analysis results presented in Table 6.4 indicate that statistically significant differences between the two stabilization methods were observed only near cracks in terms of D_0, I, and BCI. This means that FWD measurements in the HDP foam stabilized section showed better improvement at cracks compared to the cementitious grout section.

LTE was a critical parameter in selecting locations for treatment. Results indicated that LTE improved near cracks and joints in both cementitious grout and HDP foam stabilized sections. LTE measurements at cracks, although improved after HDP stabilization, did not increase to > 65% until after dowel bar retrofitting. Other critical parameters in selecting locations for treatment were D_0 and I. These values showed improvement only near cracks in the HDP foam section and only near joints in the cementitious grout section.

Although FWD measurements indicated improvements with deflections under loading and LTE, faulting measurements indicated that slabs were lifted greater than the allowed 1.3 mm during HDP stabilization. This suggests a need for better process control in vertical movement control during stabilization, particularly with the HDP stabilization method.

6.7. Summary of Key Findings

The in situ rehabilitation of pavements makes slab stabilization technology an attractive alternative to complete replacement. Yet, very little performance monitoring data are available in the literature. In this paper, a review of current slab stabilization specifications, and results of a field study comparing the performance of concrete pavement slabs stabilized with cementitious grout and injected polyurethane foam are presented. In situ testing was performed using FWD to evaluate deflections under dynamic loading, LTE near joints and cracks, and deflection basin

parameters that provide a measure of foundation layer stiffness and support conditions. Faulting near joints and cracks were monitored to assess slab movements during stabilization.

LTE, D_0, and I were critical parameters in selecting locations for treatment. LTE showed statistically significant improvement near cracks and joints in both cementitious grout and HDP foam stabilized sections. LTE measurements at cracks, although improved after HDP stabilization, did not meet the targeted criteria (> 65%) until after dowel bar retrofitting. D_0 and I values showed statistically significant improvement only near cracks (and not near joints) in the HDP foam section and only near joints (and not near cracks) in the cementitious grout section. No statistically significant improvement was determined in any of the FWD measurements obtained at the mid-panel, for both stabilization methods.

Faulting reduced by about 2.5 mm near cracks and by about 4.6 mm near shoulder after HDP foam injection. On cementitious grout section, faulting was reduced on average by about 0.5 mm near cracks and by about 2.2 mm near shoulder. These measurements indicate that slab movements were sometimes greater than the allowable 1.3 mm (per project specifications) and better process control measures are needed to control vertical movements, particularly with the HDP stabilization method.

6.8. Acknowledgements

This study was sponsored by the Federal Highway Administration under agreement No. DTFH61-06-H-00011 and Pennsylvania DOT under Transportation Pooled Fund Program TPF-5(183). Terry Kerr, Marc Gardner, Paul Majoris, Joshua Freeman, Lydia Peddicord, and several others from Pennsylvania DOT provided assistance in identifying the project, providing access to the project site, and traffic control during testing. We greatly appreciate their help.

CHAPTER 7. CONCLUSIONS AND RECOMMENDATIONS

This chapter presents an overview of the technical merit and scientific value gained from the study and an overview of the lessons learned. The conclusions are presented in five sections, which are related to the topics of this study. Recommendations for future research and practice are provided along with the conclusions.

The objectives of the study were to investigate the frost penetrations in pavement foundations using different methods and evaluate the estimates compared to the actual measurements; to assess the seasonal variations in pavement foundation mechanistic properties and compare these parameter values to the design values; to investigate the joint frost heave on deteriorated concrete pavements and determine the frost susceptibility of reconstructed foundation materials; to evaluate the stiffness and support conditions of reconstructed pavement foundation layers and evaluate to the empirical correlations in pavement design guides; and to statistically compare the pavement slab stabilizations between using cementitious grout and high density polyurethane foam based on measuring foundation properties.

Specific conclusions in terms of each objective are discussed in the previous chapters. General conclusions from this study are presented as below.

7.1. Frost Penetration Investigation

- From field measurements, the maximum frost penetration at central Iowa reached 145 cm. However, during the same winter, locations showed differences between maximum frost penetrations despite the close distance between tested sites. Different pavement types and foundation conditions influenced the measured frost penetration depths.
- Frost penetration depth estimates with the three simplified empirical equations did not match well the measured frost penetration depths.

- The modified Berggren equation used in PCASE was able to predict frost penetration in multi-layer pavements based on freezing index and soil properties. Using default values for soil properties in PCASE resulted in about 20% underestimation of the frost penetration depths.
- When using tested values for moisture contents and dry unit weights, calculations with the modified Berggren equation in PCASE provided more accurate results of predicted frost penetrations than using default soil properties values. However, the n-factor was found to have a significant influence on the accuracy of estimations, although it is difficult to determine the precise value of n at every specific location. Empirical values of n-factor may not be broadly applicable to each particular site.
- Stabilization and drainage systems utilized in foundation layers may have affected the frost penetration estimations. The possible causes may be that stabilization and drainages lead to changes in soil densities, pore conditions, and water contents.

7.2.Seasonal Variations in Foundation Properties

- On average, there was no significant difference in $k_{\text{FWD-Static-Corr}}$ values obtained in thawed condition and summer at any of the sites. The CBR values also did not show significant differences between thawed condition and summer at most of the sites, except at the Plainfield site where $\text{CBR}_{\text{SG-Weak}}$ increased from about 10 in thawed state to about 40 in summer. The $k_{\text{FWD-Static-Corr}}$ values in frozen condition was about 10% to 56% higher than in summer at four of the five sites. At one test site, the values were about the same at all testing times.
- At two of the five sites, the $k_{\text{FWD-Static-Corr}}$ values were about 1.5 to 2 times lower than the design assumed k value (41 kPa/mm) in thawed condition and in summer.

- Results indicated that the $M_{r\text{-}SG}$ values were unrealistically high when compared with the $k_{FWD\text{-}Static\text{-}Corr}$. $M_{r\text{-}SG\text{-}Weak}$ were much lower than the $M_{r\text{-}SG}$ values. A simple linear regression fit was applied to $M_{r\text{-}SG\text{-}Weak}$ versus $k_{FWD\text{-}Static\text{-}Corr}$ results, which yielded a R^2 of 0.45 with RMSE of 11.2 kPa/mm for *k* values. Compared to the linear regression fit in the data, use of the AASHTO model significantly over estimates the *k* values.
- It is important for designers and practitioners to recognize this uncertainty in the estimated values when using empirical relationships, and also the differences that exist between the values calculated from the different test methods. Also, it must be noted that *k* and M_r are stress-dependent parameters and most of the empirical relationships between CBR vs. M_r and M_r vs. *k* do not properly address this issue.
- Relationship between pavement age and PCI showed a strong linear trend with $R^2 > 0.93$. Similar linear regression relationship was documented by White and Vennapusa (2014) based on testing on low volume jointed PCC pavement test sites.
- The relationship between $k_{FWD\text{-}Static\text{-}Corr}$ and PCI also yielded a strong linear regression relationship with $R^2 > 0.95$, while the relationship between $CBR_{SG\text{-}Weak}$ and PCI yielded a strong non-linear exponential trend with PCI with $R^2 > 0.95$. These trends suggest that higher foundation layer stiffness or strength, provides a better ride quality and that ride quality is also influenced by the pavement age. Additional testing is warranted to further explore these relationships so that designers can have an empirical model that can be used to control the ride quality for a target design age, by controlling the foundation layer stiffness.

7.3. Joint Frost Heave Deterioration

- Ice lenses were found at layer interfaces of ACC, PCC, and ATB. ACC overlay and PCC showed weak structures during freezing, and stiff frozen ATB specimens showed low permeability.
- PCC specimens presented significantly higher moisture contents than other layers. This finding indicated that water was trapped at the deteriorated joint spaces at PCC layer. Microcracking on concrete under joints may contribute to water infiltration to lower base and subgrade, which may play the role of supplying water to lower layers for frost heaving.
- Vertical heaves at deteriorated joint locations reached up to 38 mm but showed non-uniformity in the transverse direction. The longitudinal width of the heaved bulge reached up to 760 mm near the shoulder.
- The greatest frost penetration in four monitored years was 1.0 to 1.1 m. A total of 59 to 94 freeze-thaw cycles were counted at the pavement surface, and no freeze-thaw cycle was found for three winters at depths over 0.7 m.
- Local freezing and thawing periods had various lengths. Freezing periods lasted two to three months, and full thawing occurred within 25 days.
- Laboratory freeze-thaw test results indicated that frost-heave and thaw-weakening might be influenced by grain size distribution. All three geomaterials from the reconstructed foundations were medium frost-heave susceptible, and the soft clayey subgrade showed high thaw-weakening susceptibility.

- Water movement after freeze-thaw cycles differed between types of geomaterials, even though the soil classifications were similar. Pore conditions may have critical influences on the amount and direction of water moving during freezing.

7.4. Stiffness and Support Conditions of Pavement Foundations

- The laboratory CBR testing showed that materials with lower fines content provided lower bearing capacity. However, the CBR values may reduce to a similar level after experiencing freezing and thawing damage.
- Aggregate segregation showed significant influence on subbase layer elastic modulus. Higher moduli values were observed in areas with high fines content.
- The k values determined from the FWD deflection basin data showed the lowest values. The $k_{PCA(1984)}$ calculated based on $CBR_{SG\text{-}Weak}$ and the $k_{FWD\text{-}Static\text{-}Corr}$ were relatively closer to the assumed design k value.
- The k values calculated using the empirical relationships between CBR and k from AASHTO (1993) produced the highest values. The average $k_{AASHTO(1993)}$ was about 2 to 4 times higher than the design k value with a wide variety.
- The $k_{FWD\text{-}Static\text{-}Corr}$ versus $CBR_{SG\text{-}Weak}$ results are in line with previously published relationships, but $k_{FWD\text{-}Static\text{-}Corr}$ versus CBR_{SG} results are not. Nevertheless, CBR versus k relationships show significant scatter and present significant uncertainty in the predictions.

7.5. Comparing Cementitious Grout and HDP Foam

- A review of current slab stabilization specifications, and results of a field study comparing the performance of concrete pavement slabs stabilized with cementitious grout and injected polyurethane foam are presented.

- LTE, D_0, and I were critical parameters in selecting locations for treatment. LTE showed statistically significant improvement near cracks and joints in both cementitious grout and HDP foam stabilized sections. LTE measurements at cracks, although improved after HDP stabilization, did not meet the targeted criteria (> 65%) until after dowel bar retrofitting.
- D_0 and I values showed statistically significant improvement only near cracks (and not near joints) in the HDP foam section and only near joints (and not near cracks) in the cementitious grout section.
- No statistically significant improvement was determined in any of the FWD measurements obtained at the mid-panel, for both stabilization methods.
- Faulting reduced by about 2.5 mm near cracks and by about 4.6 mm near shoulder after HDP foam injection.
- On cementitious grout section, faulting was reduced on average by about 0.5 mm near cracks and by about 2.2 mm near shoulder. These measurements indicate that slab movements were sometimes greater than the allowable 1.3 mm (per project specifications) and better process control measures are needed to control vertical movements, particularly with the HDP stabilization method.

BIBLIOGRAPHY

AASHTO, 1993. Guide for Design of Pavement Structures. American Association of State Highway and Transportation Officials, Washington, D.C.

AASHTO, 2008. Mechanistic-Empirical Pavement Design Guide: A Manual of Practice. 2nd Edition. American Association of State Highway and Transportation Officials, Washington, D.C.

Abu al-Eis, K., and LaBarca, I., 2007. Evaluation of the URETEK Method of Pavement Lifting. Wisconsin Department of Transportation. Madison, Wisconsin.

ACPA, 1994. Slab Stabilization Guidelines for Concrete Pavements. Technical Bulletin TB018P. American Concrete Pavement Association, Skokie, IL.

ACPA, 2012. k-value Calculator, American Concrete Paving Association (ACPA), <http://apps.acpa.org/apps/kValue.aspx> Date Accessed December 18, 2012.

Aitken, G.W., and Berg, R.L., 1968. Digital Solution of Modified Berggren Equation to Calculate Depths of Freeze or Thaw in Multilayered Systems. Special Report, SR 122. CRREL. U.S. Army.

ALDOT, 2012a. Section 452–Slabjacking of Portland Cement Concrete Pavement. Standard Specifications for Highway Construction. Alabama Department of Transportation, Montgomery, AL.

ALDOT, 2012b. Section 453–Pressure Grouting and Repair of Portland Cement Concrete Pavement. Standard Specifications for Highway Construction. Alabama Department of Transportation, Montgomery, AL.

Aldrich, H., and Paynter, H., 1953. Analytical Studies of Freezing and Thawing of Soils. Technical Report No. 42. U.S. Army Corps of Engineers.

Andersland, O. B., and Ladanyi, B., 2004. Frozen Ground Engineering. The American Society for Civil Engineers.

ASTM, 2003. Standard Test Method for Use of the Dynamic Cone Penetrometer in Shallow Pavement Applications. D-6951, ASTM International, West Conshohocken, PA.

ASTM, 2009. Standard Test Method for Deflections with a Falling-Weight-Type Impulse Load Device. D-4694, ASTM International, West Conshohocken, PA.

ASTM, 2007. Standard test method for CBR (California Bearing Ratio) of laboratory compacted soil, D-1883. Annual Book of ASTM Standard.

ASTM, 2013. Standard test methods for frost heave and thaw weakening susceptibility of soils, D-5918. Annual Book of ASTM Standard.

Baladi, G., and Rajaei, P., 2015. Predictive Modeling of Freezing and Thawing of Frost-Susceptible Soils. Final Report, RC-1619. Michigan Department of Transportation.

Baladi, G., Dawson, T., and Sessions, C., 2009. Pavement Subgrade MR Design Values for Michigan's Seasonal Changes. Final Report, RC-1531. Michigan Department of Transportation.

Barbenberg, E. J., and Petros, K. A., 1991. Evaluation of Concrete Pavements Using NDT Results, Illinois Highway Research Project IHR-512, University of Illinois and Illinois Department of Transportation, Report No. UILU-ENG-91-2006, IL.

Barker, W. R., and Alexander, D. R., 2012. Determining the effective modulus of subgrade reaction for design of rigid airfield pavements having base layers. Final Report, ERDC/GSL TR-12-20. US Army Corps of Engineers, Engineer Research and Development Center, Geotechnical and Structures Laboratory.

Barron, B., 2004. 50-50 Change: Kansas DOT Decides to go with Polyurethane to Correct 50 miles of Highway 50. Roads and Bridges. Vol.42. pp. 24-26.

Becker, P. J., White, D. J., Vennapusa, P. K. R., and Dunn, M. J., 2014. Freeze-Thaw Performance Assessment of Stabilized Pavement Foundations. Transportation Research Board, 93rd Annual Meeting, January 12–16, 2014, Washington, D.C.

Bianchini, A., and Gonzalez, C., 2012. Pavement-Transportation Computer Assisted Structural Engineering (PCASE) Implementation of the Modified Berggren (ModBerg) Equation for Computing the Frost Penetration Depth within Pavement Structures. TR-12-15. Geotechnical and Structural Laboratory. U.S. Army Corps of Engineers.

Braley, W., and Connor, B., 1989. Berg2 Micro-computer Estimation of Freeze and Thaw Depths and Thaw Consolidation. Alaska Department of Transportation and Public Facilities, Fairbanks, Alaska.

Brandl, H., 2008). Freezing-thawing behavior of soils and unbound road layers. Slovak Journal of Civil Engineering, 2008/3: 4-12.

Brewer, W. B., Hayes, C. J., and Sawyer, S., 1994. Ureteck Construction Report. OK 94(03). Oklahoma Department of Transportation.

Brown, R.J.E., 1963. Relation between mean annual air and ground temperatures in the permafrost region of Canada. Proceedings: Permafrost International Conference. November, 1963. Ottawa, Canada.

Caltrans, 2010a. Section 41-2–Pavement Subsealing. Standard Specifications. California Department of Transportation, Sacramento, CA.

Caltrans, 2010b. Section 41-3–Pavement Jacking. Standard Specifications. California Department of Transportation, Sacramento, CA.

Caltrans, 2015. Common Distresses on Rigid Pavements. Maintenance Technical Advisory Guide (MTAG), California Department of Transportation.

Cassagrande, A., Taber, S., and Watkins, W., 1931. Discussion of Frost Heaving. Highway Research Board, 165-177.

Chamberlain, E. J., 1987. A freeze-thaw test to determine the frost-susceptibility of soils. CRREL Special Report 87-1.

Chamberlain, E.J., 1986. Evaluation of Selected Frost-Susceptibility Test Methods. U.S. Army Cold Regions Research and Engineering Laboratory. CRREL Report 86-14.

Chen, D. H., and Scullion, T., 2007. Using Nondestructive Testing Technologies to Assist in Selecting the Optimal Pavement Rehabilitation Strategy. Journal of Testing and Evaluation, 35(2), 211-219. 10.1520/JTE100136.

Chen, D. H., Won, M., 2008. Field Performance Monitoring of Repair Treatments on Joint Concrete Pavements. Journal of Testing and Evaluation, 36(2), 119-127. 10.1520/JTE101362.

Chen, D. H., Won, M., and Hong, F., 2009. Investigation of Settlement of a Jointed Concrete Pavement. Journal of Performance of Constructed Facilities, 23(6), 440-446. 10.1061/(ASCE)CF.1943-5509.0000050.

Chen, D.H., Lin, D.F., Liau, P.H., and Bilyeu, J., 2005. A correlation between dynamic cone penetrometer values and pavement layer moduli. Geotechnical Testing Journal, 28 (1), 42–49.

Chen, D.H., Wang, J. N. and Bilyeu, J., 2001. Application of the DCP in Evaluation of Base and Subgrade Layers. Transportation Research Record: Journal of the Transportation Research Board. 2001, No. 1764, pp. 1–10.

Chen, X., and Wang, Y., 1988. Frost heave prediction for clayey soils. Cold Reg. Sci. Technol. 15(1988), 233-238.

Chisholm, R. A., and Phang, W. A., 1983. Measurement and prediction of frost penetration in highway. Journal of Transportation Research Board, No 918, Transportation Research Board of the National Academies, Washington D.C., 1983, pp. 1-10.

Cho, Y., Liu, C., Dossey, T., and McCullough, B. F., 1998. Asphalt Overlay Design Methods for Rigid Pavements Considering Rutting, Reflection Cracking, and Fatigue Cracking. The University of Texas at Austin, Austin, TX.

Crawley, A. B., Albritton, G. E., and Gatlin, G. R., 1996. Evaluation of the Uretek Method for Pavement Undersealing and Faulting Correction - Interim Report. FHWA/MS-DOT-RD-96-113. Mississippi Department of Transportation, Jackson, MS.

Crovetti, J. A., 1994. Evaluation of jointed concrete pavement systems incorporating open-graded bases. Ph.D. Dissertation, University of Illinois at Urbana-Champaign, IL.

Dai S, Skok, G, Westover, T., Labuz, J., and Lukanen, E., 2008. Pavement Rehabilitation Selection. Final Report, MN/RC 2008-06. Minnesota Department of Transportation.

Darter, M. I., Hall, K. T., and Kuo, C-M., 1995. Support under Portland Cement Concrete Pavements, NCHRP Report 372. Transportation Research Board, Washington, D.C.

Deblois, K., Bilodeau, J., and Dore, G., 2010. Use of falling weight deflectometer time history data for the analysis of seasonal variation in pavement response. Can. J. Civ. Eng. 37: 1224–1231 (2010). DOI: 10.1139/L10-069

DeGaetano, A.T., Cameron, M.D., and Wilks, D.S., 2001. Physical simulation of maximum seasonal soil freezing depth in the united states using routine weather observations. J. Appl. Meteor., 40:546-555.

Del Val, J., 1981. Pressure Grouting of Concrete Pavements. Transportation Research Record: Journal of the Transportation Research Board, 800, 38-40.

ERES Consultants Inc., 1982. Techniques for Pavement Rehabilitation: A Training Course. U.S. Department of Transportation, FHWA, Washington, D.C.

Farnam, Y., Bentz, D., Sakulich, A., Flynn, D., and Weiss, J., 2014. Measuring freeze and thaw damage in mortars containing deicing salt using a low-temperature longitudinal guarded comparative calorimeter and acoustic emission. Advances in Civil Engineering Materials, 3(1).

FHWA, 2005. Concrete Pavement Rehabilitation and Preservation Treatments. Tech Brief. Federal Highway Administration, Washington, D.C.

Flerchinger, G.N., Kustas W.P., and Weltz, M.A., 1998. Simulating Surface Energy Fluxes and Radiometric Surface Temperatures for Two Arid Vegetation Communities using the SHAW Model. J. Appl. Meteor., 37(5):449-460.

Freitag, D.R., and McFadden, T., 1997. Introduction to Cold Regions Engineering. The American Society for Civil Engineers.

Gaspard, K., and Morvant, M., 2004. Assessment of the Uretek Process on Continuously Reinforced Concrete Pavement, Jointed Concrete Pavement, and Bridge Approach Slabs. 03-2TA. Louisiana Department of Transportation and Development, Louisiana Transportation Research Center, Baton Rouge, LA.

Gaspard, K., and Zhang, Z., 2010. Mitigating Transverse Joint Faulting in Jointed Concrete Pavement with Polyurethane Foam." Transportation Research Record: Journal of the Transportation Research Board, 2010, 3-11. 10.3141/2154-01.

Gietz, R. H., 1979. Asphalt Pavement Distress Investigation: Final Report. Washington State Department of Transportation, Tumwater, WA.

Hansen, W., and Kang, Y., 2010. Durability Study of the US-23 Aggregate Test Road and Recent JPCP Projects with Premature Joint Deterioration. Final Report, University of Michigan, Ann Arbor, MI.

Harrington, D., and Fick, G., 2014. Guide to Concrete Overlays: Sustainable Solutions for Resurfacing and Rehabilitating Existing Pavements (3rd edition). ACPA Publication TB021.03P, National Concrete Pavement Technology Center, Iowa State University.

Hoffman, M. S., and Thompson, M. R., 1981. Mechanistic Interpretation of Nondestructive Pavement Testing Deflections. Transportation Engineering Series No. 32, Illinois cooperative Highway and Transportation Research Series No. 190. University of Illinois at Urbana-Champaign, Champaign, IL.

Hoover, J. M., Huffman, R. T., and Davidson, D. T., 1962. Soil stabilization field trials, primary Highway 117, Jasper County, Iowa. The Forty First Annual Meeting of the Highway Research Board, NAS-NRC, Washington D.C., January 1962.

Horak, E., 1987. Aspects of deflection basin parameters used in a mechanistic rehabilitation design procedure for flexible pavements in South Africa. University of Pretoria, South Africa.

Huang, Y. H., 2004. Pavement Analysis and Design. Second Edition. Pearson Prentice Hall.

IADOT, 2014. Test Sections by Milepost. Special Investigations, Special Investigations Office of Materials Highway Division, Iowa Department of Transportation, Ames, Iowa.

Ioannides, A. M., 1990. Dimensional analysis in NDT rigid pavement evaluation. Transportation Engineering Journal, ASCE, Vol. 116, No. TE1.

Iowa DOT, 2012. Section 2539–Concrete Pavement Undersealing by Pressure Grouting. Standard Specifications for Highway and Bridge Construction. Iowa Department of Transportation, Ames, IA.

Iowa DOT, 2014. Test Section by Milepost. Primary Office of Materials, Highway Division. Special Investigations Office of Materials Highway Division Iowa Department of Transportation, Ames, IA

Janoo, V. C., and Berg, R. L., 1996. PCC Airfield Pavement Response During Thaw-Weakening Periods – A Field Study. Special Report 96-12. CRREL, US Army Corps of Engineers.

Janoo, V. C., and Berg, R. L., 1998. PCC Airfield Pavement Response During Thaw-Weakening Periods. Journal of Cold Regions Engineering. Vol. 12, No. 3.

Janoo, V. C., and Shepherd, K., 2000. Seasonal Variation of Moisture and Subsurface Layer Moduli. Transportation Research Record 1709. No. 00-0929.

Janoo, V. C., Eaton, R., and Barna L., 1997. Evaluation of Airport Subsurface Materials. U.S. Army Corps of Engineering, Cold Regions Research and Engineering Laboratory, Special Report 97-13.

Johnson, A. E., 2012. Freeze-thaw performance of pavement foundation materials. Master of Science, Iowa State University, Ames, Iowa.

Jones, W., Farnam, Y., Imbrock, P., Spiro, J., Villani, C., Golias, M., Olek, J., and Weiss, W. J., 2013. An Overview of Joint Deterioration in Concrete Pavement: Mechanisms, Solution Properties, and Sealers. Purdue University, West Lafayette, Indiana.

Jumikis, A.R., 1955. The Frost Penetration Problem in Highway Engineering. Rutgers University Press.

Jury, W.A., and Horton, R., 2004. Soil Physics. Sixth Edition. Wiley.

KDOT, 2015. Section 834–Undersealing. Standard Specifications for State Road & Bridge Construction. Kansas Department of Transportation, Topeka, KS.

Khazanovich, L., and Gotlif, A., 2003. Evaluation of Joint and Crack Load Transfer. Final Report, ERES Consultants, A Division of Applied Research Associates, Inc., Champaign, IL.

Khoshkhoo, Y., Jansson, P.E., Irannejad, P., Khalili, A., and Rahimi, H., 2015. Calibration of an energy balance model to simulate wintertime soil temperature, soil frost depth, and snow depth for a 14 year period in a highland area of Iran. Cold Regions Science and Technology. 119, 47-60.

Kilareski, W. P., and Anani, B. A., 1982. Evaluation of In situ Moduli and Pavement Life from Deflection Basins. the Fifth International Conference of Asphalt Pavements, University of Michigan, Ann Arbor, MI.

Konrad, J. and Lachance, D., 2001. Use of in-situ penetration tests in pavement evaluation. Canadian Geotechnical Journal, 38 (5), 924–935.

Konrad, J-M, and Roy, M., 2000. Flexible pavement in cold regions: a geotechnical perspective. Can. Geotech. J. 37: 689–699 (2000).

Lai, Y., Zhang, S., Yu, W., 2012. A new structure to control frost boiling and frost heave of embankments in cold regions. Cold Reg. Sci. Technol. 79–80, 53–66.

Lai, Y., Zhang, X., Xiao, J., Zhang, S., Liu, Z., 2005. Nonlinear analysis for frost-heaving force of land bridges on Qing–Tibet railway in cold regions. J. Therm. Stresses 38 (3), 317–332.

Lary, J. A., Mahoney, J. P., and Sharma, J., 1984. Evaluation of Frost Related Effects on Pavements. Final Report, WA-RD 67.1. Washington State Transportation Research Center and the University of Washington.

Li, W., Pour-Ghaz, M., Castro, J., and Weiss, J., 2012. Water absorption and critical degree of saturation relating to freeze-thaw damage in concrete pavement joints. ASCE, J. Mater. Civ. Eng., 2012.24, 299-307

Louisiana DOTD, 2006. Section 602.14–Undersealing or Slabjacking Pavement. Standard Specifications for Roads and Bridges. Louisiana Department of Transportation and Development, Baton Rouge, LA.

Marks, V. J., and Anderson, C., 1993. Crack and Seat PCC Pavement Prior to Resurfacing US 59 - Shelby County. Final Report, Iowa Department of Transportation, Ames, IA.

McCracken, J. K., 2008. Seasonal Analysis of the Response of Jointed Plain Concrete Pavements to FWD and Truck Loads. MS, University of Pittsburg, Pittsburg, PA.

MIT, 1957. Frost Penetration in Multilayer Soil Profiles. Technical Report No. 67. Massachusetts Institute of Technology, Department of Civil and Sanitary Engineering. Corps of Engineers, U.S. Army.

MoDOT, 2009a. Section 625.10–Slab Undersealing. General Provisions and Supplemental Specifications to 2004 Missouri Standard Specifications for Highway Construction. Missouri Department of Transportation, Jefferson City, MO.

MoDOT, 2009b. Section 625.20–Slab Jacking. General Provisions and Supplemental Specifications to 2004 Missouri Standard Specifications for Highway Construction. Missouri Department of Transportation, Jefferson City, MO.

Muge, E.O., Liu, J., Tutumluer, E., 2016. Frost depth prediction for seasonal freezing areas in Eastern Turkey. Cold Reg. Sci. Technol. 124, 118–126

NCDOT, 2008. HDPF (High Density Polyurethane Foam) Processes–General and Slab Leveling, Undersealing and Voidfilling. Contract Proposal–Small Business Enterprise. North Carolina Department of Transportation, Greenville, NC.

NDDOT, 2015. Why there are Spring Load Restrictions. North Dakota Department of Transportation. Accessed in December 10, 2015. https://www.dot.nd.gov/divisions/maintenance/springldrestricprocedures.htm

Newcomb, D. E., and Birgisson, B., 1999. NCHRP Synthesis of Highway Practice 278: Measuring In Situ Mechanical Properties of Pavement Subgrade Soils. TRB, National Research Council, Washington, D.C.

Ni, J., and Cheng, W., 2011. Quality Control for Grouting under Rigid Pavement. Pavements and Materials. Proc., GeoHuman, pp. 183-191. 10.1061/47623(402)22.

Nixon, J.F., and McRoberts, E.C., 1973. A study of some factors affecting the thawing of frozen soils. Canadian Geotechnical Journal. 10:439-452.

NJDOT, 2007a. Section 451–Concrete Slab Stabilization. Standard Specifications for Road and Bridge Construction. New Jersey Department of Transportation, Trendon, NJ.

NJDOT, 2007b. Section 903.08.03–Grout for Undersealing of Concrete Pavement. Standard Specifications for Road and Bridge Construction. New Jersey Department of Transportation, Trendon, NJ.

Ohio DOT, 2007. Section 842–Correcting Elevation of Concrete Approach Slabs with High Density Polyurethane. Supplemental Specifications. Ohio Department of Transportation, Columbus, OH.

OKDOT, 2009. Section 426–Pressure Grouting Pavement. Standard Specifications Book. Oklahoma Department of Transportation, Oklahoma City, OK.

Opland, W. H., and Barnhart, V. T., 1995. Evaluation of the URETEK Method for Pavement Undersealing. Research Report, No. R-1340. Michigan Department of Transportation.

Orakoglu, M., Liu, J., and Tutumluer, E., 2016. Frost depth prediction for seasonal freezing area in Eastern Turkey. Cold Regions Science and Technology, 124, 118-126.

Orr, D. P., 2003. Detection of Nonresilient Behavior in Pavements with a Falling-Weight Deflectometer. Transportation Research Record 1860. No. 03-3688.

Ott, R. L., and Longnecker, M., 2001. An Introduction to Statistical Methods and Data Analysis. Duxbury, Pacific Grove, CA.

Ovik, J. M., Siekmeier, J. A., and Van Deusen, D. A., 2000. Improved Spring Load Restriction Guidelines Using Mechanistic Analysis. Final Report. 2000-18. Minnesota Department of Transportation.

Owusu-Antwi, E. B., Meyer, A. H., and Hudson, W. R., 1990. Assessing Load Transfer across Joints and Cracks in Rigid Pavements using the Falling Weight Deflectometer. The University of Texas at Austin, Austin, TX.

Packard, R. C., 1973. Design of Concrete Airport Pavement. Engineering Bulletin, Portland Cement Association.

PCA, 1984. Thickness Design for Concrete Highway and Street Pavement. Portland Cement Association.

Penn DOT, 2010. Section zITEM 9000-0001–Slab Stabilization. Supplemental Specifications. Pennsylvania Department of Transportation, Harrisburg, PA.

Penn DOT, 2011. Section 679–Slab Stabilization. Specifications. Pennsylvania Department of Transportation, Harrisburg, PA.

Penn DOT, 2005. Falling Weight Deflectometer. Roadway Inventory and Testing Section. Commonwealth of Pennsylvania Department of Transportation, Harrisburg, PA.

www.dot.state.pa.us/Internet/Bureaus/pdBOMO.nsf/infoRMRIFWD (Date Accessed: May 4, 2015).

Penner, E., and Eldred, D., 1985. Equipment and methods for soil frost action studies. National Resource Council, Canada, Div. Building Res. Intern. Rep. 503.

Ping, W. V., and Sheng, B., 2011. Developing Correlation Relationship Between Modulus of Subgrade Reaction and Resilient Modulus for Florida Subgrade Soils. Transportation Research Record: Journal of the Transportation Research Board. 2011, pp. 95–107. DOI: 10.3141/2232-10

Powell, W. D., Potter, J. F., Mayhew, H. C., and Nunn, M. E., 1984. The Structural Design of Bituminous Roads. TRRL Report LR 1132, 62 pp.

Priddy, L. P., and Newman, J. K., 2010. Full-Scale Field Testing for Verification of Mechanical Properties of Polyurethane Foams for Use as Backfill in PCC Repairs. Journal of Materials in Civil Engineering, 22(3), 245-252. 10.1061/(ASCE)0899-1561(2010)22:3(245).

Priddy, L. P., Jersey, S. R., and Reese, C. M., 2010. Full-Scale Field Testing for Injected Foam Stabilization of Portland Cement Concrete Repairs. Transportation Research Record: Journal of the Transportation Research Board, 2155, 24-33. 10.3141/2155-03.

Puppala, A. J., 2008. Estimating Stiffness of Subgrade and Unbound Materials for Pavement Design. NCHRP Synthesis 382. Transportation Research Board.

Rajaei, P., and Baladi, G.Y., 2015. Frost depth – a general prediction model. 94st Transportation Research Board Annual Meeting, Washington D.C.

Rodden, R., 2010. Drainable Base Layers Revisited. Tennessee Concrete Pavement Conference. ACPA.

Roesler, J. R., Chavan, H., King, D., and Brand, A. S., 2015. Concrete slab analyses with field-assigned non-uniform support conditions. Int. J. Pavement Eng., Vol. 17. Issue. 7, 578-589.

Rui, D., Deng, H., Nakamura, D., Yamashita, S., Suzuki, T., and Zhao, H., 2016. Full-scale model test on prevention of frost heave of L-type retaining wall. Cold Reg. Sci. Technol. 132 (2016) 89–104.

RWIS, 2016. Iowa State Environmental Mesonet, RWIS Soil Probe Download. Iowa State University, Department of Agronomy. Road Weather Information System. http://www.rwisonline.com/scanweb/swlogin.asp. Accessed December, 2016.

Schmalzer, P. N., 2006. LTPP Manual for Falling Weight Deflectometer Measurements, Version 4.1. Final Report, FHWA-HRT-06-132. Federal Highway Administration.

SDDOT, 2004a. Section 391–Undersealing. Standard Specifications for Roads & Bridges. South Dakota Department of Transportation, Pierre, SD.

SDDOT, 2004b. Section 392–Pavement Jacking. Standard Specifications for Roads & Bridges. South Dakota Department of Transportation, Pierre, SD.

Simonsen, E., Isacsson, U., 1999. Thaw weakening of pavement structures in cold regions. Cold Reg. Sci. Technol. 29, 135–151.

Smith, K. D., Wade, M. J., Bruinsma, J. E., Chatti, K., Vandenbossche, J. M., Yu, H. T., Hoerner, T. E., Tayabji, S. D., 2007. Using Falling Weight Deflectometer Data with Mechanistic-Empirical Design and Analysis, Draft Interim Report, DTFH61-06-C-0046, Federal Highway Administration, Washington, D.C.

Solanki, P., Zaman, M. and Khalife, R., 2013. Effect of Freeze-Thaw Cycles on Performance of Stabilized Subgrade. Sound Geotechnical Research to Practice, pp. 566-580.

Stefan, J., 1890. Ueber die verdampfung und die auflösung als vorgänge der diffusion. Annalen der Physik. Vol. 277, Iss. 12(1890), 725–747. DOI: 10.1002/andp.18902771206.

Stubstad, R. N., Jiang, Y. J., and Lukanen, E. O., 2006. Guidelines for Review and Evaluation of Backcalculation Results, FHWA-RD-05-152, Federal Highway Administration, Washington, D.C.

Taber, S., 1929. Frost Heaving. Journal of Geology, Vol. 37, No. 5 (1929), 428–461.

Taha, R., Selim, A., Schaefer, V., Carlson, K., and Hasan, S., 1994. Evaluation of Undersealing of Undoweled Plain Jointed PCC Pavements in South Dakota. Final Report, South Dakota Department of Transportation. Pierre, SD.

Taylor, P. C., 2011. Preventing Joint Deterioration in Concrete Pavements: A Summary of Current Knowledge. CP Road Map.

Taylor, P. C., Sutter, L., and Weiss, J., 2012. Investigation of Deterioration of Joints in Concrete Pavements. National Concrete Pavement Technology Center, Iowa State University, Ames, IA.

Thorton, S.I., 1983. Correlation of Subgrade Reaction with CBR, Hveem Stabilometer, or Resilient Modulus. Arkansas State Highway and Transportation Department.

U.S. Air Force., 1966. Airfield Rigid Pavement Evaluation--Air Force: Emergency Construction. Volume 88, Issue 40 of Air Force manual. U.S. Department of the Army, U.S. Department of the Air Force.

U.S. Army, 1965. Soils and geology – Pavement design for frost conditions. U.S. Army Corps of Engineers. Department of the Army Technical Manual TM 5-818-2.

UDOT, 2012. Section 02755–Concrete Slab Jacking. Standard Specifications for Road and Bridge Construction. Utah Department of Transportation, Salt Lake City, UT.

USDA and USDAF, 1988. Arctic and Subarctic Construction Calculation Methods for Determination of Depths of Freeze and Thaw in Soils. Technical Manual, 5-852-6. Departments of the Army and the Air Force.

Vennapusa, P. K. R., 2008. Investigation of roller-integrated compaction monitoring and in-situ testing technologies for characterization of pavement foundation layers. Ph.D. Thesis. Iowa State University. Ames, Iowa.

Vennapusa, P. K. R., and White, D. J., 2014. Field Assessment of a Jointed Concrete Pavement Foundation Stabilized with Injected Polyurethane Expandable Foam. International Journal of Pavement Engineering. Published online: 03 Nov 2014. 10.1080/10298436.2014.972917.

Vennapusa, P. K.R., and White, D. J., 2009. Comparison of light weight deflectometer measurements for pavement foundation materials. Geotechnical Testing Journal, ASTM, 32(3), 239-251.

Vennapusa, P. K.R., White, D. J., Siekmeier, J., and Embacher, R. A., 2011. In situ mechanistic characterisations of granular pavement foundation layers. International Journal of Pavement Engineering. Volume 13, 2012, Issue 1. DOI: 10.1080/10298436.2011.564281

Vennapusa, P., White, D. J., and Jahren, C. T., 2006. In-situ permeability of unbound granular bases using the air permeameter test. Proceedings of 85th Annual Transportation Research Board Conference, No. 06–1729, Transportation Research Board, Washington, D.C.

White, D. J., and Vennapusa, P. K. R., 2014. Optimizing Pavement Base, Subbase and Subgrade Layers for Cost and Performance on Local Roads. Final Report. InTrans Project 11-422. Iowa State University. Ames, IA.

White, D. J., and Vennapusa, P. K.R., Zhang, Y., and Johnson, A., 2016. Assessment of Seasonal Variations in Concrete Pavement Foundation Layers – Multiple Test Sections in Iowa. InTrans Project 09-352 Report. Iowa State University. Ames, IA. (In Progress)

White, D. J., Becker, P., Vennapusa, P. K. R., Dunn, M. J., and White, C. I., 2013. Soil stiffness of stabilized pavement foundations. Transportation Research Record: Journal of the Transportation Research Board. No. 2335, Transportation Research Board of the National Academies, Washington, D.C., 2013, pp. 99–109. DOI: 10.3141/2335-11

White, D. J., Vennapusa, P., Suleiman, M., and Jahren, C., 2007. An In-situ Device for Rapid Determination of Permeability for Granular Bases. Geotech. Test. J., ASTM. Vol. 30, No. 4.

White, D., Mekkawy, M., Sritharan, S., and Suleiman, M., 2007. Underlying causes for settlement of bridge approach pavement systems, Journal of Performance of Constructed Facilities, 21(4), 273-282

Yang, Z., Weiss, W., and Olek, J., 2006. Water transport in concrete damaged by tensile loading and freeze-thaw cycling. ASCE, J. Mater. Civ. Eng., 18(3), 424-434.

Yoder, E.J., and Witczak, M.W., 1975. Principles of Pavement Design. Second Edition. John Wiley & Sons.

Yu, L., Wang, R., and Skirrow, R., 2013. The application of polyurethane grout in roadway settlements issues. GeoMontreal. Montreal, Canada.

Yun, Y., Wu, Y.F., 2011. Durability of CFRP-concrete joints under freeze–thaw cycling. Cold Reg. Sci. Technol. 65 (3), 401–412.

Zarling, J. P., Braley, W. A., and Pelz., C., 1989. The modified Berggren method – A review. Proceedings of the Fifth International Conference, Cold Regions Engineering. 267-273. New York, NY: ASCE.

Zhang, J., White, D., Taylor, P. C., and Shi, C., 2015. A case study of evaluating joint performance in relation with subsurface permeability in cold weather region. Cold Reg. Sci. Technol. 110 (2015) 19–25.

Zhang, Y., Johnson, A. E., White, D. J., 2016. Laboratory freeze-thaw assessment of cement, fly ash, and fiber stabilized pavement foundation materials, Cold Reg. Sci. Technol. 122 (2016) 50–57.

Zorn, G., 2003. Operating manual: Light drop-weight tester ZFG2000. Zorn Stendal, Germany.

ACKNOWLEGEMENTS

First and foremost, I would like to thank my major professors, Drs. David White, Pavana Vennapusa, and Bora Cetin, for their guidance, teaching, and patience. Their technical support helped me to concentrate on this work and confidently to pursue a degree of doctor of philosophy. I am also thankful for Dr. Robert Horton, Dr. Peter Taylor, and Dr. Charles Jahren serving in my committee. Their professional advising helped me to reach the goals of this research. I would like to give special thanks to Dr. Robert Horton and Dr. Peter Taylor for their spiritual encouragements and financial support at the most difficult time to me. I would not be able to finish this study without their essential inspirations.

I am grateful for everyone who has helped me during my program of study, especially the members in the Center for Earthworks Engineering Research (CEER) and Mr. Bob Steffes in the National Concrete Pavement Technology (CPTech) Center at Iowa State University. I would like to thank Dr. Christiana White for her guidance on technical writing and Alex Johnson for sharing his previous experience.

At last, I would like to thank my deeply loving family, especially my parents, wife and parents in law, who constantly pushed me to follow my dream and gave me the greatest support on every chapter of my life.